Summer 7-6-1989

Hillslope Processes on Late Quaternary Cinder Cones of the Cima Volcanic Field, Eastern Mojave Desert, California

Claire Estelle Renault

THE UNIVERSITY OF NEW MEXICO
ALBUQUERQUE, NEW MEXICO 87131

POLICY ON USE OF THESES AND DISSERTATIONS

Unpublished theses and dissertations accepted for master's and doctor's degrees and deposited in the University of New Mexico Library are open to the public for inspection and reference work. *They are to be used only with due regard to the rights of the authors.* The work of other authors should always be given full credit. Avoid quoting in amounts, over and beyond scholarly needs, such as might impair or destroy the property rights and financial benefits of another author.

To afford reasonable safeguards to authors, and consistent with the above principles, anyone quoting from theses and dissertations must observe the following conditions:

1. Direct quotations during the first two years after completion may be made only with the written permission of the author.

2. After a lapse of two years, theses and dissertations may be quoted without specific prior permission in works of original scholarship provided appropriate credit is given in the case of each quotation.

3. Quotations that are complete units in themselves (e.g., complete chapters or sections) in whatever form they may be reproduced and quotations of whatever length presented as primary material for their own sake (as in anthologies or books of reading) ALWAYS require consent of the authors.

4. The quoting author is responsible for determining "fair use" of material he uses.

This thesis/dissertation by Claire Estelle Renault has been used by the following persons whose signatures attest their acceptance of the above conditions. (A library which borrows this thesis/dissertation for use by its patrons is expected to secure the signature of each user.)

NAME AND ADDRESS		DATE
[signature]	SUNY-Buffalo	12/92
[signature]	CalState LA	3/96

Claire Estelle Renault
Candidate

Geology
Department

This thesis is approved, and it is acceptable in quality and form for publication on microfilm:

Approved by the Thesis Committee:

, Chairperson

Accepted:

Asst. *Dean, Graduate School*

July 6, 1989
Date

HILLSLOPE PROCESSES ON LATE QUATERNARY CINDER CONES OF THE CIMA VOLCANIC FIELD, EASTERN MOJAVE DESERT, CALIFORNIA

By

CLAIRE ESTELLE RENAULT

B.A., The Colorado College, 1984

THESIS

Submitted in Partial Fulfillment of the
Requirements for the Degree of

Master of Science in Geology

The University of New Mexico
Albuquerque, New Mexico

July, 1989

ACKNOWLEDGEMENTS

The author wishes to express her appreciation to her advisor Dr. Stephen G. Wells for his guidance and support which he offered during this study. I am grateful to the following people for their comments and ideas: Dr. L.D. McFadden, Dr. R.Y. Anderson, Dr. W.E. Elston, Dr. G. Smith, Dr. F. Perry (University of New Mexico) and Dr. B. Crowe (Los Alamos National Laboratory).

Thanks is given to the director of the ZZYZX Desert Studies Consortium, Gerry Sherba, for providing housing at the ZZYZX Desert Studies Consortium during my field seasons. Special thanks to the caretakers of ZZYZX Desert Studies Consortium, Rob Fulton and Dawn VanTassle, for providing their generous friendship and support during my field seasons.

Thanks to the graduate students of the Quaternary Studies Program at the University of New Mexico for feedback during many healthy discussions.

Fiscal support by the Student Research and Allocations Committee at the University of New Mexico is appreciated and gratefully acknowledged.

My special thanks to Thomas M. Skirvin as a constant source of support and insight in the field and office.

HILLSLOPE PROCESSES ON LATE QUATERNARY CINDER CONES OF THE CIMA VOLCANIC FIELD, EASTERN MOJAVE DESERT, CALIFORNIA

By

CLAIRE ESTELLE RENAULT

ABSTRACT OF THESIS

Submitted in Partial Fulfillment of the
Requirements for the Degree of

Master of Science in Geology

The University of New Mexico
Albuquerque, New Mexico

July, 1989

HILLSLOPE PROCESSES ON LATE QUATERNARY CINDER CONES OF THE CIMA VOLCANIC FIELD, EASTERN MOJAVE DESERT, CALIFORNIA

Claire Estelle Renault

B.A., Geology, The Colorado College, 1984

M.S., Geology, University of New Mexico, 1989

Four basaltic cinder cones of the cima volcanic field were studied in an attempt to understand the geomorphic and volcanic processes involved in the constructional and degradational evolution of late Quaternary cinder cones in an arid climate. Modern hillslope processes were mapped on cone slope and soil and subsurface stratigraphy were documented in the surrounding debris-apron deposits. In addition, morphometric parameters shown to be sensitive to cinder cone age (Dohrenwend et al., 1986) were measured on the four cinder cones to evaluate previous studies which estimated the relative or absolute age of cinder cones based only on morphologic changes in the cone slope and debris apron.

Debris-flow, fluvial, and colluvial processes are the principle processes by which cinder cones degrade through time. Lithologic variations on the cone slope such as the proportion of agglutinate and proto-agglutinate to lapilli affect the rates and processes of degradation. Deeply incised debris-flow channels are more common below

agglutinate and/or proto-agglutinate. Areas on the cone slope without agglutinate and/or proto-agglutinate degrade primarily through episodic fluvial processes.

Morphometric analysis reveals that differences in slope angle, apron height, and apron length are controlled by the upslope location of agglutinate or proto-agglutinate. Therefore, the eruptive history and geomorphic evolution of cinder cones must be understood to augment morphometric analyses.

Multiple eruptions from a single vent are called polycyclic eruptions. Four geomorphic and pedologic criteria are determined to be useful for recognizing polycyclic volcanos: (1) multiple airfall-tephra deposits separated by buried soils, (2) debris-apron deposits with soils buried by airfall-tephra, (3) the presence of debris-apron deposits topographically below cone slopes with no incision, and (4) large variations in morphometric parameters sensitive to cone age.

TABLE OF CONTENTS

TABLE OF CONTENTS (cont.)

TABLE OF CONTENTS (cont.)

LIST OF FIGURES

LIST OF FIGURES (cont.)

LIST OF FIGURES (cont.)

LIST OF TABLES

INTRODUCTION

STATEMENT OF PROBLEM AND PURPOSE

Numerous studies of volcanic cinder cones have demonstrated that the eruptive processes and original constructional morphology of cinder cones are predictable (McDonald, 1972; McGetchin et al., 1974; Chouet et al., 1974; Gutmann, 1979; Settle, 1979; Cas and Wright, 1987). Others have documented systematic changes in cinder cone morphology with time since the eruptive event (Scott and Trask, 1971; Porter, 1972; Bloomfield, 1975; Wood, 1980a,b; and Dohrenwend et al., 1986). Dohrenwend et al. (1986) have postulated that debris flow, throughflow, and fluvial processes are significant in the degradation of late Pleistocene cinder cones of the Cima volcanic field, California (Fig. 1). No previous study has provided detailed documentation of the erosional and depositional processes associated with the degradation of late Quaternary cinder cones.

The primary objectives of this study are (1) to determine the types of hillslope processes responsible for the degradation of four Late Pleistocene volcanic cinder cones in the Cima volcanic field, California, and (2) to develop a better understanding of the eruptive history by enhancing relative age estimates of late Quaternary cinder

LOCATION MAP

CIMA VOLCANIC FIELD, CALIFORNIA

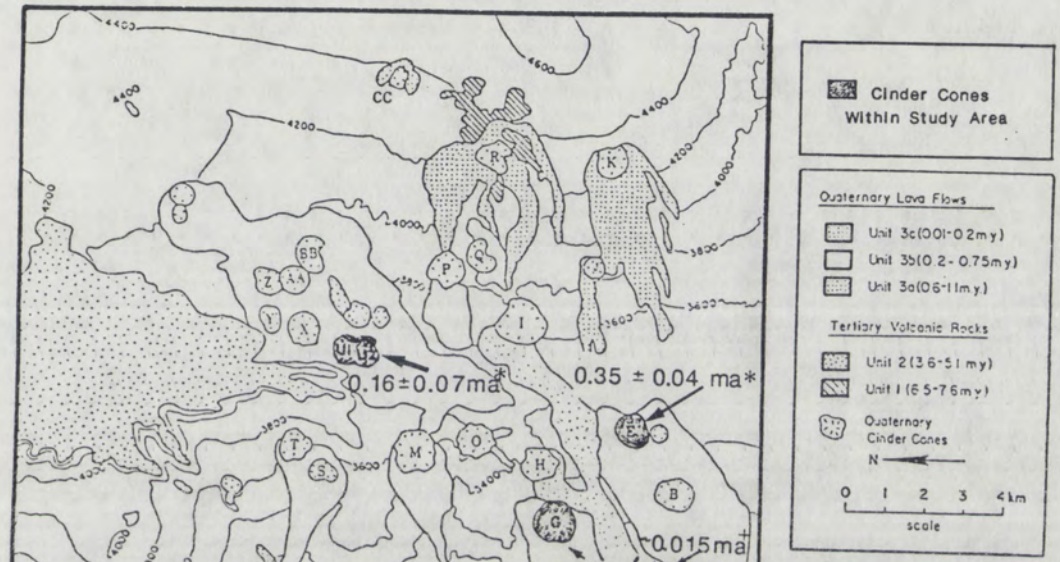

* K/Ar date from Turrin et al., 1985

\+ flow age for A2 cone, from Dorn (1984; Dorn et al. (1986)

FIGURE 1.

Generalized geologic map of the southern part of the Cima volcanic field showing location of cinder cones within the study area. (modified from Dohrenwend et.al., 1986)

cones and in arid climates.

The approach used in this study combines geomorphic field observations of hillslope processes recently active on cinder cones with analysis of sedimentologic and soil characteristics of the debris-apron deposits at the base of cinder cones. Debris aprons accumulate along the base of cinder cones due to downslope transport of pyroclastic material by mass movement and colluvial and alluvial processes. Thus, an approach that utilizes an analysis of both modern hillslope processes and the resultant debris-apron deposits will provide a better understanding of cinder cone degradation.

RESEARCH SIGNIFICANCE

Radiometric dating techniques at times yield questionable age estimates for geologically young basaltic rocks (e.g., see Sinnock and Easterling, 1983; and Crowe et al., 1989). Absolute dating of cinder cone eruptions by radiometric techniques is difficult when cone and flow field relations are unclear. A better understanding of the timing of eruptions and the degradation of cinder cones provides (1) valuable mapping tools in volcanic fields where cinder cone eruptive sequences are complex, (2) age estimates for cinder cones in volcanic fields where absolute age control is unreliable or not available (Crowe et al., 1989), and (3)

vital information for the assessment of volcanic hazards in areas of the western United States where nuclear waste disposal is planned (Wells, 1986; and Wells et al., 1988).

Results of this study will enhance an understanding of long-term hillslope processes in arid regions during the late Quaternary. Several workers have attempted to understand the evolution of hillslopes in arid regions by documenting modern processes (Yair and Lavee, 1982) or by documenting the sequence of deposits at the base of a hillslope (Wells et al., 1982). This study combines observations of the hillslope processes and Quaternary colluvial deposits resulting from hillslope degradation and should prove useful in a variety of geomorphic studies in arid regions.

LOCATION AND GEOLOGIC SETTING

The Cima volcanic field and associated study area are located approximately 20 km southeast of Baker, California in the eastern Mojave Desert (Fig.1). Access is gained from the Kelbaker road along the Rainy Day Mine road (15.4 mi from Baker, California) or the Akin Mine road (19.7 mi from Baker, California). The Cima volcanic field contains approximately 40 cinder cones and more than 60 associated basaltic flows that are extruded onto pediment surfaces and alluvial fans (Dohrenwend, et al., 1984, Wells et al., 1987; Skirvin and Wells, 1989). The four cinder cones analyzed in

this research were breached during the later stages of eruption, followed by extrusion of alkali basaltic flows through the breached openings. Original constructional forms are characteristic of relatively fluid basaltic lavas (McFadden et al., 1986) (Fig. 1). The cinder cones studied range from 2.5 km to 7.7 km apart, with average heights and widths ranging from 90 m to 155 m and 540 m to 915 m, respectively (Dohrenwend et al., 1986). Given the minimum distance between any of the cinder cones studied (2.5 km) and the much older age of adjacent cinder cones (Turrin et al., 1984; Turrin et al., 1985) the effect of pyroclastic material from adjacent eruptions on cinder cone degradation is negligible.

The alkali basalts of the Cima volcanic field possess isotopic compositions high in ENd (+9.0 - +10.06) and very low in $^{87}Sr/^{86}Sr$ (0.7029 - 0.7037). These isotopic values are expected for basalts derived exclusively from "depleted" asthenospheric mantle (Farmer et al., in press). Recent tectonic models for this portion of the Mojave Desert suggest a mechanism of Early Tertiary low-angle subduction for tectonic removal of pre-existing continental mantle beneath the Cima volcanic field (Bird, 1988) and replacement of ancient mantle lithosphere by new lithosphere composed of "depleted" asthenospheric mantle (Farmer et al., 1989 in press). North-northwest trending shear zones are aligned with and offset several volcanic flow units and cinder cones in the Cima volcanic field. This alignment and offset

suggests that volcanism is associated with structural weakness at the eastern margin of the Mojave Desert (Wilshire, 1988; Skirvin, in prep.).

Potassium - argon (K/Ar) age determinations on the lava flows associated with the three older cinder cones studied produce ages of 0.16 + 0.07 Ma, 0.22 + 0.03 Ma, 0.35 + 0.04 Ma (Fig. 1)(Turrin et al., 1985). Age determinations of the youngest cone are approximately 19,000 yrs. B.P. by cation-ratio of the rock varnish (Dorn, 1984) and 16,580 +/- 600 yrs. B.P. and 14,600 +/- 800 yrs. B.P. by radiocarbon on varnish (Dorn, 1984; and Dorn et al., 1986). These age ranges are in agreement with paleomagnetic excursion data (Wells et al., 1985, Champion, D. personal communication), and relative soil development estimates (McFadden, et al., 1984, Dohrenwend et al., 1986).

CLIMATE

At elevations of 600 to 1000 m in the eastern Mojave Desert, the climatic regime is semi-arid to arid with mean annual precipitation and mean annual temperature ranging from 12 to 25 cm and 16 to 18^{o}C, respectively (National Oceanic and Atmospheric Administration, 1978). Approximately equal proportions of precipitation fall during the summer and winter (Wells et al., 1984) with summer precipitation consisting of low-frequency high-intensity storms. Due to the sparseness of vegetation, the short-

duration, high-intensity summer storms result in local flash flooding in the typically dry washes (Wells et al., 1989).

Research by McFadden et al. (1986) and Royek (in prep.) on soil development on radiometrically dated lava flows at the Cima volcanic field indicates that soil development occurs primarily within eolian dust (loess) which accumulates on the flow surface with time. The observed soil/loess stratigraphy suggests that several loess events have occurred during the past ~1.0 Ma (McFadden et al., 1986). These loess events are attributed to past climatic changes, such as the Pleistocene-to-Holocene climate change (VanDevender, 1973; VanDevender and Spaulding, 1979; Spaulding, 1982), which resulted in the desiccation of pluvial lakes, reduction in vegetation, and exposure of loose fine materials on hillslopes and playas (McFadden et al., 1986). The resultant saline playas are likely sources for soluble salts and calcium carbonate which tend to precipitate higher in the soil profile during interglacial periods (McFadden et al, 1986).

VEGETATION

Vegetation in the eastern Mojave Desert is classified as Mojave Desert scrub (Brown, 1980). Vegetation on debris aprons include Joshua tree Yucca brevifolia, creosote bush Larea tridentata, brittle bush Eucelia farinosa, small cacti, and a variety of small annuals (Brown, 1980). The

sparse vegetation on the cone slopes consists of predominantly annual grasses and small woody shrubs with few creosote Joshua tree.

PREVIOUS WORK

Previous studies of cinder cones have documented qualitative and quantitative variations in the morphology of cinder cones and their associated debris-aprons. Colton's (1937) work in the San Francisco Mountain volcanic field of Arizona represents one of the earliest attempts to assign stages of cinder cone degradation based upon weathering. Kear (1957), Colton (1967), and Kieffer (1971), also classified cone degradational stages on the basis of weathering. Porter (1972), provided one of the first studies to quantify relations between various morphometric parameters of cinder cones. Subsequently, cinder cone degradation has been quantified by the measurement of (1) maximum cone slope angle, shown to decrease with time (Scott and Trask, 1971; and Dohrenwend et al., 1986), (2) the ratio of cone height to cone basal diameter, shown to decrease with time (Scott and Trask, 1971; Bloomfield, 1975; Wood, 1980a; Wood, 1980b; and Dohrenwend et al., 1986), (3) drainage density, which increases with time and changes in drainage morphology (Hasenaka and Carmichael, 1985; and Dohrenwend et al., 1986), and (4) the ratios of debris-apron height-to-cone height and apron length-to-cone length, shown

to increase with time (Dohrenwend et al., 1986). Wood (1980b) determined that the ratio of crater width-to-cone width is maintained through time, while Bloomfield (1975) and Dohrenwend et al. (1986) observed a decrease in this ratio. Morphometric parameters will be defined in the methodology section of this report. These studies provide insight into the morphologic changes of volcanic cinder cones, but do not provide detailed analysis of the hillslope processes responsible for morphologic changes. These studies provide insight into the morphologic changes of volcanic cinder cones, but do not provide detailed analysis of the hillslope processes responsible for morphologic changes.

METHODOLOGY

GEOMORPHIC MAPPING

The purpose of geomorphic mapping in this study is to define and correlate spatially distinct cinder cone slope volcanic and geomorphic features which are not temporally constrained to relative age-dated debris-apron deposits. Field mapping units are divided into volcanic (constructional) and geomorphic (degradational and depositional) units. Constructional volcanic units mapped in this study include primary volcanic deposits unmodified by geomorphic processes (McGetchin et al., 1974; Chouet et al., 1974; Gutmann, 1979; Settle, 1979; Wood, 1980; Cas and Wright 1987). Unique to this study, mapped degradational geomorphic units consist of areas on the cinder cone slope in which a particular modern hillslope process dominates. Depositional geomorphic units include surficial and subsurface debris-apron deposits.

A stratigraphic sequence of surficial geomorphic units was established consisting of debris-apron deposits differentiated on the basis of (1) cross-cutting stratigraphic relationships, (2) relative thickness of rock varnish on surficial clasts, and (3) relative degree of soil development. Subsurface depositional geomorphic units were

differentiated on the basis of (1) buried soil horizons, and (2) distinct sedimentologic units.

Volcanic and geomorphic units were mapped in the field on enlarged vertical black and white aerial photographs at an approximate scale of 1:10,000. Volcanic units mapped include features such as (1) garlands [g] which form during the cinder cone eruption process as talus slopes of tephra are deposited at the angle of repose of approximately 32° - 38° (McGetchin, 1975), (2) base surge deposits [bs], (3) agglutinate [ag], and (4) areas with a high frequency of bombs (proto-agglutinate) [b] (Fig. 2). Geomorphic degradational units mapped include: (1) channels with debris flow levees [df], (2) channels without debris flow levees [d], and (3) channels with high frequency of coarse material filling up to three quarters of the channel [dc] (Fig. 3). Geomorphic depositional units mapped or correlated in the subsurface include debris-apron surficial deposits [Qa1, Qa2, and Qa3] and subsurface deposits [unit 1 - unit 4 from oldest to youngest].

SOIL PROFILE FIELD DESCRIPTIONS

Because the degree of soil development of many soil properties is time dependent (Bockheim, 1980) this study uses soils as a stratigraphic tool to augment differentiation of debris-apron surface deposits where cross-cutting relationships are unavailable. Soil field

SCHEMATIC DIAGRAM OF GEOMORPHIC AND VOLCANIC FEATURES

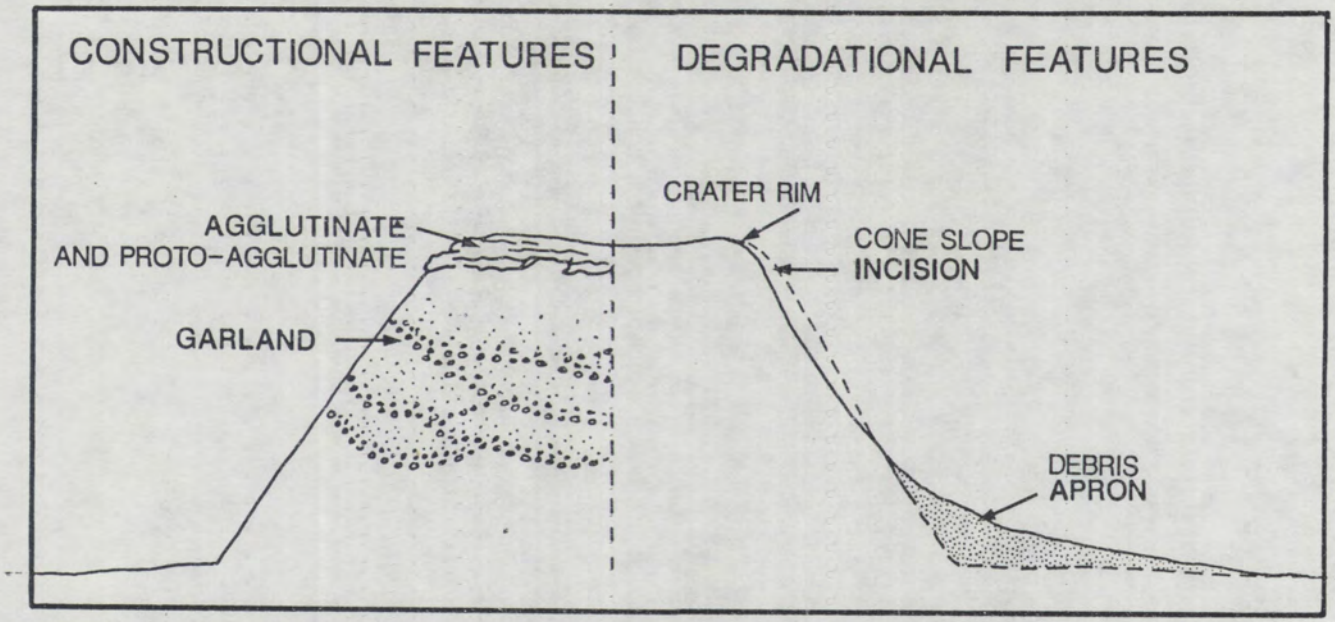

FIGURE 2. Schematic illustration of geomorphic and volcanic cinder cone features (left – constructional features; right – degradational features)

SCHEMATIC DIAGRAM OF GEOMORPHIC AND VOLCANIC FEATURES

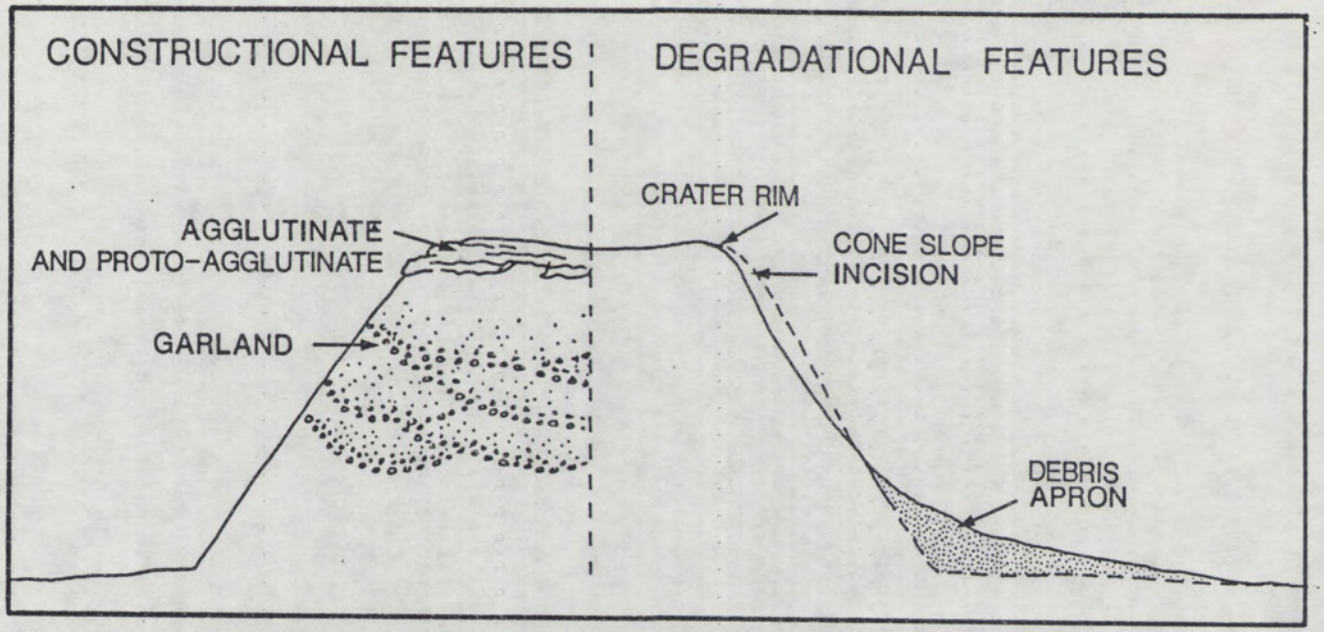

FIGURE 2. Schematic illustration of geomorphic and volcanic cinder cone features (left – constructional features; right – degradational features)

FIGURE 3. Illustration of the three types of cone slope incision: a) debris-flow channel, b) fluvial channel, and c) fluvial channel infilled with bombs and lapilli. The location of channel width and depth measurements are sketched on each diagram. D=depth

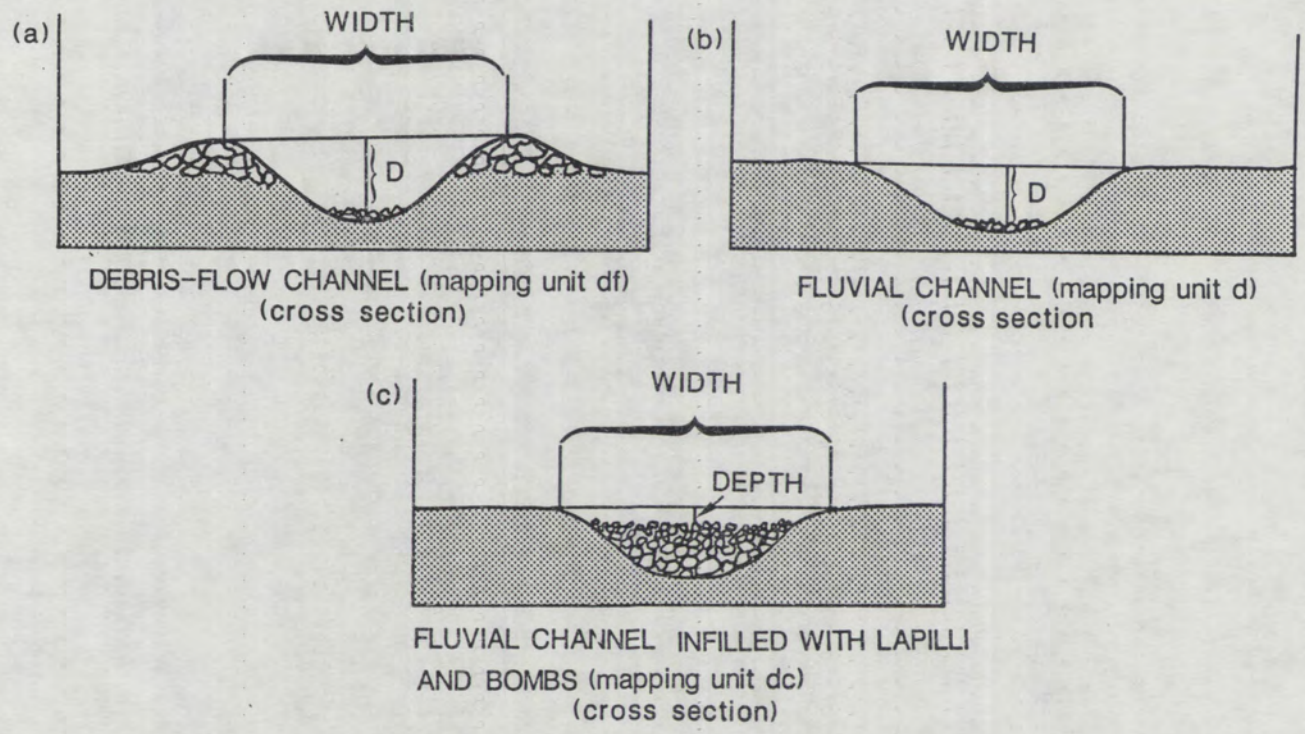

descriptions and sampling are according to the Soil Conservation Service (1981) and Birkeland (1984). Soil morphologic parameters documented in the field include: (1) horizon thickness, (2) texture, (3) stage of secondary $CaCO_3$ accumulation (Gile et al., 1966), (4) relative amount of SiO_2 and soluble salts, (5) color, from Munsell soil color chart, (6) structure, and (7) clay films. Buried soils are recognized by the presence of truncated pedogenic clay (Bt) soil horizons and buried vesicular A horizons (Av) (Fig. 4) (Birkeland, 1984; McFadden et al., 1986). Av horizons form by the entrapment of soil air that expands as the soil temperature rapidly increases after summer rainfall events (Evenari et al., 1974; and McFadden et al., 1986).

DEBRIS-APRON SUBSURFACE STRATIGRAPHIC FIELD DESCRIPTIONS

A detailed description of debris-apron subsurface stratigraphy provides the data necessary for interpretation of colluvial, alluvial, and debris flow aggradational phases. Debris apron subsurface stratigraphic sequences were differentiated on the basis of textural and bedding characteristics (Gardner and Dackombe, 1983) and described at every soil pit location (Fig. 4). Airfall tephra was distinguished from reworked tephra by the presence of aligned bombs, grain support, occasional reverse graded bedding, and alternating beds of moderately-to-well sorted

GENERAL CHARACTERISTICS OF
DEBRIS APRON, BASALTIC AIRFALL TEPHRA, AND BURIED SOILS

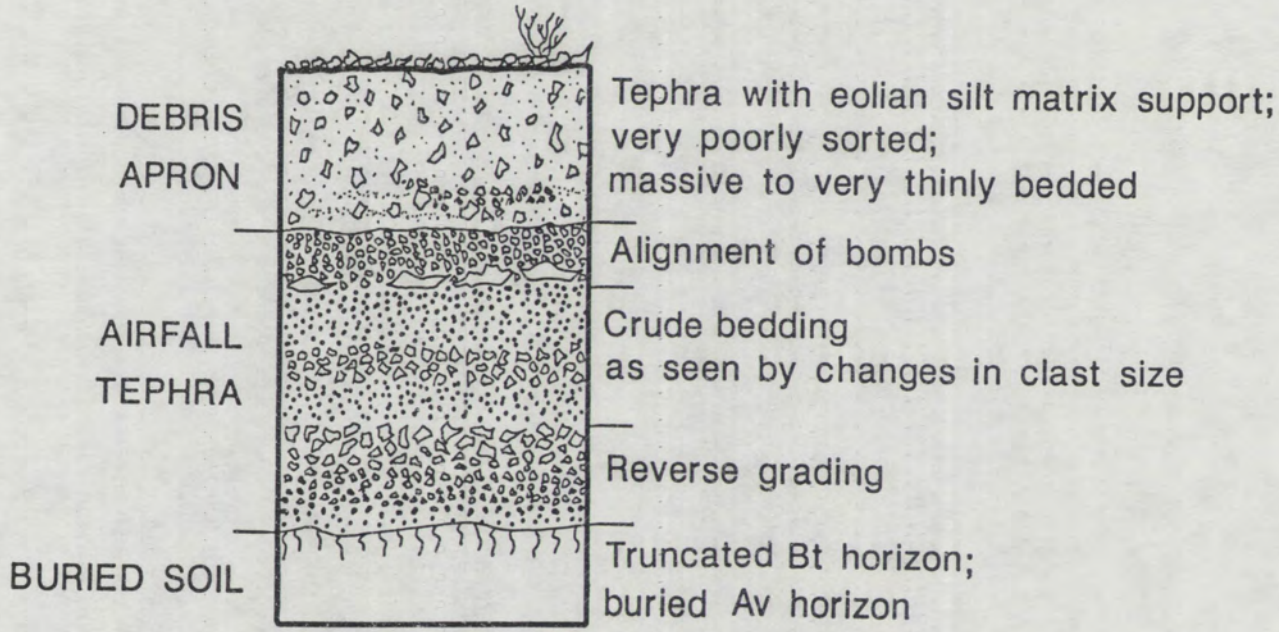

(modified from Fisher and Schmincke, 1984, and Cas and Wright, 1987)

Figure 4. Generalized stratigraphic column illustrating the different sedimentary and volcanic deposits observed.

very angular lapilli, (Write et al., 1980; Fisher and Schmicke, 1984) (Fig. 4).

MORPHOMETRIC FIELD ANALYSIS

Cone slope and debris-apron topographic profiles were measured in the field with an electronic laser theodolite perpendicular to the crater rim from the farthest point on the debris apron to the crater rim. The electronic theodolite measures at a precision up to 10^{-4}m distance and up to one second of one degree of arc. For the purpose of this study, measurements were rounded to the nearest centimeter and half-degree was sufficient. Horizontal and vertical measurements were plotted on X-Y graphs as topographic profiles (Appendix D). Several morphometric parameters sensitive to cinder cone age such as cone and debris-apron slope angle, length, and height are determined from the measured topographic profiles and summarized in Figure 5 (Porter, 1972; and Dohrenwend et al., 1986).

The dimensions of incised channels, drainage frequency and the inferred mode of sediment transport on the cone slopes are measured and described along selected transects one third-to-half way up each cinder cone slope, parallel to the crater rim. Transects are located below areas of different cone lithologies such as: (1) exposed agglutinate, (2) exposed proto-agglutinate, or (3) loose lapilli to determine

Hc = cone height
Wc = cone width
Sc = cone-slope angle
Lc = cone-slope length
Ha = apron height
La = apron length

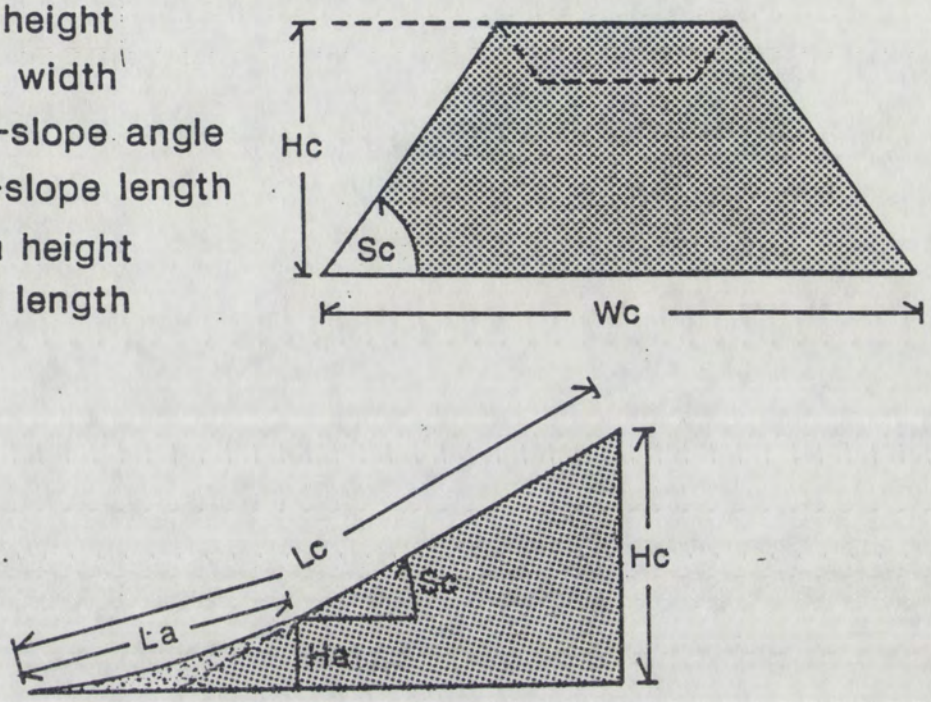

Figure 5. Morphometric parameters measured on cone slopes and debris aprons in the field (Modified from Dohrenwend et al., 1986).

the influence of lithology on channel dimensions and transport mechanisms. Cone slope channel dimensions (width and depth) are measured with a tape and Jacob staff (Fig. 3). Mode of sediment transport is differentiated in the field as (1) debris flow, indicated by incised channels with debris-flow levees and snouts (Wells et al., 1982; and Wells and Harvey, 1987), (2) fluvial processes indicated by incised channels without debris-flow levees (Dohrenwend et al., 1986), and (3) unincised cone slope with tephra accumulating up-slope of vegetation indicating gravity dominated colluvial grain flow processes. In order to establish the similarity in the proportions of debris-flow channels to fluvial channels located across transects topographically below different cone slope lithologies, a Wilcoxon-T statistical test was performed (Tate and Clelland, 1959).

RESULTS

GEOMORPHOLOGY OF CINDER CONE SLOPES AND DEBRIS APRONS

Three debris-apron geomorphic surfaces are delineated for each cinder cone and are labeled Qa1, Qa2, and Qa3 from oldest to youngest. Debris-apron geomorphic surfaces are unique to each cinder cone and not correlated between cinder cones. Subsurface stratigraphic type sections for each debris apron are described in detail providing insight into the complex history of debris-apron sedimentation.

Geomorphology of the A-Cone Complex

The A-cone complex consists of a 0.015 Ma cinder cone (here determined as A2 cone) (Dohrenwend et al., 1986) adjacent to an older cone (here determined as A1 cone) of unknown age which is partially buried by tephra erupted from A2 cone (Fig. 6). The A2 cone is 90 m high and 540 m wide (mean) (Dohrenwend et al., 1986) and has the greatest slope angle of all cones measured in this study (31.3°). The A1 cone has a mean height of 91 m, a mean width 476 m, and has the lowest slope angle of all cones measured in this study (21.0°).

Cone-slope degradational units associated with the A2 cone slope are predominantly garland features (unit g), and to a lesser degree isolated debris flow channels (unit df)

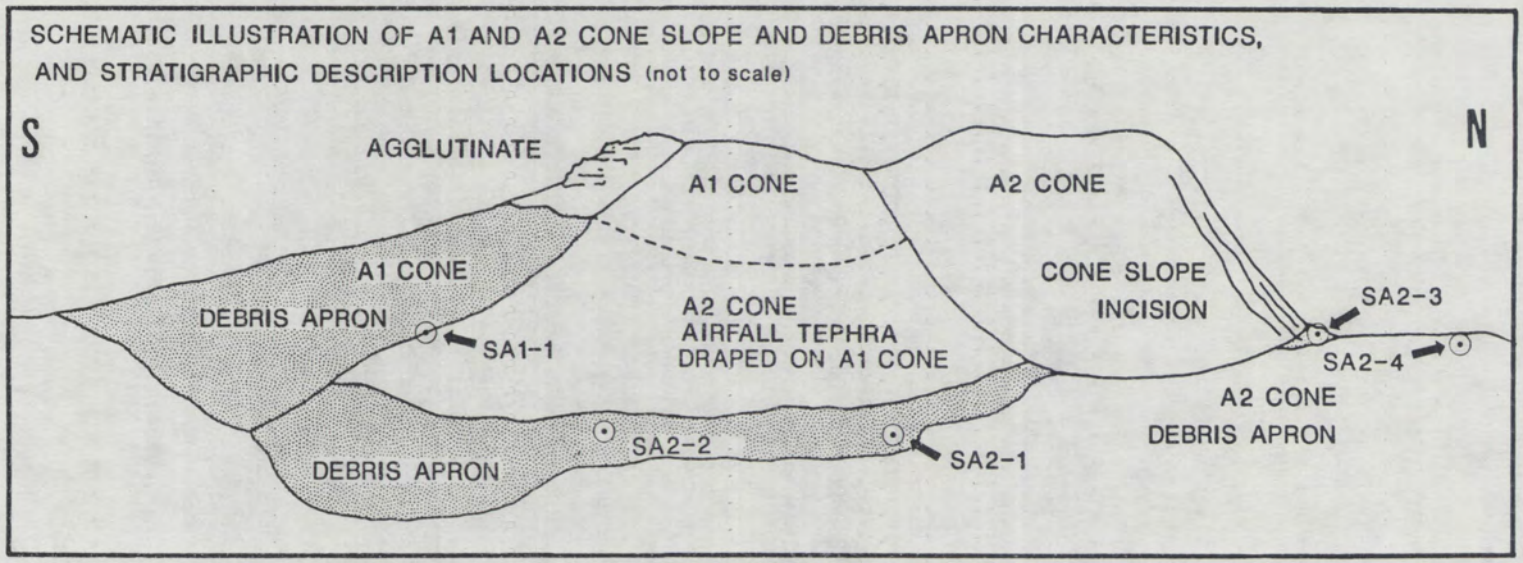

FIGURE 6. Illustration of draped tephra from A2 cone and the location of debris-apron soil and subsurface stratigraphic descriptions.

and fluvial channels (unit d) located topographically below proto-agglutinate (unit b) at the crater rim (Fig. 7). Debris-flow and fluvial channels also occur below proto-agglutinate on the A1 cone where tephra from the A2 cone eruption is draped over the slopes of the A1 cone.

The greatest depth of incision and drainage frequency on the A-cone complex occurs on A1 cone (measurements made on draped tephra) (Table 1). In contrast, a lower drainage frequency and a lower average depth of incision were found on A2 cone, with large areas that are unincised.

TABLE 1. PERCENTAGES OF INCISED CHANNEL PROPERTIES ALONG SELECTED TRANSECTS ON THE A-CONE COMPLEX

CONE TRANSECT	% df	% d	% dc	DRAINAGE FREQUENCY	AVE WIDTH	AVE DEPTH	AVE W/D
A1-1	50	50	0	36.1	1.63	0.32	6.20
A1-2	74	26	0	25.6	1.68	0.31	7.86
A2-3	50	50	0	18.3	1.64	0.19	8.98
A2-4	0	0	0	00.0	0.00	0.00	0.00

(Transect location map - Figure 8)

df = debris flow channel
d = fluvial channel
dc = channels with high frequency of coarse material filling up to three quarters of the channel
W/D = width-to-depth ratio

LOCATION AND CONE SLOPE CHARACTERISTICS:
A1-1 : east side A1 draped with tephra from A2; proto-agglutinate
A1-2 : east side of A1; proto-agglutinate
A2-3 : east side A2
A2-4 : east side A2 on garlands

af	airfall
ag	agglutinate
b	proto-agglutinate (concentration of bombs)
bs	base surge
d	incised fluvial channels
dc	channels infilled with lapilli + bombs
df	incised debris flow channels
g	garlands
ls	landslide
Qau	Quaternary debris apron undifferentiated
Qa1-Qa3	Quaternary debris-apron geomorphic surfaces
Qv	Quaternary vent undifferentiated
Qvf	Quaternary lava flow
Tg	Tertiary fanglomerates
====	Crater rim
~	Contact

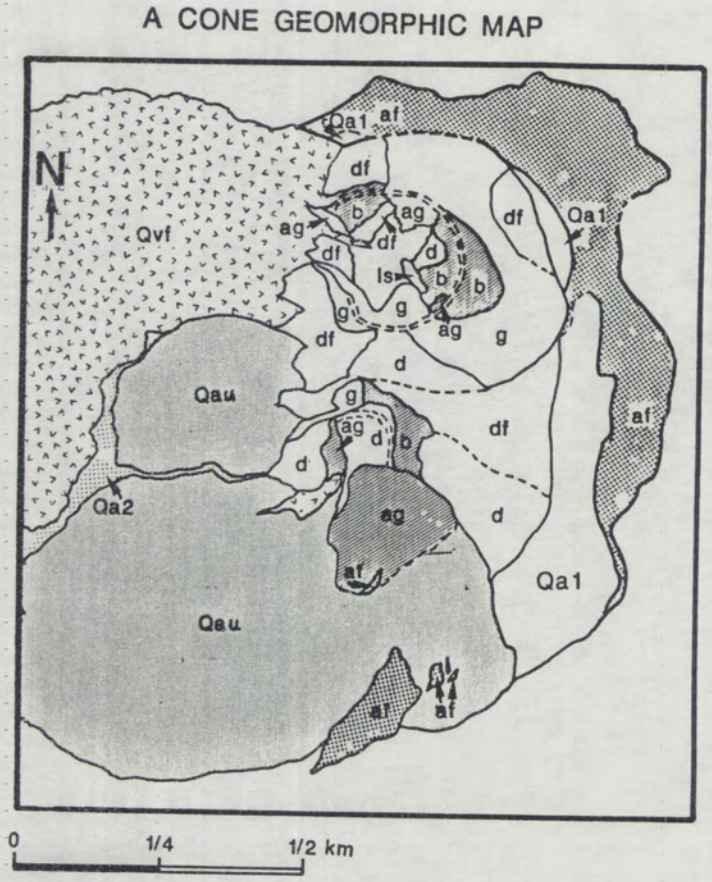

Figure 7. Geomorphic map of A-cone complex.

Geomorphic surface stratigraphic units associated with the debris-apron consist of units Qa1, Qa2 (modern channel deposits), and Qau (undifferentiated) with Qa1 being the oldest mapped unit adjacent to A2 cone. The A1 cone apron unit Qau was not mapped in detail; however, this debris-apron surface possesses the strongest soil development of all debris-apron units. Debris-apron deposits exist at the base of the A2 cone only below unincised slopes with garland features. No apron is found below unincised garland units (Fig. 8). In addition, the A1 cone apron is 48 times larger in areal extent than the A2 cone apron (0.48 versus 0.01 km^2, respectively) (Table 2).

TABLE 2 SUMMARY OF THE AREAL EXTENT OF GEOMORPHIC MAP UNITS AT SELECTED VOLCANIC CENTERS

CONE	TOTAL CONE AREA (KM^2)	APRON AREA (KM^2)	INCISED AREA (%)	GARLAND AREA (%)	AGGLUTINATE AREA (%)
A1 CONE	0.12	0.48	74	3	23
A2 CONE	0.12	0.01	40	59	1
U1 CONE	0.22	0.24	58	38	0.5
U2 CONE	0.16	0.08	16	80	0
G CONE	0.49	0.76	93	5	2

Morphometric measurements on A1 cone were made on tephra-draped and non-draped areas. The A1 cone has the lowest slope angle (21.0°) of the four cones measured (Table 3). The apron height-to-cone height ratio (Ha/Hc) and apron length-to-cone length ratio (La/Lc), which are measured on the tephra-draped portion of A1, are higher than all the other regions of the A-cone complex (Table 3).

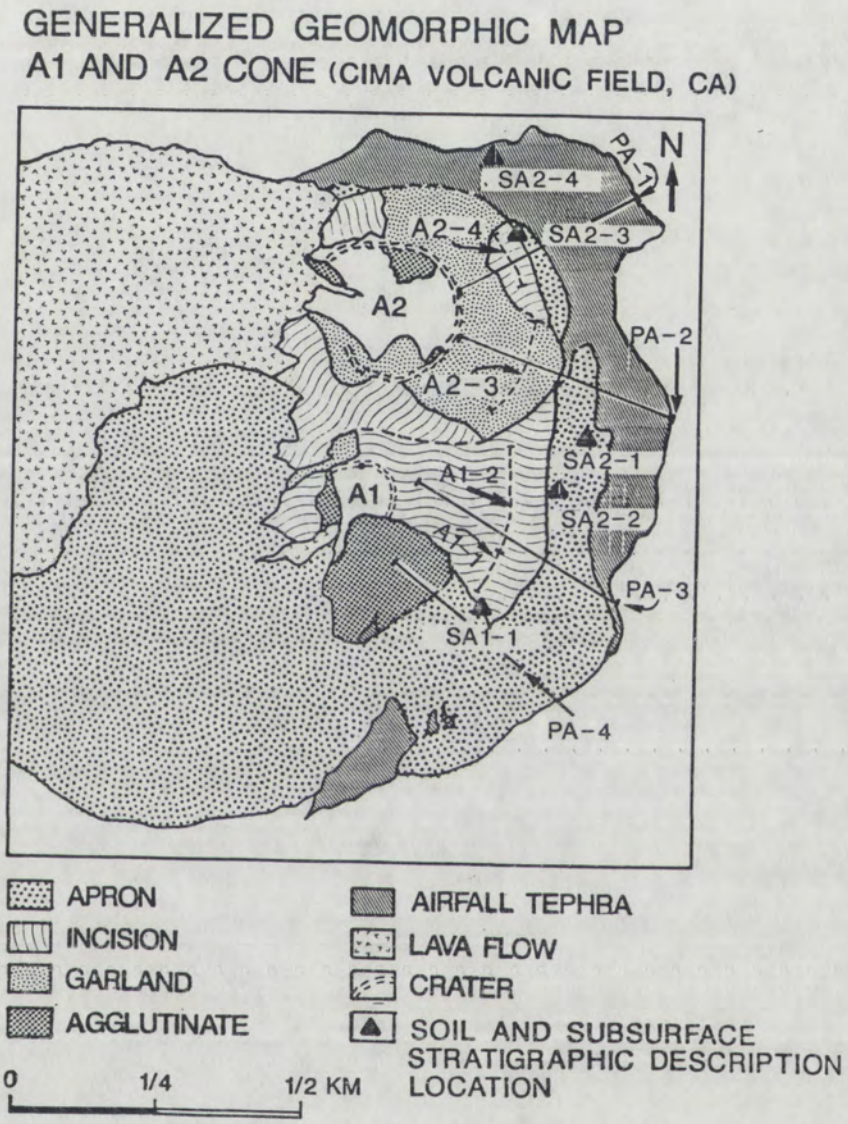

Figure 8. Generalized geomorphic map of the A-cone complex and location map of (1) stratigraphic and soil pit locations (SA1-1, SA2-1, SA2-2, SA2-3, SA2-4), (2) topographic profile measurements lines (PA-1, PA-2, PA-3, PA-4), and (3) incision measurement transects (A1-1, A1-2, A2-1, A2-2, A2-3).

TABLE 3 A CONE MORPHOMETRIC MEASUREMENTS

CONE C PROFILE	Sc (deg)	Sa (deg)	Hc (m)	Ha (m)	Lc (m)	La (m)	La/Lc	Ha/H
A1-1	23.6	4.6	78.7	11.1	386.8	125.6	0.32	0.14
A1-2	21.0	12.4	--	--	--	--	--	--
A2-3	28.2	--	91.1	--	184.7	--	--	--
A2-4	31.3	8.2	87.1	3.0	172.9	20.9	0.12	0.03

(Cone profile location map - Figure 8)

LOCATION:
A1-1 : east side A1 draped with tephra from A2
A1-2 : east side of A1
A2-3 : east side A2 on garland unit
A2-4 : east side A2 on garlands between interfluves

LEGEND:
Sc = cone slope angle
Sa = debris apron angle
Hc = Height of cone
Ha = Height of apron
Lc = Length of cone + apron
La = Length of apron
(symbols from Dohrenwend et al., 1986)

Geomorphology of U-Cone Complex

The U-cone complex consists of two adjacent eruptive vents (U1 and U2 cones) in the northern portion of the study area (Fig. 1). The U2 cone consists of a 0.16 + 0.07 Ma cinder cone (Turrin, 1985) erupted adjacent to the southern portion of U1 cone. The U2 cone is 240m high and 570m wide (mean) (Dohrenwend et al., 1986) with a maximum slope angle of 29.5°. The U1 cone has a mean height of 220 m, a mean width of 570 m, (Dohrenwend et al., 1986), and a maximum slope angle of 29.3°. Field observations indicate that the crater rim of U2 crosscuts the crater rim of U1 cone indicating U2 cone is younger than U1 cone.

The distribution of degradational units on the slope of U1 and U2 cones is such that garland features with no incised channels cover 38% of U1 cone and 80% of U2 cone (Figs. 9 and 10). The area of cone slope with incised channels with debris-flow levees cover 88% of the U1 cone slope.

On the U1 cone, incised channels with debris flow levees, the greatest drainage frequency, deepest rilling, and lowest width-to-depth ratio of channels are all found below exposures of agglutinate at the crater rim (Table 4). Debris-apron deposits are present below garland units on the eastern side of U2 cone.

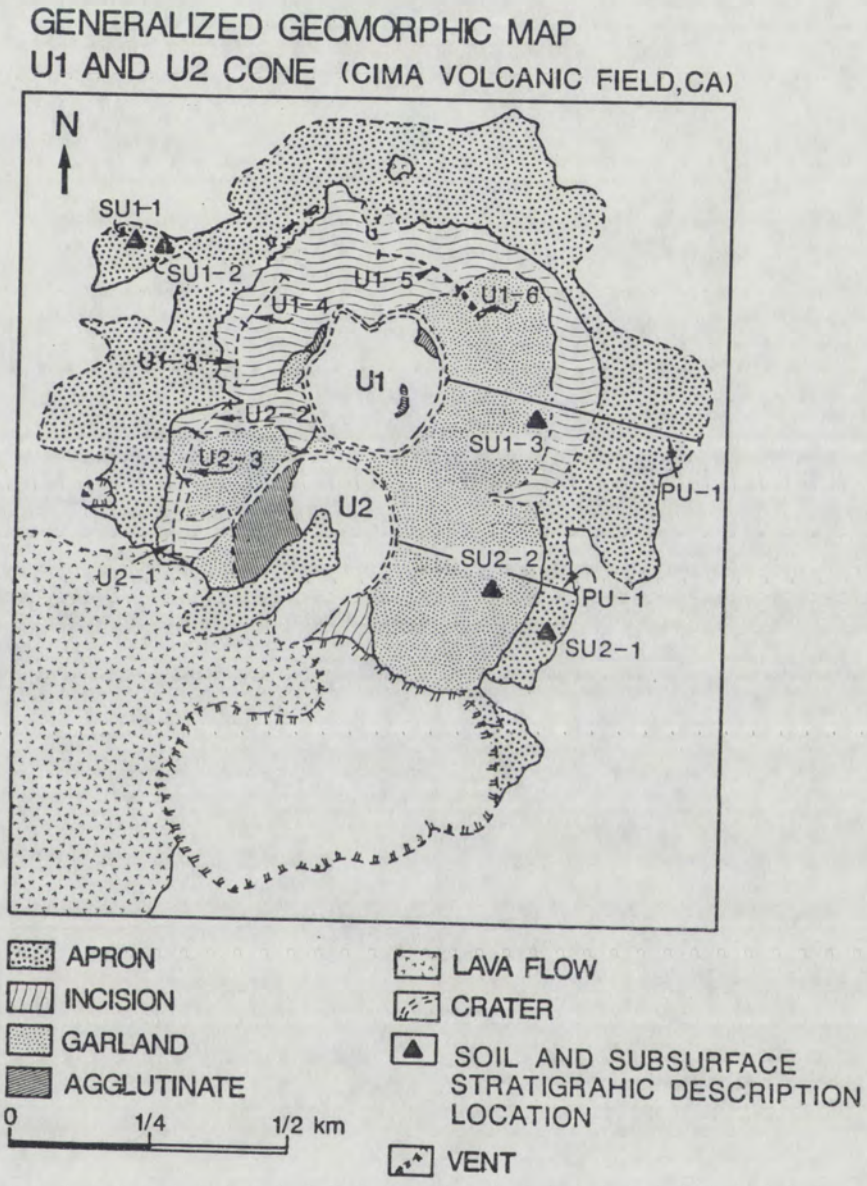

Figure 9. Generalized geomorphic map of U1 and U2 cone and location map of (1) stratigraphic and soil pit locations (SU1-1, SU1-2, SU1-3, SU2-1, SU2-2), (2) topographic profile measurements lines (PU-1, PU-2), and (3) incision measurement transects (U2-1, U2-2, U2-3, U1-3, U1-4, U1-5, U1-6).

af	airfall
ag	agglutinate
b	proto-agglutinate (concentration of bombs)
bs	base surge
d	incised fluvial channels
dc	channels infilled with lapilli + bombs
df	incised debris flow channels
g	garlands
ls	landslide
Qau	Quaternary debris apron undifferentiated
Qa1-Qa3	Quaternary debris-apron geomorphic surfaces
Qv	Quaternary vent undifferentiated
Qvf	Quaternary lava flow
Tg	Tertiary fanglomerates
====	Crater rim
~~	Contact

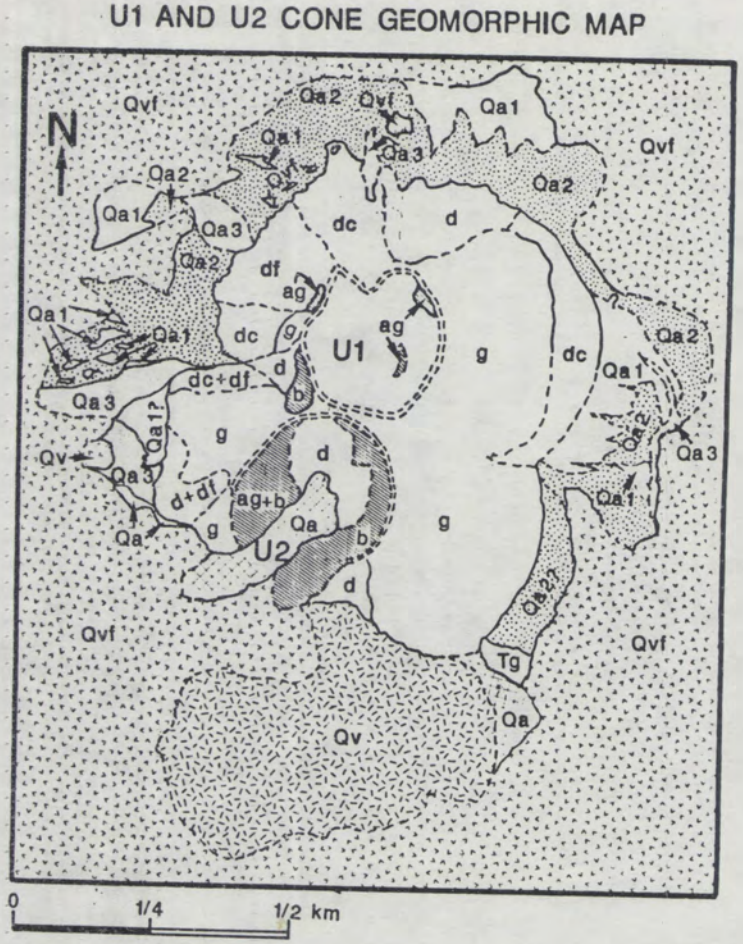

Figure 10. Geomorphic map of U1 and U2 cones.

Debris-apron units at U1 and U2 cones display interesting distribution patterns. At the base of U1 and U2 cones debris-apron unit Qa3 dominates topographically below areas of exposed agglutinate, proto-agglutinate, and debris-flow channels on the cone slope. Debris-apron unit Qa1 is preserved primarily at the distal portions of the debris apron, surrounded by debris-apron units Qa2 and Qa3 (Fig. 10). In addition, the area of U1 cone debris-apron area is three times greater (0.24 km^2) than that of the U2 cone (Table 2).

TABLE 4. PERCENTAGES OF INCISED CHANNEL PROPERTIES ALONG SELECTED TRANSECTS ON THE U1 AND U2 CONES

CONE TRANSECT	% DF	% D	% DC	DRAINAGE FREQUENCY	AVE WIDTH	AVE DEPTH	AVE W/D
U1-3	40	30	30	25.4	3.13	0.14	23.87
U1-4	88	6	12	52.6	3.06	0.21	16.03
U1-5	11	67	22	17.2	3.60	0.17	23.00
U1-6	0	0	0	00.00	0.00	0.00	00.00
U2-1	33	67	0	13.8	5.13	0.37	14.86
U2-2	17	17	66	13.0	1.79	0.11	15.59
U2-3	0	0	0	00.00	0.00	0.00	00.00

(Transect location map - Figure 9)

LOCATION, AND CONE SLOPE AND APRON CHARACTERISTICS:
U1-3 : west side, Qa1 and Qa2 on apron
U1-4 : west side, agglutinate (cone) and Qa3 (apron)
U1-5 : north side, no agglutinate
U1-6 : north side, garlands on cone slope
U2-1 : west side, proto-agglutinate and agglutinate
U2-2 : west side, proto-agglutinate
U2-3 : east side, garland

Morphometric parameters measured at the U-cone complex reveal that slope angles of cones and debris aprons are higher on the eastern flank of the U2 than on the U1 cone (Table 5) and La/Lc and Ha/Hc ratios are two times higher on the older U1 cone.

TABLE 5 U1 AND U2 CONE MORPHOMETRIC MEASUREMENTS

CONE PROFILE	Sc (deg)	Sa (deg)	Hc (m)	Ha (m)	Lc (m)	La (m)	La/Lc	Ha/Hc
U1 cone	29.3	13.7	124.4	31.9	358.5	168.2	0.47	0.26
U2 cone	29.5	14.8	121.5	15.3	272.5	63.3	0.23	0.13

(Profile location map - Figure 9)

LOCATION:
U1 cone: east side on garland unit
U2 cone: east side on garland unit

Geomorphology of G cone

The G cone consists of a single vent, 0.22 + 0.03 Ma cinder cone (Turrin et al., 1985) primarily erupted as loose tephra and agglutinate with minor episodes of hydrovolcanic base surge activity. The G cone has a mean height of 180 m, a mean width of 915 m (Dohrenwend et al., 1986), and a maximum slope angle of 29.6°. The northeastern portion of the cinder cone was not mapped in detail due to the complexity volcanic units exposed in this region.

Debris-flow channels represent 54% of all incised channels measured on the eastern side of G cone directly below exposed agglutinate and indurated base-surge deposits (Fig. 11). Unincised garland areas with no incised channels on the south side of G cone cover 5% of the total cone slope and are stratigraphically above areas of deeply incised cone slope (Fig. 12 and Table 2).

Statistical analysis of the areal extent of incised channels indicates that the greatest drainage density and width-to-depth ratios occur topographically below proto-agglutinate exposed at the crater rim. Topographically below areas of exposed agglutinate on the northwestern cone slopes debris-flow activity dominates by 69% (Table 6).

A 0.76 km^2 area of debris apron surrounds the G cone and consists of debris-apron surface units Qa1, Qa2, and Qa3 (Fig. 11). Debris-apron unit Qa3 predominantly occurs topographically below cone slope debris-flow units on the northwestern flank of G cone. In addition, unit Qa3 emerges from volcanically and erosionally breached areas of the G cone. Unit Qa1 primarily occurs adjacent to the cone slope below unit g and unit dc. Debris apron surface unit Qa2 shows no consistent spatial pattern.

af	airfall
ag	agglutinate
b	proto-agglutinate (concentration of bombs)
bs	base surge
d	incised fluvial channels
dc	channels infilled with lapilli + bombs
df	incised debris flow channels
g	garlands
ls	landslide
Qau	Quaternary debris apron undifferentiated
Qa1-Qa3	Quaternary debris-apron geomorphic surfaces
Qv	Quaternary vent undifferentiated
Qvf	Quaternary lava flow
Tg	Tertiary fanglomerates
====	Crater rim
~	Contact

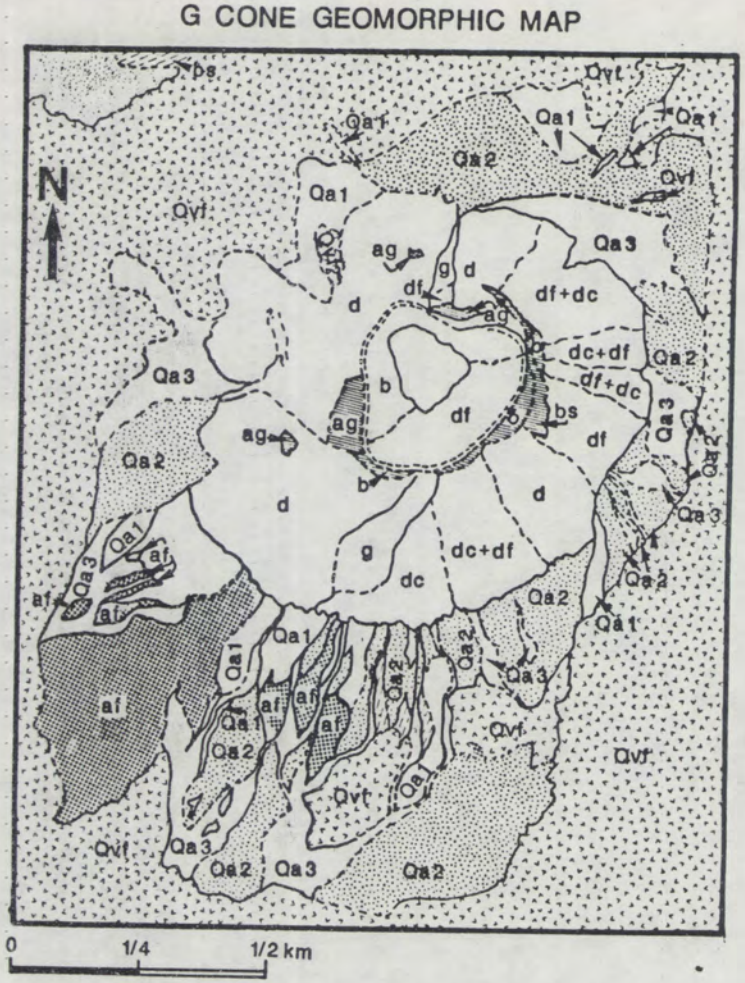

Figure 11. Geomorphic map of G cone.

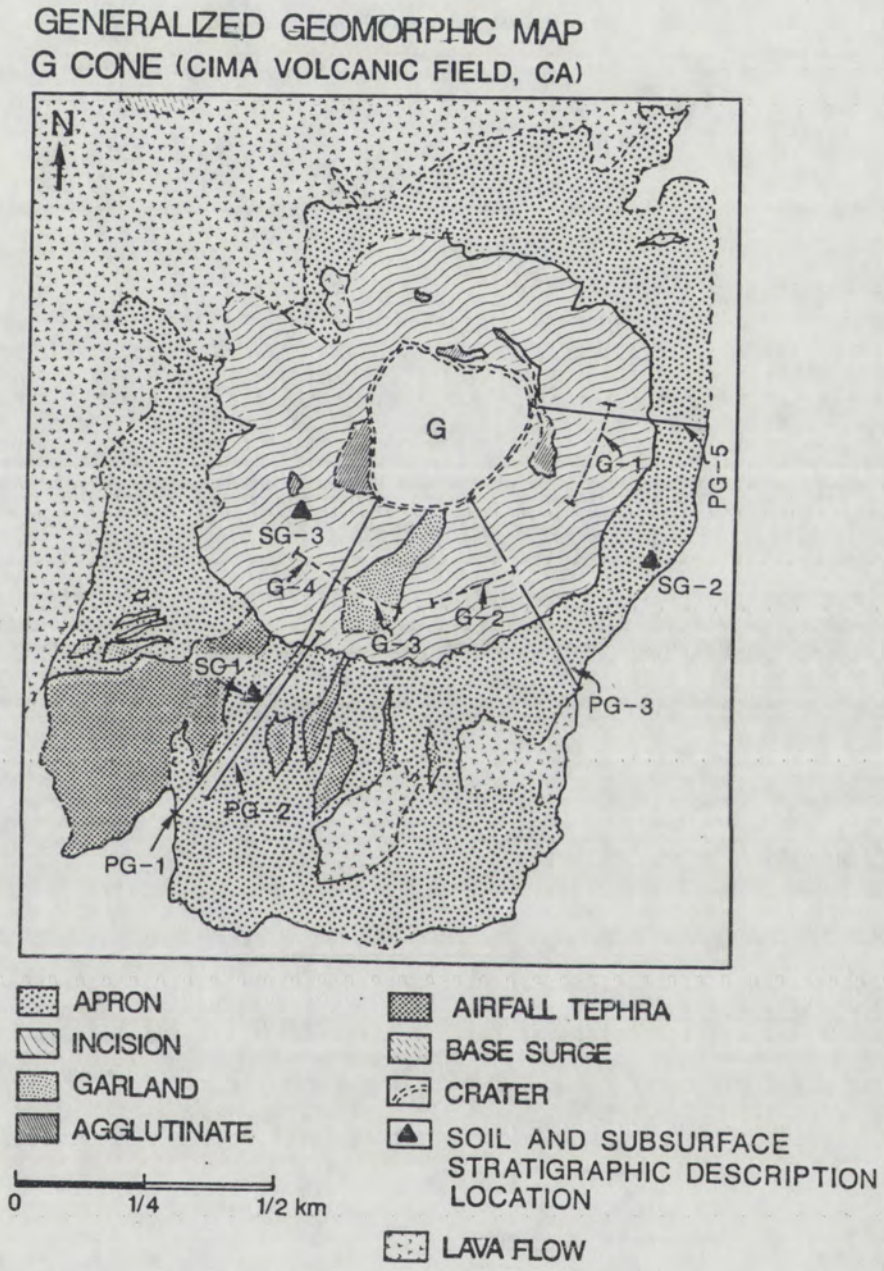

Figure 12. Generalized geomorphic map of G cone and location map of (1) stratigraphic and soil pit locations (SG-1, SG-2, SG-3), (2) topographic profile measurements lines (PG-1, PG-2, PG-3, PG-4, PG-5), and (3) incision measurement transects (G-1, G-2, G-3, G-4).

TABLE 6. PERCENTAGES OF INCISED CHANNEL PROPERTIES ALONG SELECTED TRANSECTS ON THE G CONE

CONE TRANSECT	% DF	% D	% DC	DRAINAGE FREQUENCY	AVE WIDTH	AVE DEPTH	AVE W/D
G-1	69	28	3	71.4	3.20	0.30	12.52
G-2	54	47	0	48.4	2.89	0.34	9.37
G-3	0	0	0	00.00	0.00	0.00	0.00
G-4	0	0	100	93.2	1.92	0.10	21.15

(Transect location map - Figure 12)

LOCATION, AND CONE SLOPE AND APRON CHARACTERISTICS:
G-1 : east side, agglutinate (cone) and Qa3 (apron)
G-2 : southeast side, proto-agglutinate (cone) and Qa2
G-3 : south side, garlands
G-4 : south side, proto-agglutinate

Morphometric measurements for G cone are summarized in Table 7. Cone slope angles vary from 28.2° to 29.6° around the cone. Large variations exist in apron length-to-cone length ratios (La/Lc) (0.33 to 0.58) and apron height-to-cone height ratios (Ha/Hc) (0.17 to 0.29) around the G cone.

TABLE 7 G CONE MORPHOMETRIC MEASUREMENTS

CONE PROFILE	Sc (deg)	Sa (deg)	Hc (m)	Ha (m)	Lc (m)	La (m)	La/Lc	Ha/Hc
G-1	--	14.7	--	64.8	--	587.0	--	--
G-2	28.2	15.6	210.2	59.9	754.2	434.1	0.58	0.29
G-3	29.6	17.0	151.8	26.3	376.6	124.1	0.33	0.17
G-4	29.3	19.8	177.5	42.5	454.4	170.1	0.37	0.24

(Profile location map - Figure 12)

LOCATION:
G-1 : south side, profile of modern channel on apron
G-2 : south side, profile up Qa1 and cone slope
G-3 : east side, adj. to exposed base surge dep on cone
G-4 : southeast side, profile up Qa2 and and cone slope

Geomorphology of E cone

The E cone has a mean height of 160 m and a mean width 690 m (Dohrenwend et al., 1986) 0.35 + 0.04 Ma cinder cone (Turrin et al., 1985) which erupted through an older degraded cinder cone to the north (Fig. 13). The relative age of a smaller cone located to the south of E cone is difficult to assess due to unclear stratigraphic relationships with the dated portion of the E cone. Therefore, the older center and southern center were not examined in this study.

Geomorphic mapping and analysis of incision data indicate that the highest percentage of debris-flow channels per transect (62% and 79%) occur topographically below agglutinate and proto-agglutinate exposed at the crater rim (Table 8). The greatest depth of incision (0.28 m) and lowest width-to-depth ratios per transect (9.74 m) are located topographically below proto-agglutinate and agglutinate on the east side of E cone. Garlands are dissected and poorly preserved on the northeastern flanks of the E cone where fluvial channels and debris-flow channels occur in equal proportions.

af	airfall
ag	agglutinate
b	proto-agglutinate (concentration of bombs)
bs	base surge
d	incised fluvial channels
dc	channels infilled with lapilli + bombs
df	incised debris flow channels
g	garlands
ls	landslide
Qau	Quaternary debris apron undifferentiated
Qal-Qa3	Quaternary debris-apron geomorphic surfaces
Qv	Quaternary vent undifferentiated
Qvf	Quaternary lava flow
Tg	Tertiary fanglomerates
====	Crater rim
~	Contact

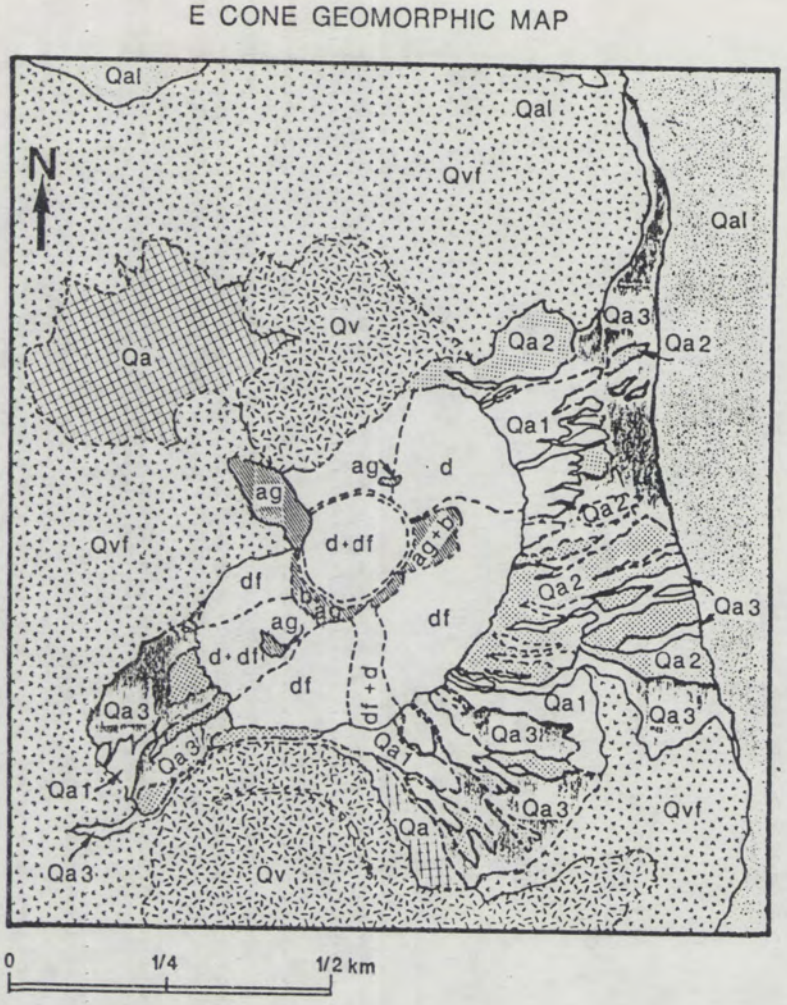

Figure 13. Geomorphic map of E cone.

TABLE 8. PERCENTAGES OF INCISED CHANNEL PROPERTIES ALONG SELECTED TRANSECTS ON THE E CONEE CONE

CONE TRANSECT	% DF	% D	% DC	# CHANNEL PER RADIAN	AVE WIDTH	AVE DEPTH	AVE W/D
E-1	79	21	0	32.7	2.21	0.28	9.74
E-2	62	31	7	93.8	1.80	0.14	13.77
E-3	52	48	0	60.4	1.74	0.16	13.24

(Transect location map - Figure 13)

CONE SLOPE AND APRON CHARACTERISTICS:
E-1 : east side, proto-agglutinate (cone) and Qa3 (apron)
E-2 : east side, proto-agglutinate and agglutinate (cone)
E-3 : northeast side, degraded garlands

An extensive debris-apron surrounds the E cone except where lava flows cover a portion of the southwestern cone slope (Fig. 14). Debris-apron geomorphic surface units include units Qa1, Qa2, and Qa3 (Fig. 13). Deeply incised areas of unit Qa1 are typically located adjacent to the cone slope; however, where proto-agglutinate and agglutinate dominate the cone slope, units Qa2 and Qa3 lie adjacent to the cone slope (Fig. 13).

Values for debris-apron length-to-cone length ratios (0.53-0.67) and debris-apron height-to-cone height ratios (0.20-0.30) are more consistent and high compared to all other cones measured in this study (Table 9). Cone slope angles vary from 27.9 to 28.4°.

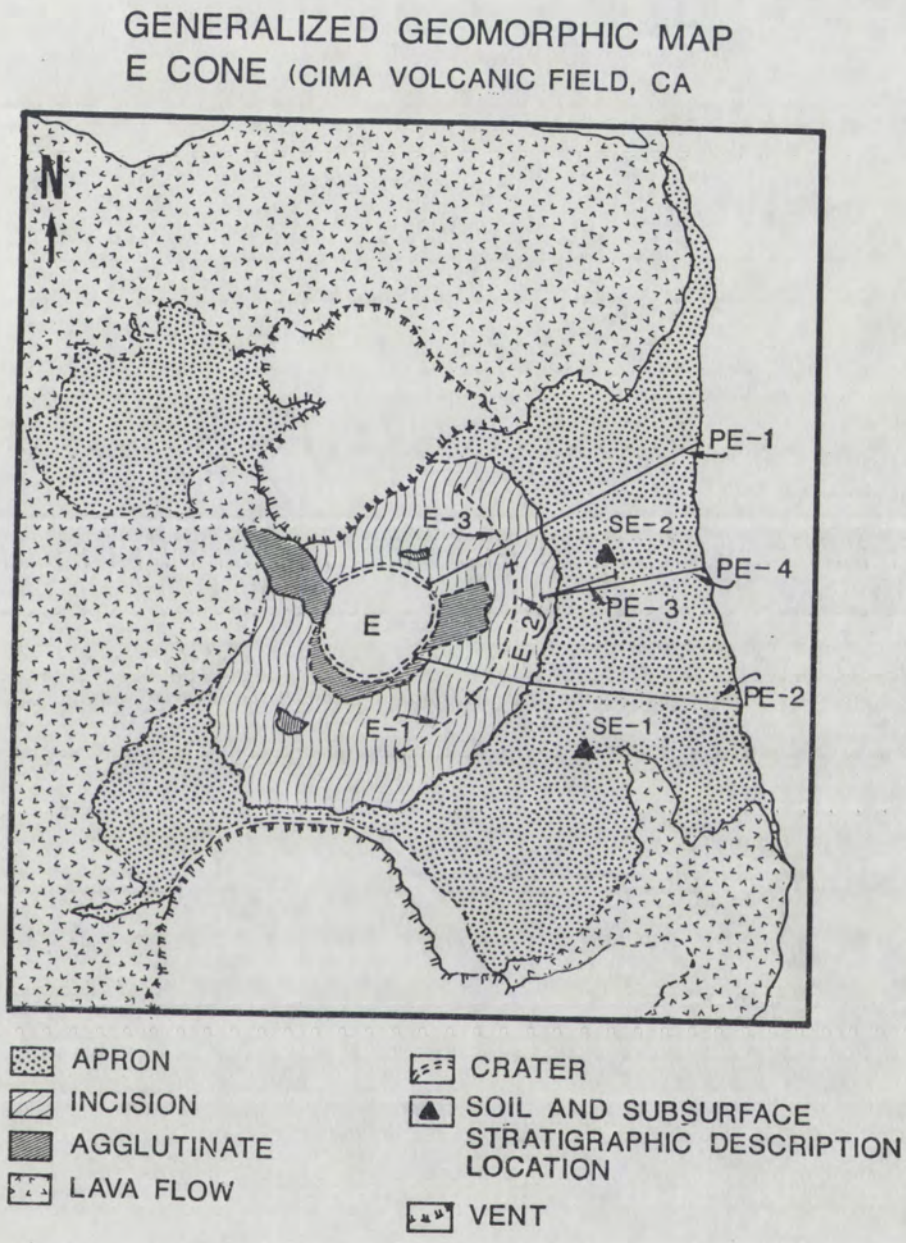

Figure 14. Generalized geomorphic map of E cone and location map of (1) stratigraphic and soil pit locations (SE-1, SE-2), (2) topographic profile measurements lines (PE-1, PE-2, PE-3, PE-4), and (3) incision measurement transects (E-1, E-2, E-3).

TABLE 9 E CONE MORPHOMETRIC MEASUREMENTS

CONE C PROFILE	Sc (deg)	Sa (deg)	Hc (m)	Ha (m)	Lc (m)	La (m)	La/Lc	Ha/H
E-1	28.4	14.-	163.7	31.0	586.3	308.2	0.53	0.20
E-2	27.9	14.2	156.4	47.1	727.5	488.0	0.67	0.30
E-3	--	17.8	--	--	--	--	--	--
E-4	--	11.8	--	26.3	--	322.8	--	--

(Profile location map - Figure 13)

LOCATION:
E-1 : east side, Qa3 and proto-agglutinate on cone slope
E-2 : east side, Qa1 and cone slope
E-3 : east side, up Qa1 apron only
E-4 : east side, up Qa3 apron only

STATISTICAL ANALYSIS

A Wilcoxon-T statistical test (Tate and Clelland, 1959) was performed for each cinder cone in order to establish the similarity or difference between the proportion of debris-flow channels to fluvial channels located topographically below the different cone lithologies studied. The null hypothesis that the percentage areal extent of debris-flow channels is the same when topographically below resistant cone slope lithologies (agglutinate and proto-agglutinate) or non-resistant lithologies is rejected at alpha = 0.05 (calculated T value = 43.5; table T value = 53) (see Appendix C). This test supports field observations that the percentage of debris-

flow activity is higher below agglutinate and proto-agglutinate than elsewhere on the cinder cone.

A second Wilcoxon-T statistical test was performed for each cinder cone in order to establish the similarity or difference in the depths of incised channels located topographically below different cone lithologies studied (Tate and Clelland, 1959). The null hypothesis that the areal extent of deeply incised channels are the same when topographically below resistant cone slope lithologies (agglutinate and proto-agglutinate) versus non-resistant lithologies is rejected at alpha = 0.05 (calculated T value = 17.5; table T value = 22) (see Appendix C). This test indicates that the depth of incision is greater below agglutinate and proto-agglutinate than elsewhere on the cinder cone.

SOIL AND STRATIGRAPHY OF VOLCANIC, COLLUVIAL, ALLUVIAL DEPOSITS

Quaternary Geology of the A-cone complex

Two detailed soil profiles and five subsurface stratigraphic sections are described in the A1 and A2 cone debris-apron deposits (Fig. 8). The soil and subsurface stratigraphic type-sections (SA2-1) of the A2 cone debris apron are described in the surface debris-apron unit Qa1 (Fig. 15). From the oldest to the youngest, the subsurface debris-apron stratigraphy at SA2-1 consists of two airfall-tephra deposits (units 1 and 2) separated by a buried soil with Bk soil characteristics and Stage I secondary carbonate morphology (see Appendix B). A thinly bedded subsurface debris-apron deposit (unit 3) buries unit 2. The unit 2 exhibits soils with Bt horizon development and Stage I secondary carbonate morphology. Detailed soil and subsurface stratigraphic descriptions of the other four A cone sections can be found in Appendix A and Appendix B. A fence diagram showing all five described sections at the A-cone complex illustrates the stratigraphic correlation between surface and subsurface debris-apron units and volcanic units (Fig. 16).

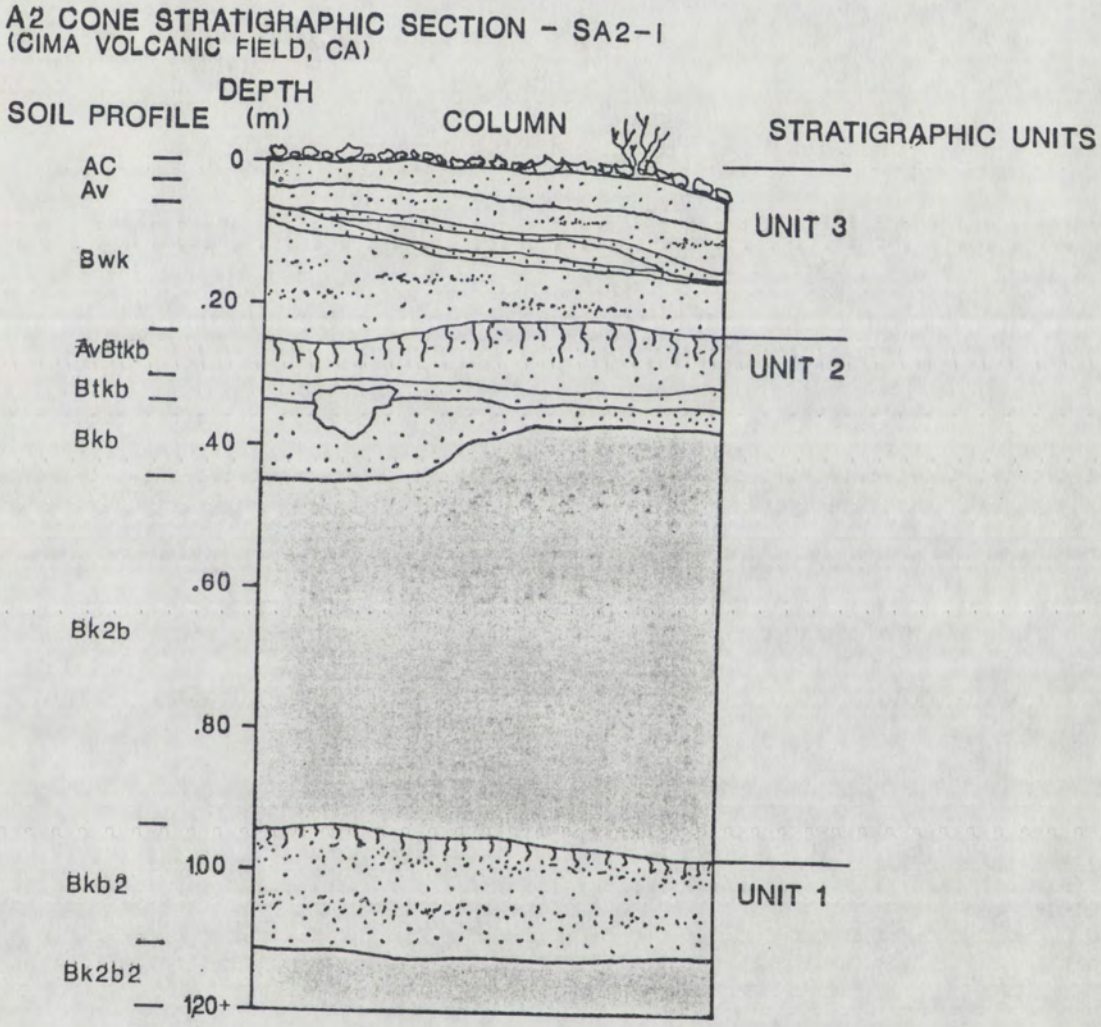

Figure 15. SA2-1 debris-apron stratigraphy and soil profile horizons described in the field.

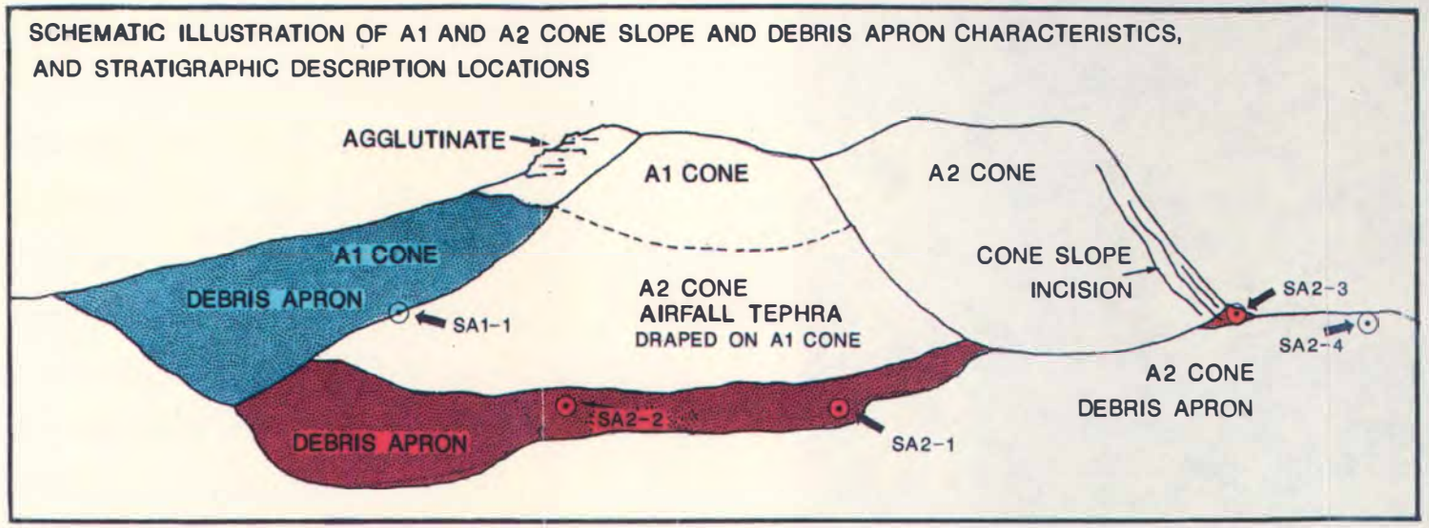

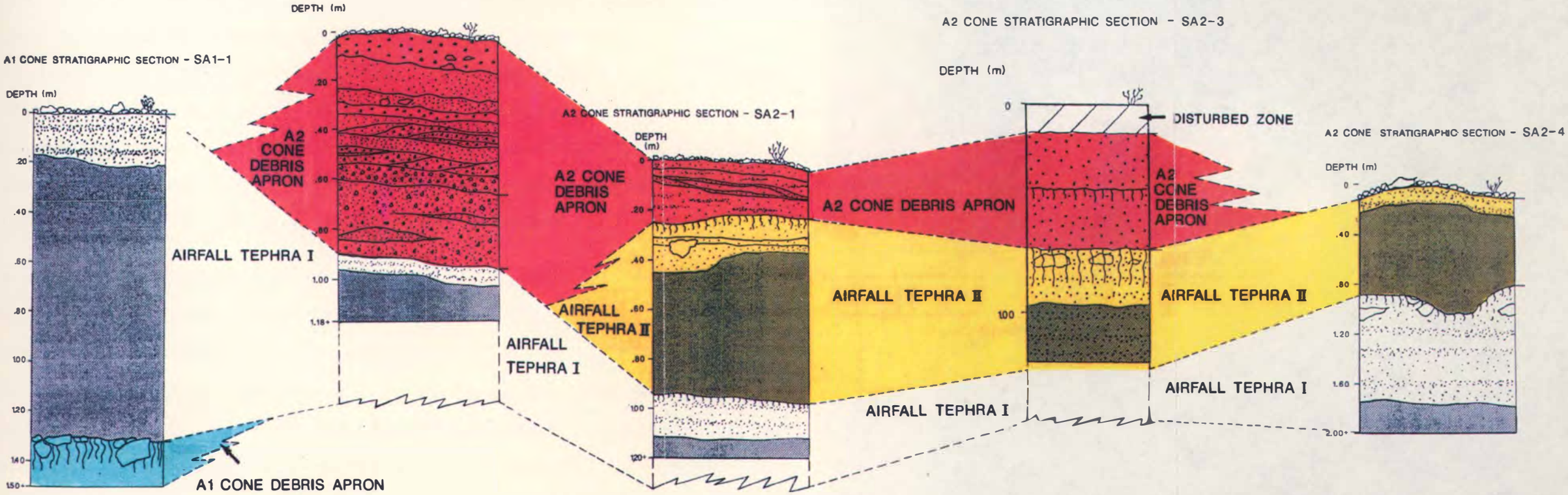

Figure 16. Fence diagram of debris-apron stratigraphy along the base of A1 and A2 cones.

Quaternary Geology of U1 Cone

Two detailed soil profiles and subsurface stratigraphic sections are described in U1 cone debris-apron deposits (Fig. 9). The soil and subsurface stratigraphic type-sections (SU1-1) of the U1 cone debris-apron are described within the surface debris-apron stratigraphic unit Qa1. From the oldest to the youngest, the debris-apron subsurface stratigraphy at SU1-1 consists of four stratigraphic units (Fig. 17). Subsurface debris-apron unit 1 exhibits soils with Bt soil horizon development and Stage III-IV secondary carbonate morphology and is truncated by the airfall-tephra deposit of unit 2 (see Appendix B). Units 3 and 4 bury unit 2 and are separated by a truncated buried soil with Btky soil characteristics and local Stage II secondary carbonate morphology. Detailed soil and subsurface stratigraphic debris-apron descriptions of the other U1 cone section (SU1-2) can be found in Appendix A and Appendix B .

A single stratigraphic section, SU1-3, is described on the U1 cone slope (Fig. 18). From the oldest to the youngest, the cone slope subsurface stratigraphy at SU1-3 consists of three units. Unit 1 consists of airfall-tephra with Btky soil characteristics and Stage II-III secondary carbonate morphology. This airfall-tephra and soil is buried by Unit 2 which displays Bwk soil characteristics and Stage I-II secondary carbonate morphology. Subsurface debris-apron stratigraphic unit 3 overlies unit 2 and consists of seven

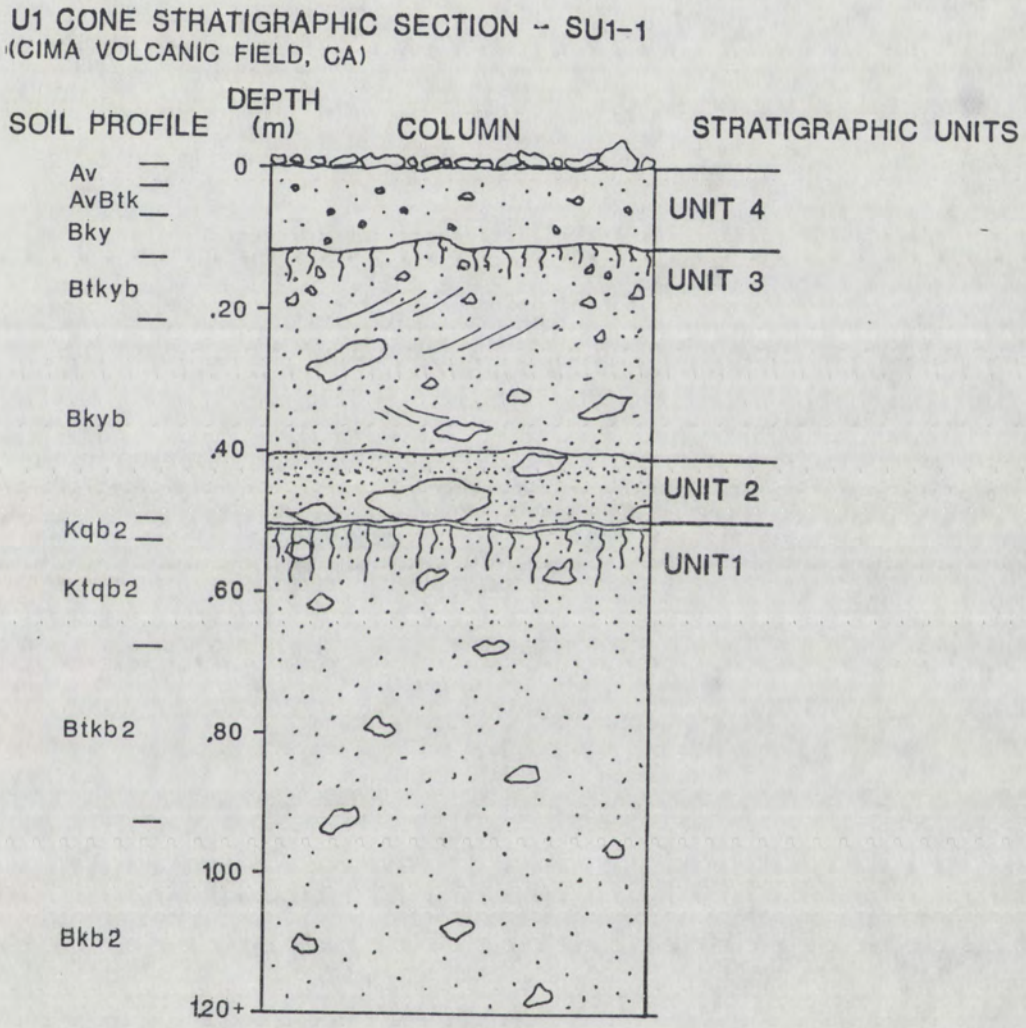

Figure 17. SU1-1 debris-apron stratigraphy and soil profile horizons described in the field.

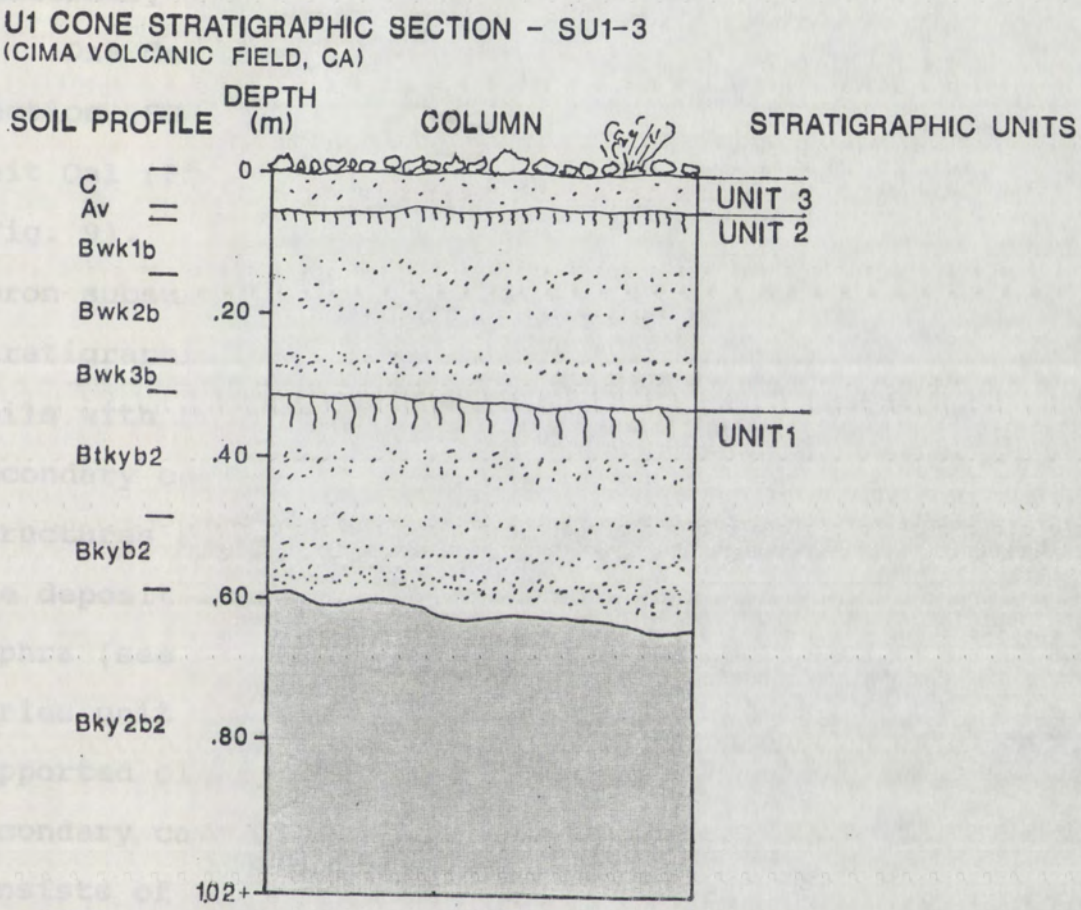

Figure 18. SU1-3 cone-slope stratigraphy described in the field.

centimeters of loose unstratified reworked tephra and weak Stage I secondary carbonate morphology.

Quaternary Geology of U2 Cone

One detailed soil profile and subsurface stratigraphic section, SU2-1, is described in the surface debris-apron unit Qa1 (Fig. 19) of the U2 cone debris-apron deposits (Fig. 9). From the oldest to the youngest, the debris-apron subsurface stratigraphy at SU2-1 consists of three stratigraphic units. In unit 1 pedogenesis consisting of soils with Btk soil horizon development and Stage III+ secondary carbonate morphology obscures sedimentary structures such that it is difficult to determine whether the deposit consists of primary airfall tephra or reworked tephra (see Appendix B). Subsurface debris-apron unit 2 buries unit 1 and consists of grain and eolian matrix supported clasts with Bwk soil characteristics and Stage I+ secondary carbonate morphology. The overlying unit 3 consists of very thinly-bedded tephra with Bwk soil characteristics and weak Stage I secondary carbonate morphology.

A single stratigraphic section, SU2-2, is described on the U2 cone slope (Fig. 9). In contrast to SU1-3 of the U1 cone slope, SU2-2 includes only two stratigraphic units. From the oldest to the youngest, the cone slope subsurface stratigraphy at SU2-2 is very simple (Fig. 20): unit 1 consists of airfall tephra with Bkq and Bwk soil horizon

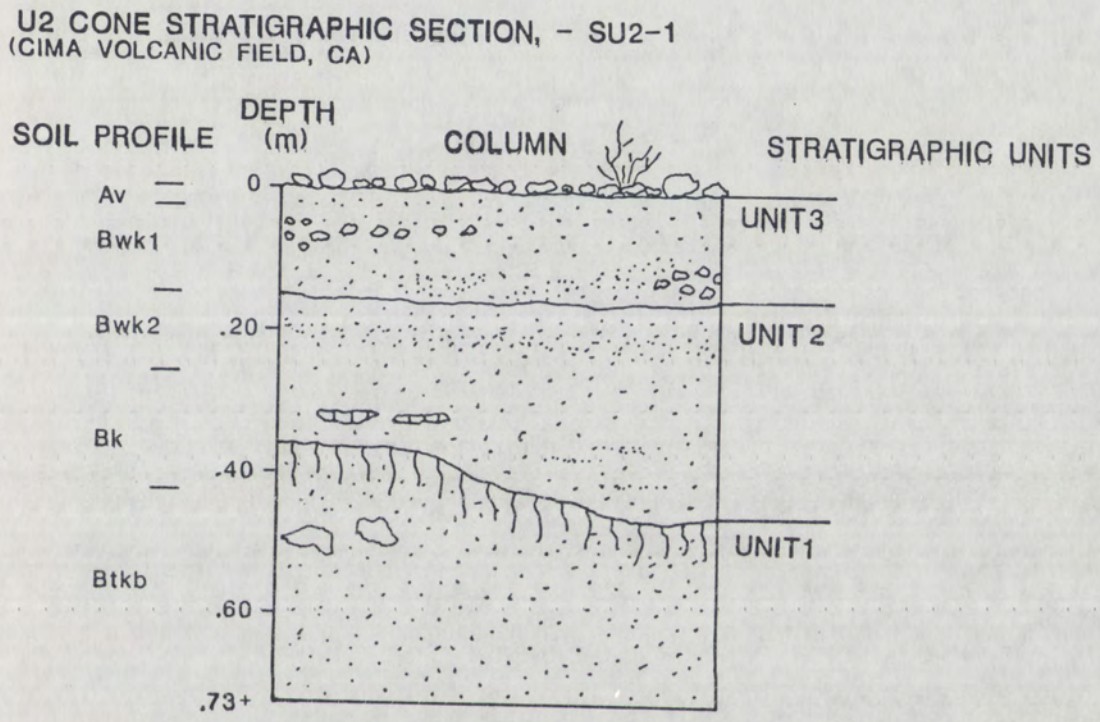

Figure 19. SU2-1 debris-apron stratigraphy and soil profile horizons described in the field.

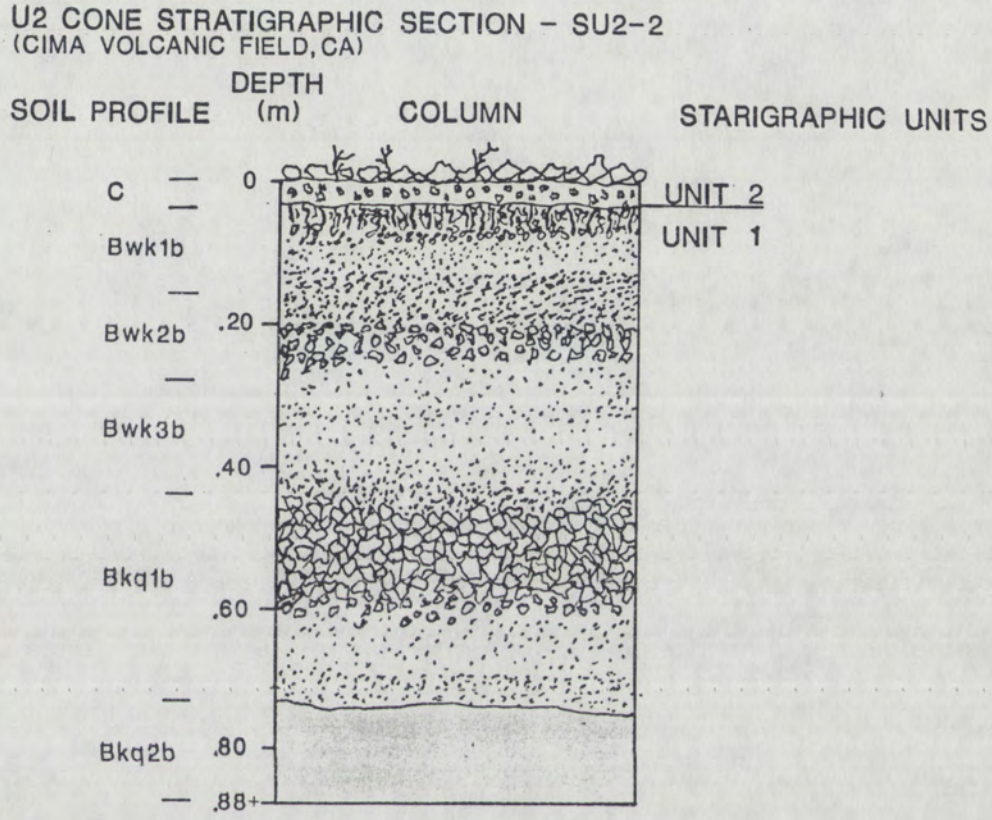

Figure 20. SU2-2 cone-slope stratigraphy described in the field.

development and Stage I-II secondary carbonate morphology overlain by four centimeters of loose unstratified reworked tephra (unit 2) with weak Stage I secondary carbonate morphology.

Quaternary Geology of the G Cone

Two detailed soil profile and subsurface stratigraphic sections are described in the G cone debris-apron deposits (SG-1 and SG-2) (Fig. 12). No type-section was extracted from the stratigraphic and soil data due to the complexity and variability observed in the subsurface debris-apron stratigraphy at SG-1 and SG-2; therefore, both SG-1 and SG-2 will be described in detail.

From the oldest to the youngest, the subsurface debris-apron stratigraphy at SG-1 consists of four stratigraphic units described in the surface debris-apron unit Qa1 (Fig. 21). Subsurface debris-apron stratigraphic unit 1 consists of primary airfall tephra with Bky and Kyb soil horizon development and Stage III - IV secondary carbonate morphology (see Appendix B). The overlying unit 2 consists of very thinly bedded and massive sediments with Bky soil characteristics and Stage II+ to local Stage IV secondary carbonate morphology. A buried soil with preserved Av horizon characteristics separates Unit 2 from Unit 3, which consists of clast-supported tephra with AvBtk soil horizon development and Stage II secondary carbonate morphology.

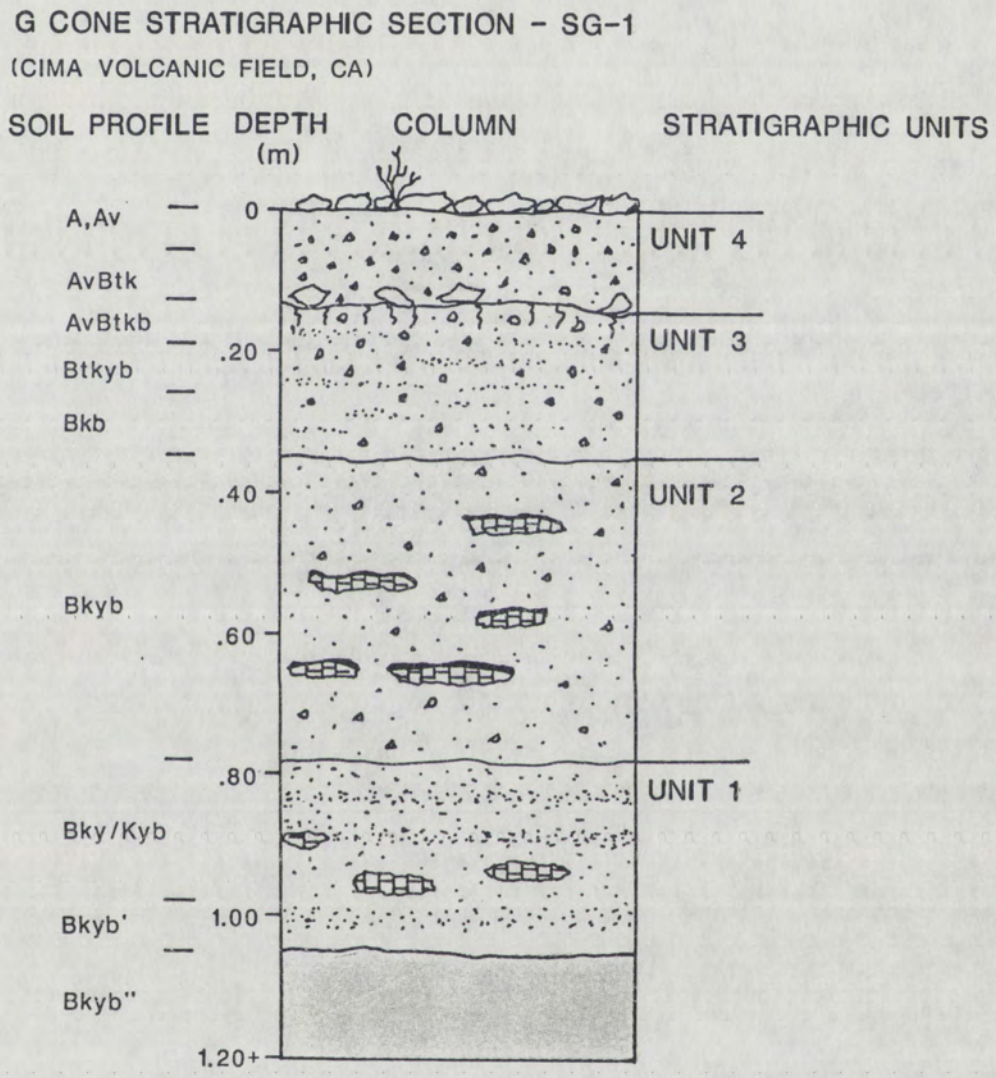

Figure 21. SG-1 debris-apron stratigraphy and soil profile horizons described in the field.

Subsurface debris-apron unit 4 overlies units 3 and consists of grain and eolian matrix-supported tephra with Avbtk soil horizon development and Stage I secondary carbonate morphology.

From the oldest to the youngest, the subsurface debris-apron stratigraphy at SG-2 consists of four stratigraphic units described in the surface debris-apron unit Qa2 (Fig. 22). Subsurface debris-apron stratigraphic unit 1 consists of primary airfall tephra with Bky soil characteristics and Stage II secondary carbonate morphology (see Appendix B). Unit 2 and Unit 3 consist of very thinly bedded and crossbedded tephra separated by a buried soil with AvBtky soil horizon development and Stage I to Stage II secondary carbonate morphology. The overlying subsurface debris-apron unit 4 consists of thinly bedded tephra with Bky soil horizon development and Stage I secondary carbonate morphology.

A single stratigraphic section, SG-3, is described on the G cone slope (Fig. 12). From the oldest to the youngest, the cone slope subsurface stratigraphy of SG-3 consists of three stratigraphic units (Fig. 23). Unit 1 consists of airfall tephra with Stage I-II secondary carbonate morphology. The overlying unit 2 buries unit 1 and consists of primary airfall tephra with Stage I secondary carbonate morphology. Unit 3 overlies and buries Unit 2 and consists of four centimeters of loose,

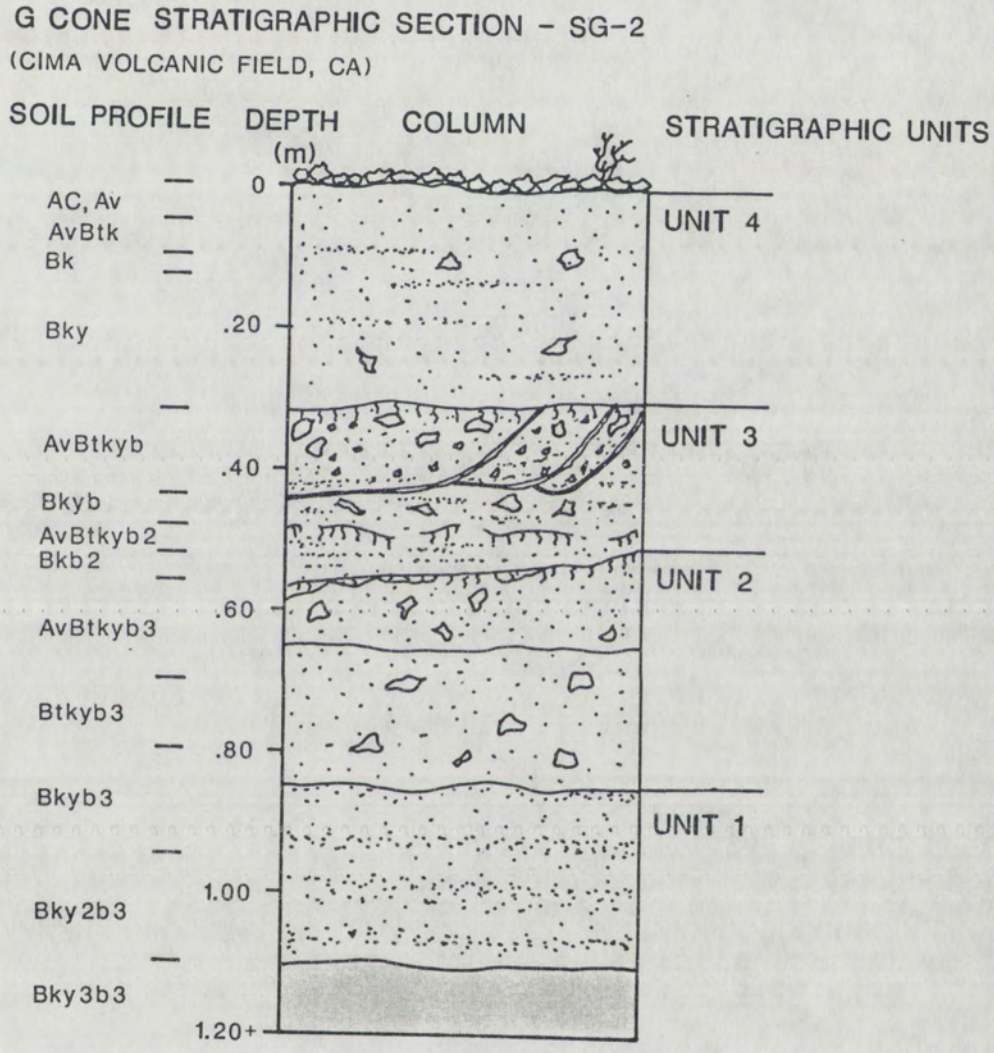

Figure 22. SG-2 debris-apron stratigraphy and soil profile horizons described in the field.

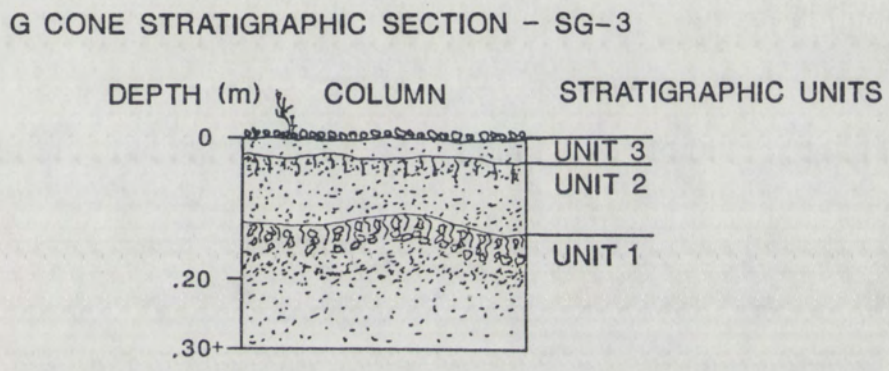

Figure 23. SG-3 cone-slope stratigraphy described in the field.

unstratified, reworked tephra with weak Stage I secondary carbonate morphology.

Quaternary Geology of the E cone

Two detailed soil profile and subsurface stratigraphic sections are described in the E cone debris-apron deposits (SE-1 and SE-2) (Fig. 13). No type-section was extracted from the stratigraphic and soil data due to the complexity and variability observed in the subsurface debris-apron stratigraphy at SE-1 and SE-2; therefore, both SE-1 and SE-2 are described in detail.

From the oldest to the youngest, the subsurface debris-apron stratigraphy at SE-1 consists of three stratigraphic units described in the surface debris-apron unit Qa1 (Fig. 24). Subsurface debris-apron stratigraphic unit 1 consists of primary-airfall tephra with Bky soil characteristics and Stage III- IV secondary carbonate morphology (see Appendix B). The overlying unit 2 consists of very thinly bedded tephra with Bky soil characteristics and Stage II+ secondary carbonate morphology. Subsurface debris-apron unit 3 overlies unit 2 and consists of matrix-supported tephra with Bky and Btky soil horizon development and Stage 1 secondary carbonate morphology.

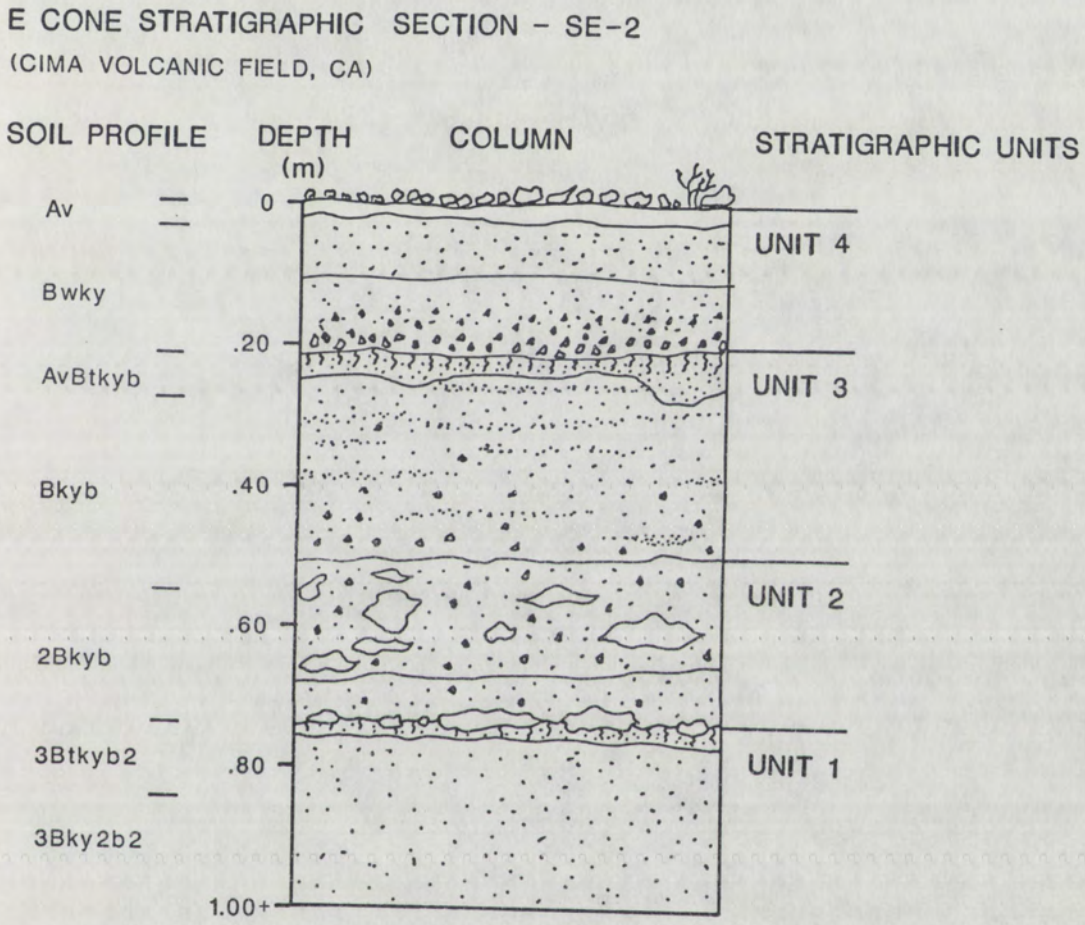

Figure 24. SE-2 debris-apron stratigraphy and soil profile horizons described in the field.

From the oldest to the youngest, the subsurface debris-apron stratigraphy of SE-2 consists of four stratigraphic units described in the surface debris-apron unit Qa2 (Fig. 25). Subsurface debris-apron stratigraphic unit 1 consists of grain and eolian matrix-supported tephra with Btky soil horizon development and Stage III secondary carbonate morphology (see Appendix B). Unit 2 overlies unit 1 and consists of poorly sorted tephra with bedding layers composed of aerodynamically aligned bombs characteristic of primary airfall tephra. The soil within unit 2 possesses Bky soil horizon development and Stage 1 secondary carbonate morphology. In contrast, the overlying unit 3 contains very thinly bedded tephra with Btky and Bky soil characteristics and Stage I secondary carbonate morphology. The overlying subsurface debris-apron unit 4 consists of a fining upward sequence of tephra with Bwky soil horizon development and Stage I secondary carbonate morphology.

The soil data from the four cinder cones does not suggest a strong soil stratigraphic relationship among all debris-aprons studied (Table 10). However, the two youngest debris-apron geomorphic surfaces (Qa2 and Qa3) appear to correlate between each cinder cone in terms of the degree of soil development in these surfaces. The Qa2 and Qa3 surfaces appear to be late Holocene to early Pleistocene in age as estimated by the degree of soil development.

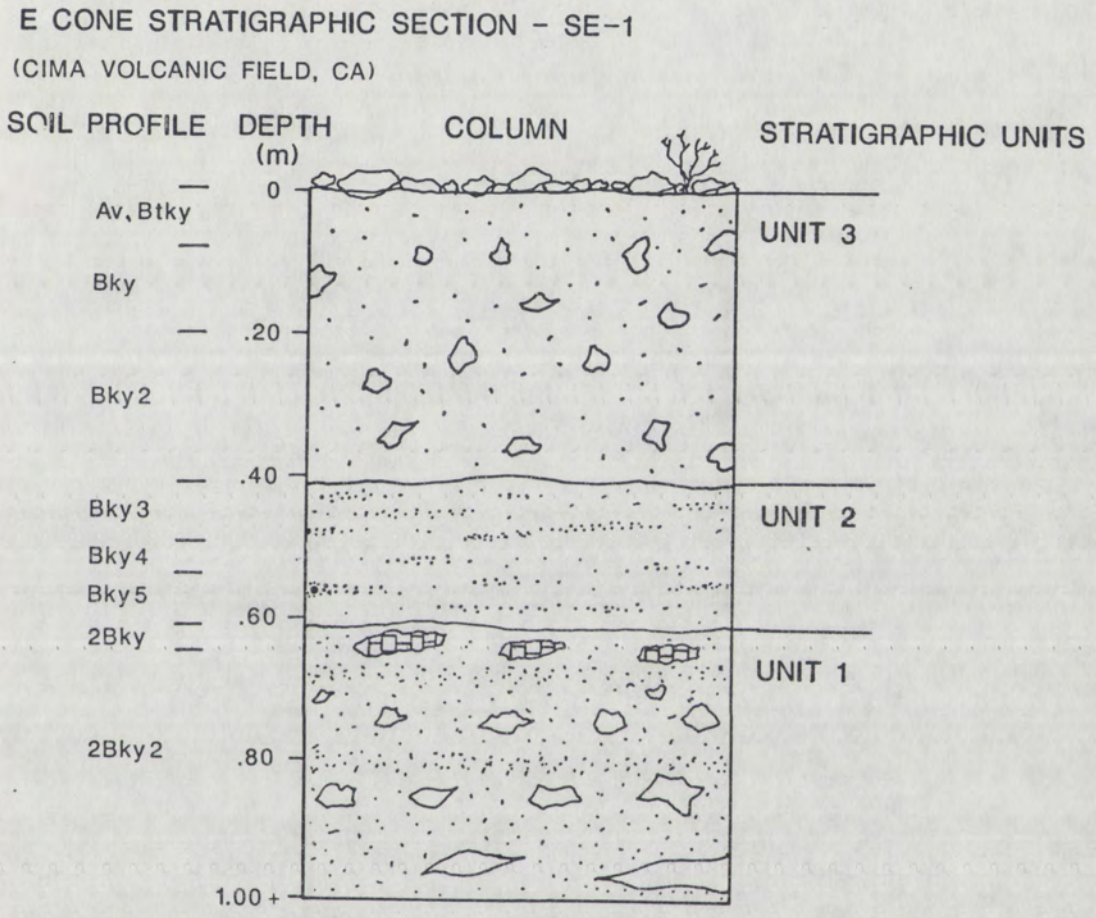

Figure 25. SE-1 debris-apron stratigraphy and soil profile horizons described in the field.

Table 10. Summary of (1) soil horizon thickness, (2) type of depositional process , and (3) stage of secondary carbonate morphology for all soils described.

A-CONE COMPLEX

SA2-1

DEPTH	SOIL HORIZON	DEPOSITIONAL PROCESSES
0 - 3	Av	Fluvial &
3 - 23	Bwk	Debris Flow
23 - 32	AvBtkb	Primary
32 - 35	Bkb	Airfall
35 - 45	Bk2b	Tephra II
45 - 95	Bk3b	"
95 - 111	Bkb2	Primary
111 - 135	Bk2b2	Airfall
		Tephra I

SA2-2

DEPTH	DEPOSITIONAL PROCESSES
0 - 19	Fluvial
19 - 118	Airfall Tephra I

SA2-3

DEPTH	SOIL HORIZON	DEPOSITIONAL PROCESSES
0 - 2	Av	Debris Flow
2 - 27	Bwk	"
27 - 31	AvBtkb	"
31 - 56	Bkb	"
56 - 62	AvBtkb2	Primary
62 - 71	Bkb2	Airfall
71 - 79	Bk2b2	Tephra II
79 - 113	Bk3b2	"

U-CONE COMPLEX

SU1-1

DEPTH	SOIL HORIZON	DEPOSITIONAL PROCESSES
0 - 3	Av	Eolian
3 - 7	AvBtk	"
7 - 13	Bky	"
13 - 22	Btkyb	Fluvial
22- 51	Bkyb	Airfall II (40 - 51 cm)
51 - 53	Kqb2	Pedogenesis
53 - 69	KBqb2	Obscures
69 - 94	Bkkb2	Sedimentary
94 - 130	Bkb2	Features

SU1-2

DEPTH	SOIL HORIZON	DEPOSITIONAL PROCESSES
0 - 2	Av	Fluvial
2 - 14	Bwk	"
14 - 36	Bwkb	"
36 - 81	Bkb	"
81 - 83	KBtqb2	Pedogenesis Obscures Sedimentary Features
83 - 115	Bk2b2	

SU2-1

DEPTH	SOIL HORIZON	DEPOSITIONAL PROCESSES
0 - 3	Av	Fluvial
3 - 13	Bwk	"
13 - 26	Bwk2	"
26 - 43	Bk	"
43 - 73	Btkb	Pedogenesis Obscures Sedimentary Features

G CONE

SG-1

DEPTH	SOIL HORIZON	DEPOSITIONAL PROCESSES
0 - 6	Av	Airfall
6 - 13	AvBtk	Tephra II
13- 19	AvBtkb	Fluvial
19 - 26	Btkyb	"
26 - 37	Bkb	Pedogenesis
37 - 78	Bkyb	Obscures Sedimentary Features
78 - 98	Ky3	Airfall
98 - 105	2Bkb	Tephra I
105 - 125	Bkyb	"

SG-2

DEPTH	SOIL HORIZON	DEPOSITIONAL PROCESSES
0 - 5	Av	Fluvial
5 - 8	AvBtk	"
8 - 11	Bk	"
11 - 30	Bky	"
30 - 43	AvBtkyb	"
43 - 49	Bkyb	"
49 - 52	AvBtkyb2	Debris Flow
52 - 56	Bkb2	"
56 - 70	AvBtkyb3	"
70 - 80	Btkyb3	"
80 - 95	Bkyb3	Airfall
95 - 109	Bky2b3	Tephra I
109 - 120	Bky3b3	(85 - 125cm)

E CONE

SE-1

DEPTH	SOIL HORIZON	DEPOSITIONAL PROCESSES
0 - 2	Av	Debris flow
2 - 8	Btky	"
8 - 20	Bky	"
20 - 41	Bky2	"
41 - 51	Bky3	Fluvial
51 - 54	Bky4	"
54 - 61	Bky5	"
61 - 65	2Bky	Airfall
65 - 127	2Bky2	Tephra

SE-2

DEPTH	SOIL HORIZON	DEPOSITIONAL PROCESSES
0 - 5	Av	Fluvial
5 - 24	Bwky	"
24 - 33	AvBtkyb	"
33 - 55	Bkyb	Debris Flow
55 - 71	2Bky2b	(52 - 85cm)
71 - 85	3Btkyb2	Airfall
85 - 112	3Bkyb2	Tephra
112 - 122	3Bky2b2	"
122 - 144	3Bky3b2	"
144 - 157	3Bkb2	"

SECONDARY CARBONATE MORPHOLOGY

- Stage I
- Stage II
- Stage III
- Stage IV [local]

~~~~ = buried soil boundary
~~~~

DISCUSSION

HILLSLOPE PROCESSES ON CINDER CONES

One of the objectives of this study is to determine the long-term processes of hillslope degradation on late Quaternary cinder cones. Geomorphic data of cone slopes provides documentation of modern hillslope processes dominant on the cone slope. Debris-apron soil characteristics and subsurface stratigraphy provide information about the depositional processes active for periods of time during degradation of the cinder cone slope. The combination of modern hillslope process data and debris-apron soil and subsurface stratigraphic data provides the information needed to determine the hillslope processes active since the initiation of cone slope degradation. Ultimately, the formulation of a hillslope evolution model for late Pleistocene cinder cones is developed based on an evaluation of the geomorphic evolution on each cone in the study.

Statistically Significant Cone Slope Relations

The Wilcoxin-T statistical test (alpha = 0.05) was performed to evaluate any relationship between the type of incision and cone slope lithology. The test reveals a statistically significant relationship between the

dominance of debris flow activity on the cone slope below agglutinate and proto-agglutinate. In addition, field relations suggest that debris flow activity primarily occurs below areas of agglutinate and proto-agglutinate due to the production of runoff from these virtually impermeable "bedrock" areas. This indicates that cinder cone primary volcanic lithologies play an important role in the evolution of processes responsible for cone degradation.

Relations Between Cone-Slope Geomorphic Units and Debris-Apron Soil and Stratigraphic Units.

The A2 cone

A comparison of degradational features on cone slopes and debris-apron deposits provide critical information for understanding the degradation of the A2 cone since the initial eruptive event at ~ 19 Ka. The A2 cone-slope degradational units at transect A1-2 (Fig. 8) correlate with the upper subsurface debris-apron stratigraphic units of SA2-1 (Fig. 15). The underlying debris-apron stratigraphic units, however, provide additional information as to the previous hillslope processes active on the cone slope (Fig. 26).

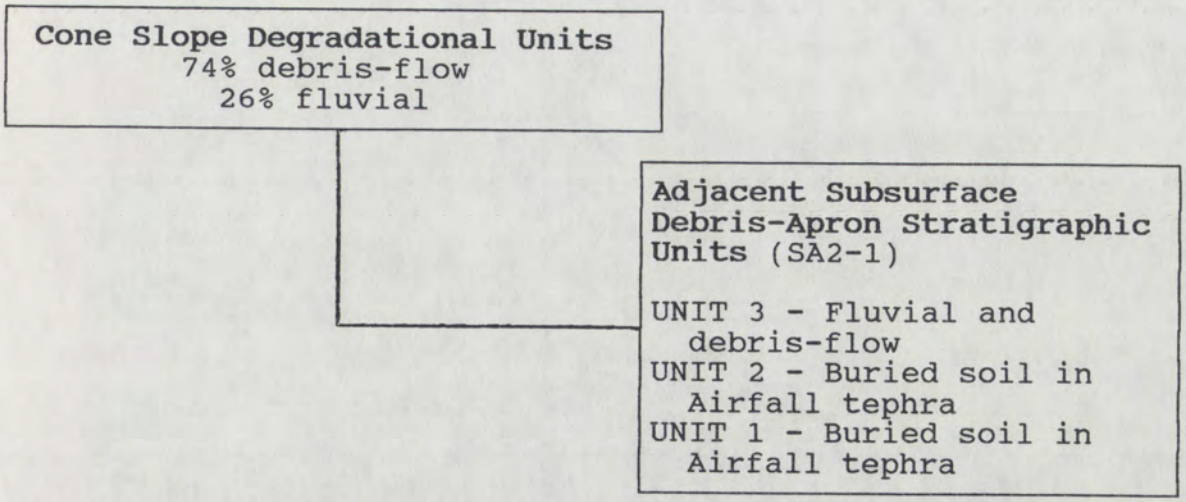

Figure 26. A comparison of modern cone slope degradational units on the A2 cone slope (box to the left) and A2 cone debris-apron stratigraphic units of SA2-1 topographically below the cone slope (box to the right).

The buried soil developed at the unit 1 and unit 2 boundary indicates that sufficient time elapsed between the eruption of unit 1 airfall tephra and unit 2 airfall tephra to allow for surface stabilization and pedogenesis. The absence of a debris-apron unit between the primary airfall-tephra of unit 1 and unit 2 of SA2-1 indicates that very little erosion of the cone slope and concomitant debris-apron deposition occurred during the time between the two airfall events. The buried soil developed on unit 2 and the overlying debris-apron unit (unit 3) indicates that cone-slope stability continued for a period following deposition of unit 2. Erosion and transport of tephra by fluvial and debris-flow processes resulting in the deposition of Unit 3 of SA2-1 probably reflects an increase in runoff and a reduction in permeability on the cone slope

(Dohrenwend et al., 1986) due to enhanced soil development after deposition of unit 2 airfall tephra.

Sedimentologic and soil stratigraphic variations also occur in the subsurface debris-apron stratigraphy at soil pit SA2-3. The presence of a buried soil within the subsurface debris-apron Unit 2 of SA2-2 (Fig. 16) indicates episodic deposition of debris-apron sediment. Climatic fluctuations creating increased runoff and transport of material off hillslopes has been documented in this portion of the Mojave Desert (Wells et al., 1984; McFadden et al., 1986) and may be the causal mechanism for this type of episodic movement of material from cone slopes to the debris aprons.

The debris-apron stratigraphy of SA2-2 (Fig. 8) consists of a package of fluvial debris-apron sediments thicker than that found at SA2-1 (Fig. 16). The increased thickness of the fluvial deposits and lack of debris-flow sedimentary structures suggests that this region of the cone slope has been dominated by fluvial processes since the eruption of airfall unit I. However, incision data (Table 1) shows that this portion of the cone slope has 50% channels with debris flow levees consists of 50% fluvial channels. The lack of debris flow sedimentary structures within the debris apron suggests that either (1) the debris-flow levees on the cone slope are relic and these channels have served only as conduits for the fluvial

transport subsequent to initial debris-flow activity or that (2) the debris flow sediments at the base of the cone slope have been reworked by fluvial processes. Erosional studies at the Paracutin cinder cone in Mexico indicate tephra draped on adjacent hillslopes erodes quickly due to the effect of runoff production from preexisting impermeable surfaces (Segerstrom, 1950). The thickness of the debris-apron deposits at SA2-2 may be due to a similar phenomena, that is, increased sediment transport as a result of similar runoff production from preexisting impermeable surfaces related to the older A1 cone.

The lack of preservation of airfall unit II at SA2-2 and further south at SA1-1 suggests that Airfall II had a limited extent and was not deposited in significant amounts south of the main A2 cone structure (Fig. 16). This is supported by the increased depth of incision, lower width-to-depth ratio (Table 1), and lack of preserved garlands (Fig. 8) on A1 cone, all of which indicate a more advanced stage of cone slope degradation.

U1 cone

For a given element of a cone slope, it is necessary to examine multiple apron surfaces topographically below it to fully understand the history of hillslope processes active on the cone slope with time. The cone-slope degradational features on the western portion of the U1 cone slope include 40% debris-flow and 60% fluvial incision

which do not correlate with the eolian stratigraphic features found in unit 4 at the top of the subsurface stratigraphy of SU1-1 (Fig. 9).

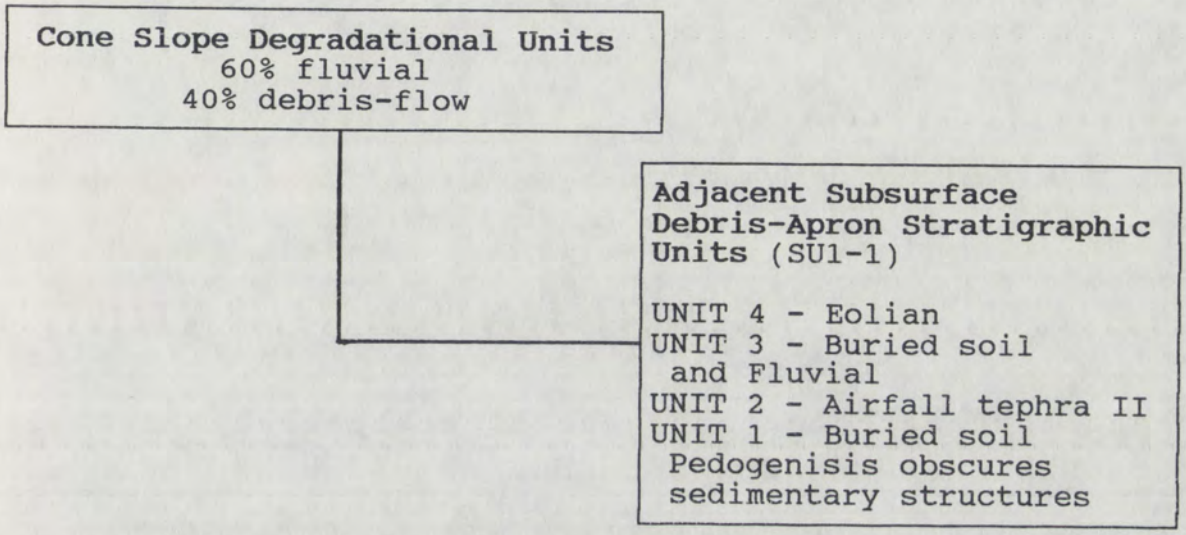

Figure 27. A comparison of modern cone slope degradational units on the U1 cone slope (box to the left) and U1 cone debris-apron stratigraphic units of SU1-1 topographically below the cone slope (box to the right).

The lack of correlation between cone slope and debris apron units may be due to (1) the antiquity of this debris-apron surface and/or (2) abandonment and subsequent deposition of eolian material on the debris-apron surface unit Qa1. The U1 cone apron lies adjacent to a major active wash which heads in Tertiary fanglomerates and may provide a local source for the eolian material.

Subsurface debris-apron unit 3 at SU1-1 contains fluvial sedimentary structures which indicate that fluvial processes were active on this portion of the U1 cone debris apron prior to burial by unit 4. The buried soil

separating unit 3 and unit 4 indicates that unit 3 was exposed at the surface long enough for a soil with Btky soil characteristics to develop prior to deposition of eolian unit 4. Unit 3 buries the airfall tephra of unit 2, an airfall deposit from the second eruption of the U cone complex (U2 cone). No evidence of a buried soil between the airfall deposit of unit 2 and the overlying unit 3 suggests that cone slope degradation occurred rapidly after the eruption of U2 cone. Rapid degradation of U2 airfall tephra off of U1 cone may be due to enhanced runoff and transport capabilities on preexisting drainages and resistant cone lithologies of U1 cone. A well developed truncated buried soil impregnated with secondary carbonate separates unit 2 from the underlying unit 1 which indicates that unit 1 was abandoned prior to the eruption of U2 cone. Unit 1 may represent airfall from U1 cone eruption; however, pedogenesis largely obscures sedimentary structures making facies classification difficult.

The U2 cone

Complex relationships between cone slope and subsurface debris-apron stratigraphic units at U2 cone best illustrate the need for detailed stratigraphic analysis of all aspects of cinder cone complexes when trying to understand their degradational and eruptive evolution. Figure 28 schematically illustrates the relationship between cone slope degradational features at transect U2-3

(Fig. 9) and the resultant adjacent debris-apron deposits of SU2-1 (Fig 19).

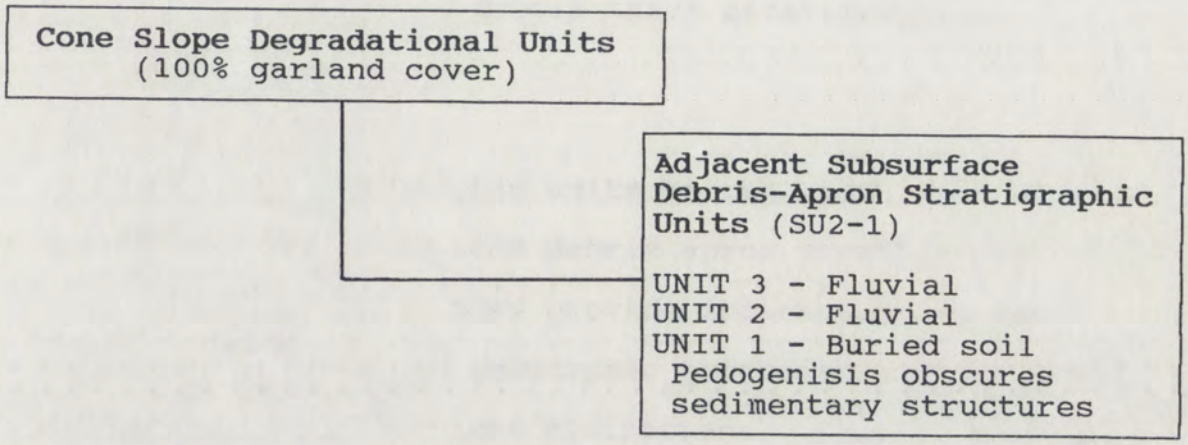

Figure 28. A comparison of modern cone slope degradational units on the U2 cone slope (box to the left) and U2 cone debris-apron stratigraphic units of SU2-1 topographically below the cone slope (box to the right).

Areas of unincised garland cover 100% of the eastern U2 cone slope at the location of SU2-1. Topographically below this portion of the cone slope are debris-apron deposits which cannot be derived from the U2 cone slope due to the lack of any geomorphic evidence of transport of tephra on the hillslope such as no debris-flow or fluvial channels. Unit 1 of SU2-1 consists of a very well developed buried soil with pedogenic characteristics comparable to unit 1 in SU1-1 and SU1-2 of the U1 cone debris-apron (see Fig. 17 and Appendix A). In addition, the overlying units 2 and 3 consist of fluvial sediments with no corresponding cone slope fluvial or debris-flow channels. It follows that the debris-apron deposits at SU2-1 must have been generated by the degradation of U1

cone prior to the eruption of U2. These interesting relations demonstrate the complexity of cinder cone eruptive processes and debris-apron stratigraphy.

The G cone

Cone slope geomorphic units on the south side of G Cone do not correlate with debris apron stratigraphic units below it at SG-1, but they provide information on the nature of volcanic and geomorphic processes active on the cone slope during the late Pleistocene. Fluvial processes cover 100% of the cone slope topographically above SG-1 (Table 6). The uppermost stratigraphic unit of SG-1 consists of airfall tephra (Unit 4) from the most recent recorded eruption of G cone (Airfall II) (Fig. 29).

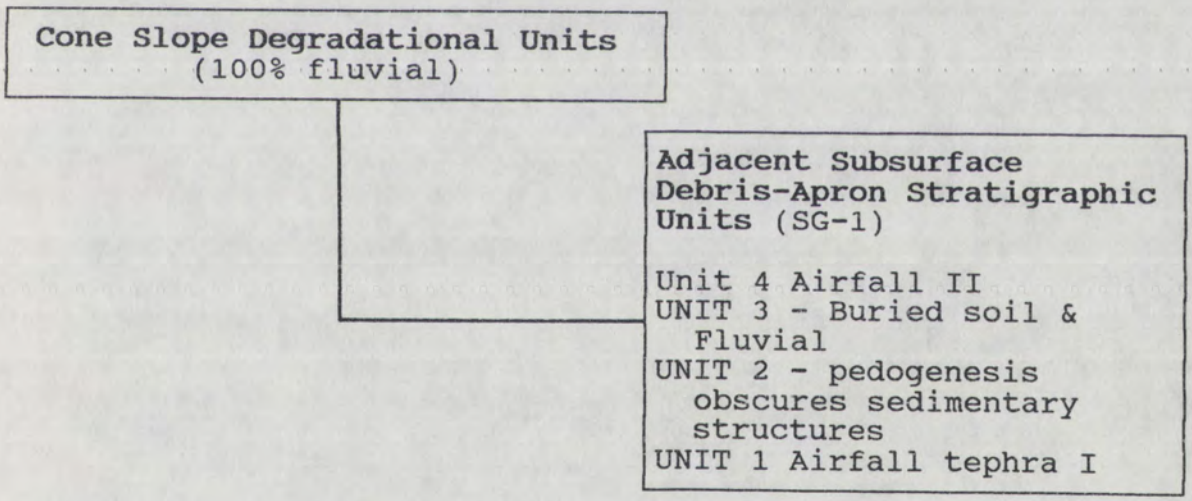

Figure 29. A comparison of modern cone slope degradational units on the G cone slope (box to the left) and G cone debris-apron stratigraphic units of SG-1 topographically below the cone slope (box to the right).

Beneath Unit 4 is a buried soil with desert pavement developed within fluvial sediments (unit 3) indicating that fluvial processes were also the dominant geomorphic process on the cone slope during unit 3 time. The buried soil indicates this surface was abandoned and stable enough for a desert pavement and a soil to develop prior to the eruption of Airfall II. Pedogenesis (local Stage IV secondary carbonate morphology) obscures the sedimentary features of Unit 2 making it impossible to determine the hillslope processes active at this time. Airfall I of Unit 1 represents the earliest evidence of cinder cone building at G cone.

On the eastern side of G cone, the subsurface debris-apron stratigraphy at SG-2 (Fig. 22) correlates with cone slope hillslope processes of transect G-1 in a complex manner (Fig. 12) providing critical information about the degradation of the G cone since the initial incision of the cone slopes (Fig. 30).

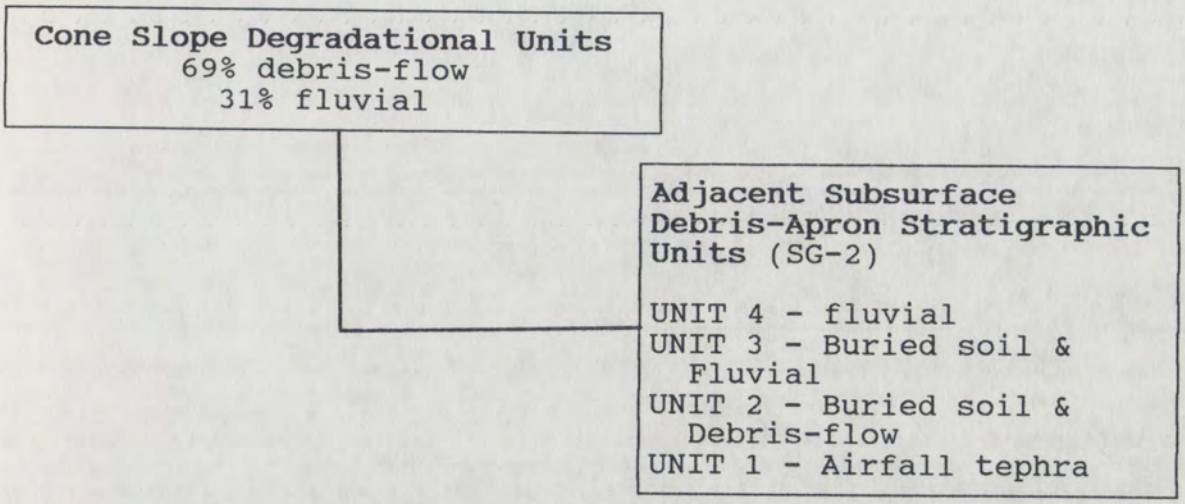

Figure 30. A comparison of modern cone slope degradational units on the G cone slope (box to the left) and G cone debris-apron stratigraphic units of SG-2 topographically below the cone slope (box to the right).

The debris-flow deposits of unit 2 are overlain by fluvial deposits of unit 3 and 4. This same sequence is recorded on the cone slope by the presence of old degraded debris-flow levees whose channels are currently dominated by fluvial processes. The buried soils between units 3 and 4 and within unit 3 again provides evidence for episodic cone slope processes. Therefore, deposition of unit 2 and subsequent development of a soil with Btky characteristics was followed by episodic fluvial sedimentation that masked the evidence of earlier debris-flow activity.

The E cone

The E cone Cone slope degradational units on E Cone correlate well with debris-apron stratigraphic units of SE-1 in such a way that they provide abundant information about the timing of hillslope processes on the E cone (Fig. 31).

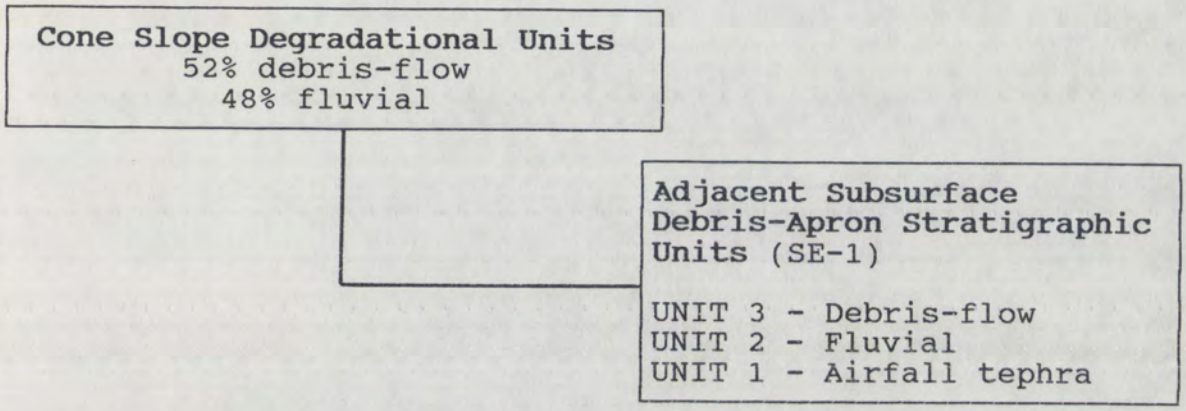

Figure 31. A comparison of modern cone slope degradational units on the E cone slope (box to the left) and E cone debris-apron stratigraphic units of SE-1 topographically below the cone slope (box to the right).

On the cone slope above SE-1 fluvial and debris-flow processes are active in approximately equal proportions (Table 8). Subsurface debris-apron Unit 1 represents airfall tephra from the latest eruption of E cone. Unit 2 buries unit 1 and consists of fluvial sediments which indicate an earlier depositional mode during which fluvial processes dominated on the debris apron and possibly on the cone slope. Unit 3, consisting of debris-flow deposits, buries unit 2. This change from fluvial to debris-flow sedimentation may be due to the exhumation of agglutinate

and proto-agglutinate by fluvial processes (unit 2) resulting in an increase in runoff conditions on the cone slope. The lack of buried soils in any of the subsurface units indicate either (1) a lack of episodicity in sedimentation or (2) that the high degree of soil development within each unit obscures soil stratigraphy.

Figure 32 shows the cone slope degradational features at transect E-2 (Fig. 13) and the resultant adjacent debris-apron deposits of SE-2 (Fig. 25) which provide additional information about the degradation of the E cone subsequent to initial incision of the cone slopes.

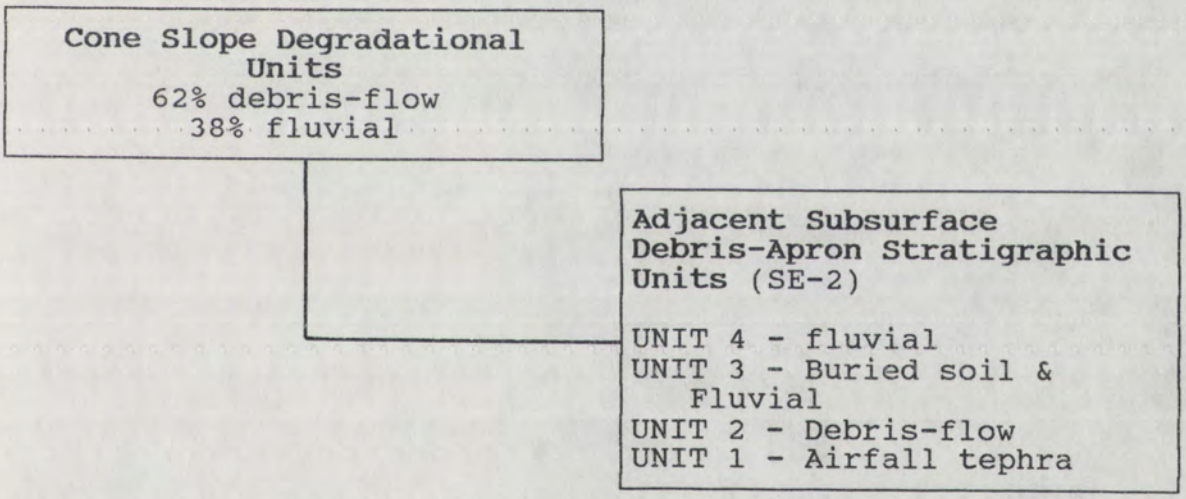

Figure 32. A comparison of modern cone slope degradational units on the E cone slope (box to the left) and E cone debris-apron stratigraphic units of SE-2 topographically below the cone slope (box to the right).

The airfall tephra of subsurface stratigraphic unit 1 again represents the most recent eruption of E cone. Unit 1 is capped by a buried soil with a desert pavement which

indicates that a period of cone slope and debris apron stability with little or no downslope movement of tephra occurred prior to deposition of the overlying apron Unit 2. Debris-flow activity resulting in deposition of unit 2 may have been initiated at this time because of increasing soil development accompanied by a reduction in permeability and increased runoff on the cone slope. A period of episodic fluvial sedimentation on the cone slope resulted in deposition of units 3 and 4 on top of unit 2. This change in deposition from debris-flow activity (deposition of unit 2) to episodic fluvial activity (deposition of units 3 and 4) may have been caused by subsequent utilization of debris flow channels by fluvial processes.

Climate fluctuations most certainly affect cinder cone degradation by creating changes in infiltration, runoff, and soil development on hillslopes. The two youngest debris-apron geomorphic surfaces (Qa2 and Qa3) correlate between each cinder cone in terms of the degree of soil development on these surfaces (Table 10). The Qa2 and Qa3 surfaces appear to be late Holocene to early Pleistocene in age as estimated by the degree of soil development and may represent climatically controlled debris-apron sedimentation during this time period. However, the effects of climate variations are difficult to properly assess by studying a single volcanic field and not intended as a purpose of this study. Future studies of cinder cone degradation in a variety of climates are necessary to fully

understand the influence of climate on hillslope processes on cinder cones.

COMPARISON OF HILLSLOPE DEGRADATION ON ALL CONES STUDIED

Buried soils in airfall deposits of SA2-1, SA2-3 and SE-2 reveal that negligible erosion and transport of tephra occurred on A cone or E cone slopes following their most recent eruptions, most likely due to cone slope stability as a result of the high infiltration capacity of tephra. With time, soil development sufficiently reduces cone-slope permeability which increases runoff potential. The dominant mechanism of transport of tephra is by debris-flow processes if agglutinate or proto-agglutinate are exposed and by fluvial processes if little or no agglutinate or proto-agglutinate are exposed.

At A2, U1, and U2 cones, incision of cone slopes by debris flows and rilling appears to be initiated on the finer grained portions of garlands where permeability is reduced and soil development is enhanced by the rapid accumulation of eolian material within the smaller pore spaces of fine grained tephra. Birkeland (1984) and Gile (1987) have shown that soil development is accelerated within soil parent material with small pore spaces as compared to large pore spaces due to the reduction in permeability in finer grained materials. Reduction in permeability due to soil development and the accumulation

of eolian material in the finer gained portions of garlands makes these areas prone to rilling and debris-flow activity. Prior to deposition of eolian material and soil development discontinuous channels with sediment plugs form on the slopes of U2 cone and E cone because runoff production is not capable of transporting sediment downslope. The lack of significant soil development in addition to the trapping of eroded tephra upslope of vegetation within the upper 4 cm of garland units on the cone slope of A1, U1, U2 and G cones (SG-3, SU1-3, and SU2-2) indicates that this upper 4 cm is not stable and is probably moving downslope by gravity sliding.

Multiple weakly developed buried soils within debris aprons and the presence of sediment plugs within cone slope channels at A2, G, and E cones indicates that fluvial sedimentation is episodic. Only in the subsurface stratigraphy of SA2-2 on the A cone debris apron are debris-flows involved in episodic sedimentation (i.e. debris-flow sediments separated by a buried soil).

In contrast, rapid and relatively continuous downslope transport of tephra by fluvial processes occurs on cone slopes buried by airfall tephra from adjacent eruptions (U1 cone and A1 cone). Previous drainage development and exposed resistant lithologies enhance runoff and result in rapid stripping of tephra (Segerstrom, 1950) and deposition on debris-aprons prior to development of soils on the cone

slope and airfall tephra deposits. No buried soils are therefore seen in the airfall deposits at SA2-2 and SU1-21-2. Additional evidence for the more rapid erosion of A1 and U1 cones is seen in the high drainage frequency on tephra draped portions of the cinder cones (Table 1 and 4). Erosional studies at Paracutin cinder cone in Mexico report similar accelerated erosion on tephra-draped surfaces adjacent to the main eruptive center due to the higher potential for runoff from preexisting exposures of bedrock (Segerstrom, 1950).

The type of hillslope process responsible for cone slope degradation is largely dependent upon the lithology exposed on the cone slopes of U1 , U2 , G , and E cones. Results of the Wilcoxon-T statistical test (alpha = 0.05) support the field observations that debris-flow processes dominate slopes which are topographically below exposures of agglutinate and proto-agglutinate. Because channel depths are also greater below exposed agglutinate or proto-agglutinate than on other portions of an isochronous cone slope, the implications is that initial exhumation of agglutinate may greatly increase the rate of incision and downslope transport of material.

PROCESS-RESPONSE MODEL FOR CINDER CONE DEGRADATION

The sequence of cinder cones selected for this study provide the opportunity to examine hillslope evolution by representing time via spatially distinct dated cinder cones (see Wells et al., 1985 for a similar approach as applied to lava flows). By comparing the morphometric parameters and hillslope process evolution of all cones discussed in this study, it is possible to develop a process-response model which illustrates the sequence of cinder cone degradation. The proposed model is applicable to cones less than 350,000 years old in arid climates.

PHASE I - CONE SLOPE STABILITY AND SOIL DEVELOPMENT

After eruption, the cone slope stabilizes as a result of slow movement of tephra downslope by gravity sliding to the angle of repose (31-38°) (Mcgetchin et al., 1974) forming garlands. Soil development is enhanced in finer grained portions of garlands due to lower permeability. (example: A2, U1, and U2 cones)

PHASE II - INITIATION OF DISCONTINUOUS CHANNELS

Small discontinuous debris-flow channels with low width-to-depth ratios are initiated in the fine grained portions of garlands where enhanced soil development and an inferred reduction in permeability results in local runoff generation. Discontinuous debris-flow channels may also be generated where agglutinate and/or proto-agglutinate are exposed at the crater rim. During this phase of degradation little to no debris apron is produced. (examples: A2, U1, and U2 cones)

PHASE III - CONTINUOUS CHANNEL DEVELOPMENT

Debris-flow processes and minor fluvial processes continue to occur below relatively impermeable areas on the cone slope, such as where agglutinate, proto-agglutinate, or well developed soils are exposed. As areas of exposed agglutinate and/or proto-agglutinate increase due to stripping of overlying tephra, runoff generation increases and small discontinuous, incised channels downslope are integrated into continuous channels capable of transporting increased quantities of sediment from the crater rim to the debris apron. In addition, high apron height-to-cone height ratios develop due to a larger volume of debris-apron accumulation. (examples: U1, G, and E cones)

Where no agglutinate and/or proto-agglutinate is exposed episodic fluvial processes may become active in preexisting debris-flow channels (Dohrenwend et al., 1986). If a large amount of loose tephra is available, channels may be shallow and largely infilled with sediment. In addition, a low-frequency, high-magnitude precipitation event that exceeds a threshold of transport capability may be necessary to mobilize and transport sediment from the cone slope channels to debris-aprons. Because of the low frequency of such events, long-term debris-apron accumulation is slow and result in low apron height-to-cone height ratios and older apron units abutting the cone slope. (examples: U1, G, and E cones)

PHASE IV - CONTINUOUS CHANNELS WITH INCISION INTO DEBRIS APRON

The runoff generating capacity of the upper cone slope greatly increases as (1) soil development on the cone slope increases, and (2) tephra continues to be eroded and relatively impermeable layers become exposed on the cone slope. Increased runoff results in greater incision into the debris-aprons. The rates of erosion and deposition of tephra down slope become so great on E cone that modern roads cutting across the cone slope and debris apron are obliterated by erosion and deposition. Debris-apron incision results in the abandonment of debris-apron

surfaces and the formation geomorphic surfaces of different ages.

APPLICATIONS TO THE ERUPTIVE HISTORY OF SMALL BASALTIC CINDER CONES:

POLYCYCLIC VOLCANISM IN THE CIMA VOLCANIC FIELD

Previous studies describe strombolian eruptions as primarily monogenetic, discrete eruptions lasting a few days to twenty years (Blackburn et al, 1976; Williams and McBirney, 1979; Hasenaka and Carmichael, 1985; Cas and Wright, 1987). Recent studies utilizing radiometric dating of lava flows associated with cinder cones in the Cima volcanic field, California (Turrin and Renne, 1987; Turrin et al., 1984; Wells et al, 1984) and geomorphic and pedologic techniques at Lathrop Wells cone, Nevada (Wells, 1986; Wells et al., 1988; Crowe et al., 1988; Renault et al., 1988) indicate a complex history of episodic (polycyclic) small volume eruptive events of compositionally uniform magma occurring over time spans of 10^3-10^5 years. Petrologic models are currently being developed and tested by Bruce Crowe of Los Alamos National Laboratory and Frank Perry of the University of New Mexico in order to understand the volcanic processes involved in polycyclic cinder cone eruptions (Crowe et al., 1989).

Evidence for polycyclic volcanism in the Cima volcanic field, California is shown by detailed geomorphic maps, soil and stratigraphic features, and morphometric analyses of parameters shown to be sensitive to cone age (Dohrenwend et al., 1986; Renault, 1988; Wells et al., 1989 in press). Geomorphic and pedologic criteria useful in the interpretation of strombolian eruptive sequences are listed in Figure 33.

Figure 33. A summary of the criteria useful in the interpretation of polycyclic cinder cone volcanism.

1. Buried soils which separate multiple airfall deposits erupted from a single vent indicate that a period of surface stability and soil development has occurred on the volcanic units prior to a second eruption. This relationship may be found either on the cone slope or within the subsurface debris-apron stratigraphy.

2. Subsurface debris-apron stratigraphic units buried by airfall deposits.

3. Debris-apron found topographically below a cone slope with no incised channels.

4. Slope angle decreases with time and the ratio of apron length-to-total length and apron height-to-cone height increases with time as the debris apron builds (Dohrenwend et al., 1986). Polycyclic volcanism may be responsible for large variations in morphometric parameters on overlapping cinder cones.

The first criterion is exemplified by relations at the A2 cone; here SA2-1 and SA2-4 display two airfall units separated by a buried soil which indicates a period of quiescence following the first eruption of airfall (Fig.16). A2 cone is the youngest cinder cone in the Cima

volcanic field, indicating that this second airfall unit must have come from the A2 cone vent.

A similar sequence of buried soils between airfall deposits is found on the cone slope of U1 cone. The initial eruption of U1 cone was followed by enough time to enable formation of a soil on the cone slope. Subsequently, the eruption of U2 cone which buried the cone-slope soil with an airfall unit (Airfall II of SU1-3) (Fig. 18). The degree of soil development of the buried U1 cone-slope soil is comparable to a phase 1 soil described by McFadden et al. (1986) estimated to represent less than 0.14 +\- 0.04m.y. of soil development. A similar sequence of buried cone-slope soils can be found in the stratigraphic section SG-3 on the G cone (Fig. 23).

The second criterion (Table 33) recognizes polycyclicity by other relations observed at the A-cone complex. Subsurface debris-apron stratigraphic units are buried by airfall from secondary eruptions of virtually the same vent. These phenomena have generated the subsurface stratigraphy of SA1-1 at the A cone complex, where A1 cone apron has been buried by airfall from the subsequent eruption of A2 cone (Fig. 16). The degree of soil development of the buried A1 cone debris-apron is comparable to a phase 2 soil described by McFadden et al. (1986) estimated to represent 0.14 +\- 0.04m.y. to 0.70 +\- 0.06 m.y. of soil development.

Criterion #2 may be complicated by the presence of interbedded debris-apron deposits. The debris apron of U1 cone at SU1-1 displays complex subsurface stratigraphy characterized by debris-apron deposits buried successively by airfall tephra and debris-apron deposits (Fig. 17). This indicates that the initial eruption of U1 cone was followed by a sufficient amount of time to allow for debris-apron development prior to the eruption and burial by the U2 cone airfall.

The third criterion (Table 33) useful in determining the polycyclic nature of cinder cones is the presence of a debris apron below a cone slope with no incised channels. On the east side of U2 cone the cone slope is unincised and dominated by garland features. Debris apron deposits are located at the base of this unincised slope (Fig. 9). At A2 cone, debris aprons have been shown to form only where there are incised channels on the cone slope. On the basis of this observation, it is postulated that the debris apron at U2 cone is not associated with U2 cone but rather with the degradation of U1 cone prior to the eruption of U2 cone. Therefore, a sufficient amount of time elapsed after the eruption of U1 cone to allow for debris-apron development prior to the eruption of U2 cone, demonstrating the polycyclic nature of the U-cone complex.

The fourth criterion (Table 33) useful for recognizing polycyclic cinder cones is the presence of multiple overlapping cinder cones of different age as estimated by geomorphic parameters shown to be sensitive to cone age (Dohrenwend et al., 1986). Previous workers have demonstrated that slope angle decreases with time and the ratios of apron length-to-total length and apron height-to-cone height increase with time as the debris apron builds (Scott and Trask, 1971; Porter, 1972; Bloomfield, 1975; Wood, 1980b; Dohrenwend et al., 1986). When two cones are overlapping one may use these parameters to determine if a significant amount of time has passed between eruptions.

An example which demonstrates the applicability of the fourth criterion is found at the A cone complex where striking differences in cone morphology exist between the A1 cone and the younger A2 cone. The cone slope angle is greater on A2 cone than A1 cone, while the ratios of apron length-to-cone length and apron height-to-cone height are greater on A1 cone than on A2 cone (Fig. 34). In addition, the area covered by the debris apron of A1 cone and the amount of incision on the A1 cone slope are much greater than for the A2 cone (Fig. 34). These differences indicate that after the eruptions of A1 cone, sufficient time elapsed to allow a reduction in the slope angle and formation of a debris apron before the eruptions of A2 cone. Similar morphometric relationships between polycyclic cinder cones are present at U1 and U2 cone;

however, the differences are less dramatic indicating that less time elapsed between eruptions (Fig. 34).

The presence of polycyclic volcanism may have profound effects on the type and rate of hillslope processes responsible for cinder cone degradation. If a subsequent eruption of a cinder cone does not completely cover the cone surface, useful cone age geomorphic parameters will be highly variable across the different age deposits. Such cone-slope variations occur at the G cone where areas of recently erupted tephra with garlands and no incised channels are juxtaposed with older, deeply incised cone slopes which lie topographically above complex debris-apron deposits (Fig. 11).

Additional complications arise when younger airfall tephra is deposited on older adjacent cone slopes. In this situation, erosion of the cone slope may be accelerated by the presence of preexisting impermeable cone slope material which provides the runoff capable of rapidly degrading the deposited airfall tephra (Segerstrom, 1950). A1 and U1 cones provide an excellent example of such complications where debris-flow stratigraphy reflects non-episodic, high-volume sedimentation below areas covered with younger airfall-tephra deposits which drape older surfaces (see Appendix A).

An increased understanding of the polygenetic nature of cinder cones will be helpful in understanding the

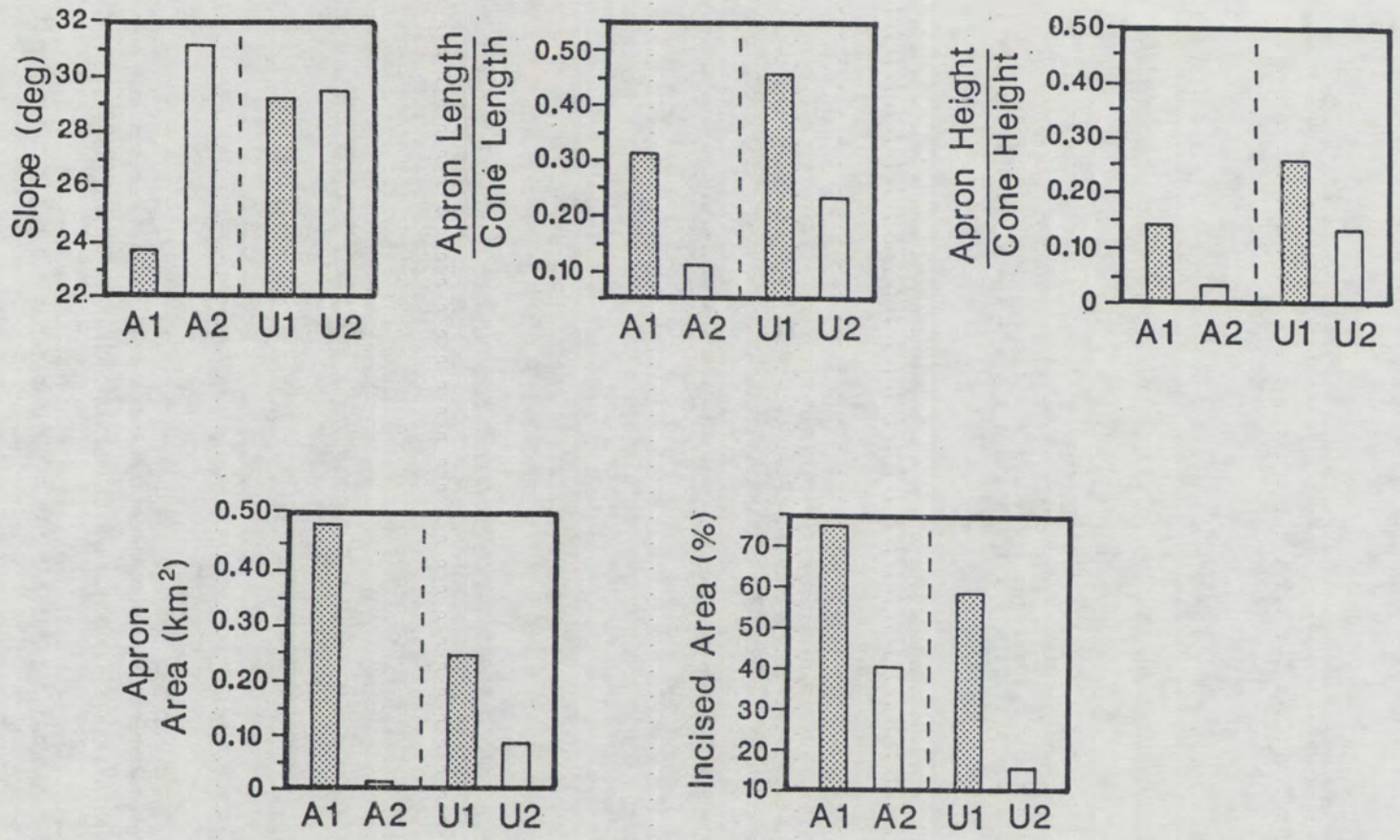

Figure 34. Bar graph comparing A1 and A2 cone morphometric parameters and U1 and U2 cone morphometric measurements.

complexities in strombolian eruptive events, especially where K/Ar dates are not available or where cinder cone / flow relationships are not clear. In addition, an improved understanding of the eruptive history of cinder cones is helping in the ongoing assessment of volcanic hazards at the proposed nuclear waste repository adjacent to the Nevada Test Site in Nevada.

IMPLICATIONS FOR AGE DATING

The process-response model presented for cinder cone degradation in the Cima volcanic field is useful for predicting hillslope processes involved in sediment transport to adjacent debris aprons and provides a supplemental tool when using morphometric measurements for estimating the relative age of cinder cones with poor radiometric age control. One may use the different phases of degradation outlined in the model section to approximate the age of the most recent eruption of late Quaternary cinder cones. However, it is important to be aware of the complicating factors brought forth in this study. For example, significant differences in cinder cone morphology such as a decreased slope angle, increased apron height, or increased apron length may result in erroneous relative age estimates if they are measured below agglutinate or proto-agglutinate. The presence of polycyclic volcanism may also complicate the cone slope and debris-apron record of cone

degradation. Multiple eruptions of a cinder cone may accelerate erosion on adjacent slopes as well as complicate and alter morphometric and geomorphic parameters described within the proposed model. Careful documentation of debris-apron and cone-slope stratigraphy and variations in cone-slope morphology will alert one to potential complications. In conclusion, this study shows that morphometric measurements provide an accurate tool for determination of relative ages of late Quaternary cinder cones in an arid climate when they are combined with a detailed analysis of volcanic and hillslope processes.

CONCLUSIONS

This study reveals that debris-flow, fluvial, and colluvial processes are the principal mechanisms by which cinder cones degrade through time. Lithologic variations on cone slopes such as the proportion of agglutinate and proto-agglutinate to lapilli affect the rates and processes of degradation. Deeply incised debris-flow channels are more common below agglutinate and/or proto-agglutinate. Areas on the cone slope without agglutinate and/or proto-agglutinate degrade primarily through episodic fluvial processes.

Morphometric analysis on different portions of the study cinder cones reveals that significant differences in slope angle, apron height, and apron length are controlled by the upslope location of agglutinate or proto-agglutinate. Therefore, estimates of the relative or absolute age of cinder cones based solely on morphometric measurements may lead to erroneous results. The eruptive history and geomorphic evolution of a cinder cone must be understood to augment morphometric analyses.

The primary geomorphic and pedologic criteria useful for determining the presence of polycyclic volcanoes are (1) multiple pyroclastic airfall deposits separated by buried soils, (2) buried soils developed in primary airfall tephra on the cone slope, (3) debris-apron deposits with

soils buried by airfall tephra deposits, (4) the presence of debris apron deposits below cone slopes with no incision, and 5) large variations in morphometric parameters sensitive to cone age. Estimates of the amount of time elapsed between eruptive events from polycyclic volcanoes may be obtained by (1) estimating the age of a buried soil between two primary airfall deposits, and (2) calculating the difference in ages of two cones based on calibration of morphometric parameters sensitive to cone age. The former method probably offers more potential for future studies because of (1) the recent advances made in Quaternary geochronologic techniques, and (2) the problematic nature of obtaining reliable age estimates based on changes in cone morphology.

APPENDIX A

STRATIGRAPHIC SECTIONS

A2 CONE STRATIGRAPHIC SECTION - SA2-2

(CIMA VOLCANIC FIELD, CA)

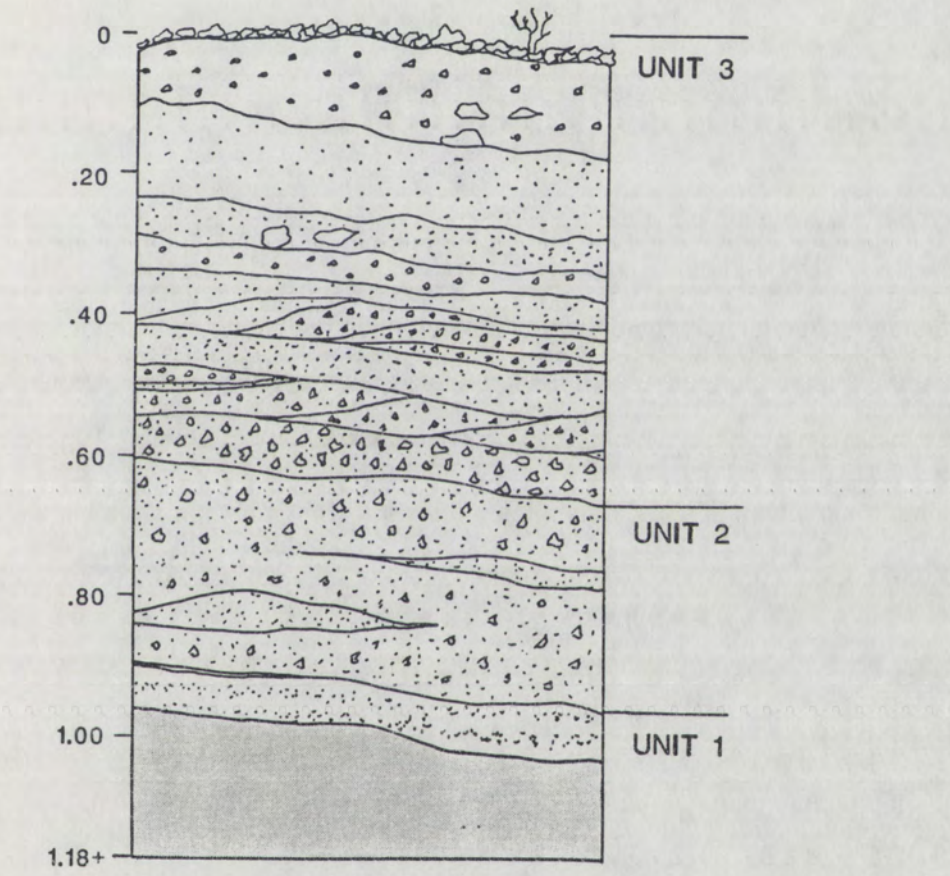

A2 CONE STRATIGRAPHIC SECTION - SA2-3

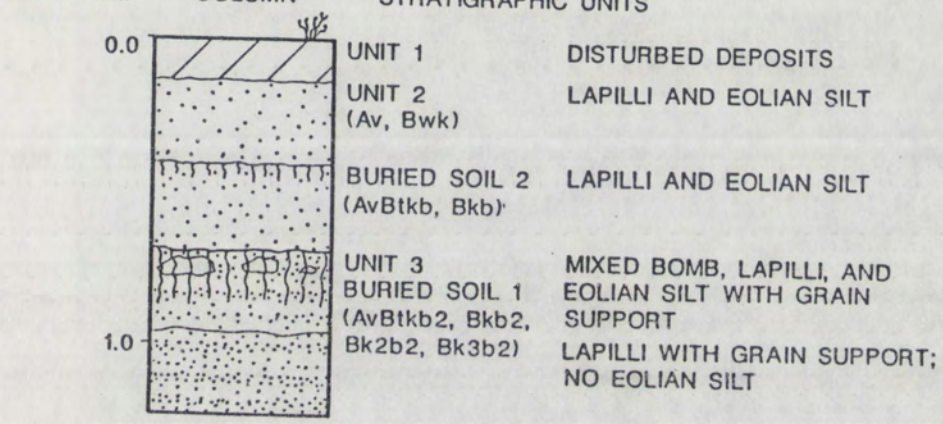

(modified from Wells et al. in prog)

A2 CONE STRATIGRAPHIC SECTION - SA2-4

(CIMA VOLCANIC FIELD, CA)

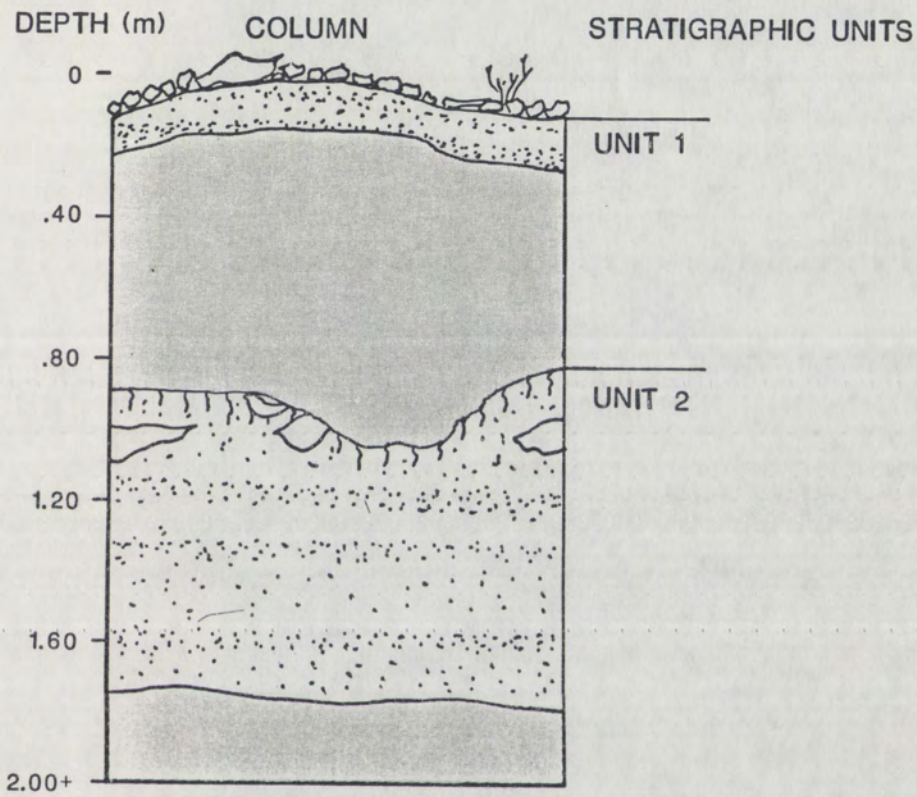

A1 CONE STRATIGRAPHIC SECTION – SA1-1
(CIMA VOLCANIC FIELD, CA)

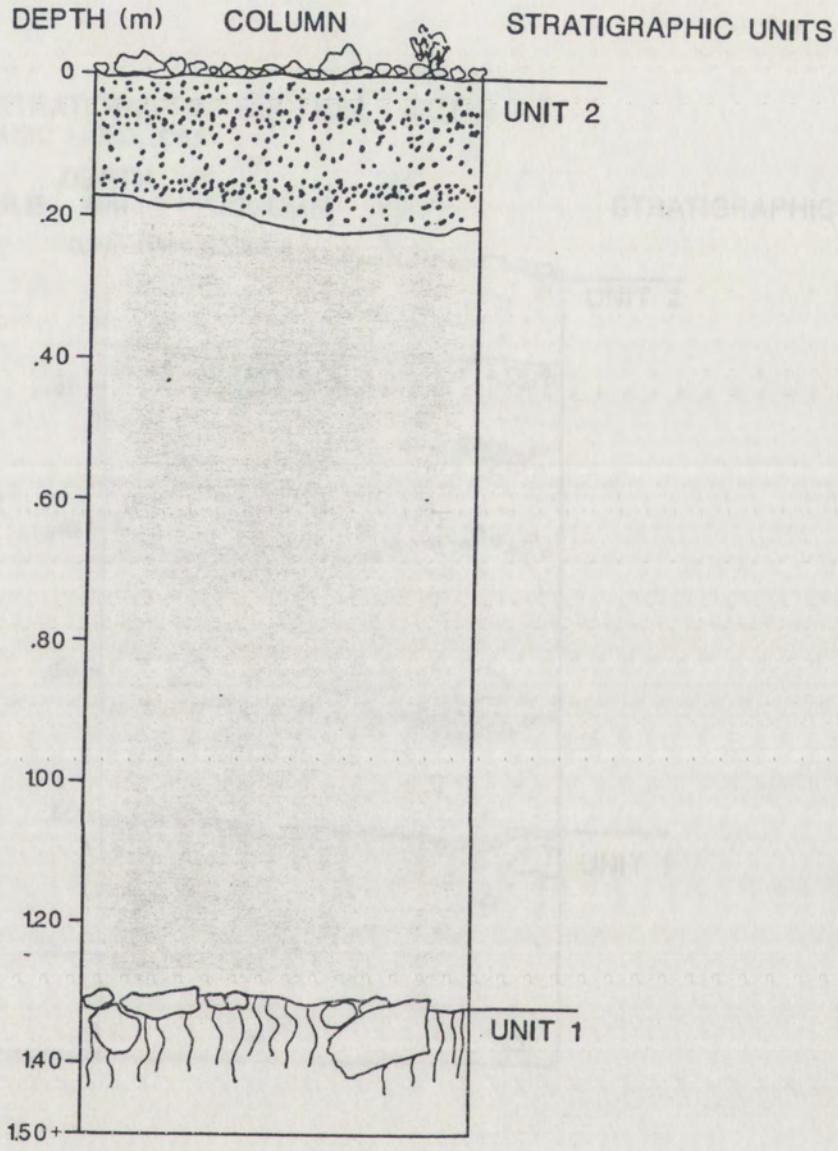

U1 CONE STRATIGRAPHIC SECTION - SU1-2
(CIMA VOLCANIC FIELD, CA)

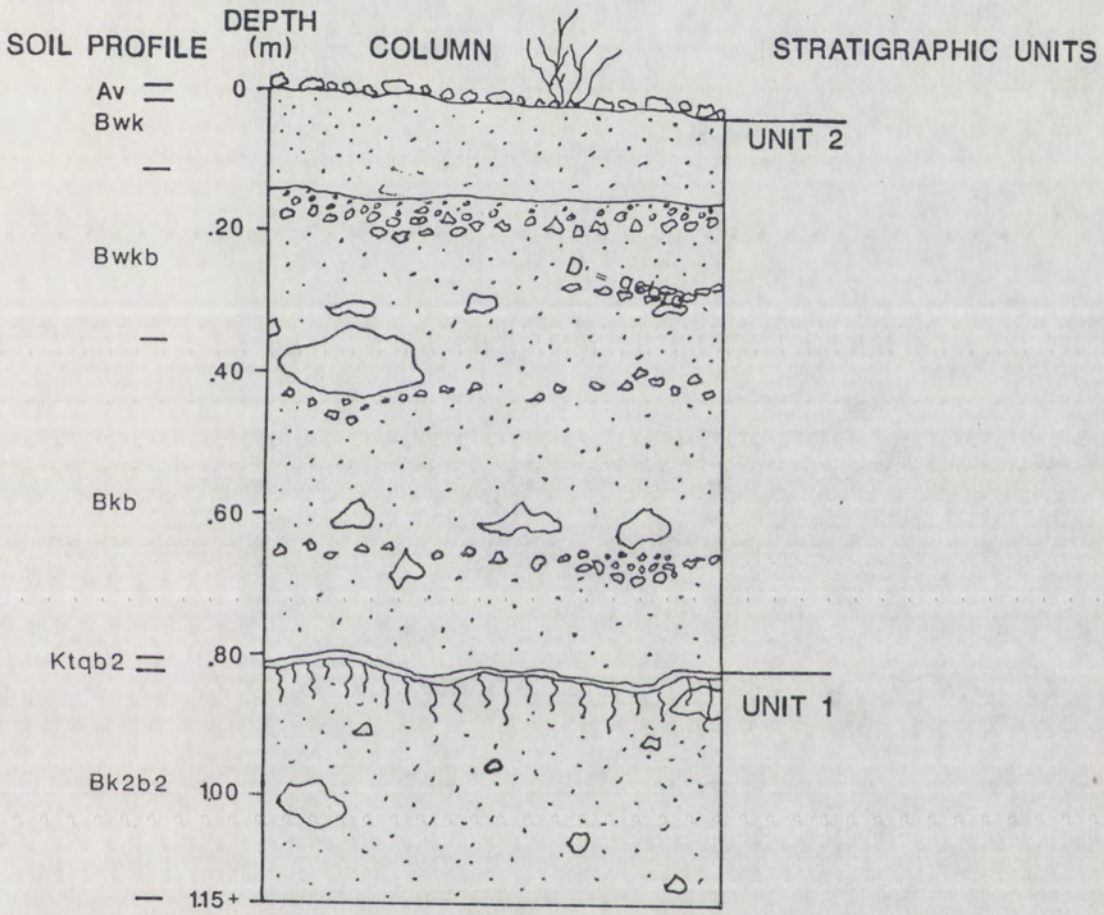

APPENDIX B

SOIL DESCRIPTIONS

Summary of morphological data for soil SA2-1 developed in the debris-apron of the A2 cone. Visual assessment of pebble roundness (Krumbein, 1941).

Location:	Cima Volcanic Field, E side of A cone, Apron	Sample Label:	CVCA-2 (STRATA-2)
Elevation (feet):		Date:	6/5/87
Topographic Position:	4 degree slope	Described by:	Claire Renault
Climate:	Arid	Project:	Master's Thesis
Vegetation:	creosote bush, small woody shrubs, annuals		
Desert Pavement:	Poorly dev. composed of lapilli		

Horizon SA2-1	Depth (cm) top-base		Boundary	Color dry	Color wet	Texture % grvl	Texture matrix	Structure Primary	Structure Secondary	Consistance dry	Consistance wet	CaCo3 matrix	CaCo3 gravel	Clay Films	Roots	Pores	Salt Gravel	Salt Matrix	Parent Material	Comments
AC	0	0.4	cs	10YR6/4	5/3	30	L	sg	--	lo	so,po	no	e	no	3vf	no	no	no	lapilli	lapilli 0.2-.5cm; roundness 0.2
Av	0.4	3	cs	10YR6/4	7/3	<5	SL	1m sbk	--	so	so,ps	no	no	no	3vf	3vf dis v	no	no	lapilli dust	lapilli 0.2-.5cm; roundness 0.2 fluvial
Bwk	3	23	aw	10YR7/4	4/3	30	LS	1m sbk	--	so	so,po	no	e	vln br	3f	2vf dis v	no	no	lapilli dust	lapilli 0.2-1.5cm; roundness 0.5 fluvial
AvBtkb	23	32	vaw	(inside ped) 10YR7/3	5/4 (outside ped) 10YR8/3	35	SL	3co abk	--	h-vh	ss,ps	e	dis n bot	2n po,	3vf	3vf dis v	no	no	lapilli dust	lapilli 0.2-1.5cm; roundness 0.2 fluvial
Bkb	32	35	cs	10YR8/3	5/4	30	SL	3co sbk	--	sh	so-ss,po	in:ev outres	nodules dis sed	2n po	2vf	2f dis v,i	no	NaCl (taste)	lapilli bombs dust	lapilli, bombs 0.2-20cm; roundness 0.3 bombs laterally discontinuous laminar carbonate airfall I
Bk2b	35	45	gw	10YR6/4	4/3	45	SL	sg	--	lo	ss,ps	ev	cont n-a bot	2 Co	2vf	no	no	NaCl (taste)	lapilli dust	lapilli 0.2-1.0cm; roundness 0.2 airfall I
Bk3b	45	95	cs	------	--	98	--	--	--	--	--	no	dis n bot decr down	no	no	3m-co cont i	no	no	lapilli	lapilli 0.2-1.0cm; roundness 0.2 top of lapilli is red airfall I
Bkb2	95	111	cs	10YR6/4	4/3	85	CoS	sg	--	lo	so,po	es	dis n bot	no	no	3m-co cont i	no	no	lapilli dust	lapilli 0.2-3cm; roundness 0.1 very little red on top of lapilli airfall II
Bk2b2	111	133+	--	------	--	--	--	--	--	--	--	--	es n bot	no	no	3m-co cont i	no	no	lapilli	lapilli 0.2-2cm; roundness 0.1 very little red on top of lapilli airfall II

Summary of morphological data for soil SA2-3 developed in the debris-apron of the A2 cone. Visual assessment of pebble roundness (Krumbine, 1941).

Location: Cima volcanic field, NE side of A2 cone
Elevation (feet):
Topographic Position: 8 degree slope
Climate: Arid
Vegetation: Few creosote, small woody shrubs approx every 3m, dried annuals.
Desert Pavement: Poorly developed composed of lapilli and bombs

Sample Lable: CVCA-1 (STRATA-3)
Date: 6/4/87
Described by: Claire Renault
Project: Master's Thesis

in = inside ped
out = outside ped

Horizon SA2-3	Depth (cm) top-base	Boundary	Color dry	Color wet	Texture % gravel	Texture matrix	Struc-ture	Consistence dry	Consistence wet	CaCO3 matrix	CaCO3 gravel	Clay Films	Roots	Pores	Parent Material	Comments
AC	0 0.4	as	10YR6/4	4/3	35	--	sg	lo	-----	no	no	no	2vf	no	lapilli dust	lapilli 0.2-1cm
Av	0.4 2	as	10YR7/3	5/3	7	LS	1c-vc pl	so	so,po	in: es out: s	no	no	3vf-f	3vf dis v	lapilli dust	lapilli 0.2-0.5cm colluvium
Bwk	2 27	cw	10YR6/4	5/3	50	SL	sg	lo	so,ps	es	dis n bot & sides reworked 2nd CaCO3	2 co	2vf	2f dis v	lapilli dust	lapilli 0.3-4cm roundness 0.2 colluvium
AvBtkb	27 31	cs	(inside ped) 10YR7/3 (outside ped) 10YR8/3	5/4 5/3	35	SL	2c sbk	sh	ss,ps	ev	dis n bot	1n po siltans in pores	3vf	3vf-f dis v	lapilli dust	lapilli 0.3-4cm roundness 0.2-0.3 colluvium
Bkb	31 56	as	10YR6/4	5/3	55	SL	1m gr	so	so,ps	es	dis n bot	2 co	2vf	1vf-f dis v	lapilli dust	lapilli 0.3-4cm roundness 0.3 colluvium
AvBtkb2	56 62	cw	10YR6/3 10YR7/3	5/4 5/3	20	L	2c sbk	sh	ss,sp	in: s out: ev	dis n bot weak sot.	2n po siltans in pores	2f	---	lapilli bombs dust	bombs 20cm lapilli 0.5-4cm roundness 0.2 airfall deposit
Bkb2	62 71	cw	10YR6/4 10YR6/4	4/4 5/4	7	SL	1m-c sbk	sh	so,po	ev	cont n bot & sides	n.o.	1f	no	lapilli dust	lapilli 0.5-2cm, roundness 0.1 airfall deposit
Bk2b2	71 79	cw	10YR6/4	4/4	60	SL	sg	lo	so,ps	ev	cont n bot & sides some top	2n co	3f	3vf dis v	lapilli dust	lapilli 0.2-2cm roundness 0.1 airfall deposit
Bk3b2	79 1.13+	--	-----	---	95	SL	-----	lo	so,ps		cont n bot & sides			no	lapilli	lapilli 0.2-2cm roundness 0.1 airfall deposit

Summary of morphological data for soil SUI-1 described in the surface debris-apron unit Qal of the UI cone.
Visual assessment of pebble roundness (Krumbein, 1941)

Location: Cima volcanic field, W side of UI cone, Qal surface
Elevation (feet):
Topographic Position: 1 - 3 degree slope
Climate: Arid
Vegitation: Creosote bush (6m apart), few annuals, Yucca (on edge of surface remnant), small woody shrubs
Desert Pavement: Interlocking pavement, variable grain size, 40% < 8cm, 40% 10 - 30cm

CVCUI-1
1/12/89
Claire Renault and Tom Shirvin
Master's Thesis

Horizon SUI-1	Depth (cm) top-base	Boundary	Color (ped) dry	Color wet	Texture % gravel	Texture matrix	Structure Primary	Consistence dry	Consistence wet	CaCO3 matrix	CaCO3 gravel	Clay Films	Roots	Pores	Salt Gravel	Salt Matrix	SiO2	Parent Material	Comments
Av	0 3	as	ins: 10YR7/3 outs: 10YR6/4	4.5/4 4/4	5	L	3cpl	h	ss ps	es	cv out ped es in ped	n.o.	n.o.	3vf-fdv 1codv	n.o.	n.o.	n.o.	lapilli ash loess	lapilli 0.2-0.7cm; roundness 0.2-0.3
AvBtk	3 7	aw/ ai loc	ins: 10YR6/4	4/4	7	CL	3vcpl	h	s p	esd out es-ev on bot ped esd in	n.o.	2nbr 1npo,pf	n.o.	3vf-fdv 1vfdt	n.o.	n.o.	n.o.	lapilli ash loess	lapilli 0.2-2cm; roundness = 0.3
Bky	7 13	ab	10YR6.5/4	4.5/4	3	SL	1f-vcsbk	so	ss vps	ed	CaCO3 along roots Stage I n dis bot	n.o.	3vf	1vfdt 3vfdi	gyp xtl bot clt	gyp fill in peds	n.o.	lapilli ash loess	lapilli 0.2-1.5cm; roundness = .3-.2
Btkyb	13 22	cw	10YR7/4	4/4	20	LS	2m-vcabk	vh	so po	ev on bot ped	n dis bot Loc Stage II	1nbr	n.o.	2vfdt 1vfdi	gyp xtl bot clt	gyp fill in peds & on bot	n.o.	lapilli ash	lapilli 0.2-2mm; roundness not possible to measure due to coating of CaCO3
Bkyb	22 51	aw	10YR7/3	4/3	30	LS	1f-csbk	sh	so po	----	Stage II+ Loc Stage III n dis bot CaCO3 along roots	n.o.	1vf	1vfdt 1vf-fdi	n gyp on bot		n.o.	lapilli bombs ash	lapilli 0.2-8cm; roundness = .1
Ekyb2	51 53	cw	10YR7/4	4/3	40	LS	2cosbk 2mabk	vh	-- --	es top ev bot of peds	loc Stage IV cont at top .5-1mm bot cont	t.o.	n.o.	1vfdt	few gyp xtl bot		in bands with CaCO3 on bot	lapilli	roundness not possible to measure due to coating of CaCO3
Kt2b2	53 69	aw	7.5YR7/4	10YR4/4	50	LS	m	vh	so po	cont bot peds	along roots Loc Stage IV	1nbr	n.o.	3vfdt 1vfdi	n.o.		n.o.	lapilli	roundness not possible to measure due to coating of CaCO3 lapilli 0.2-5cm
Btkb2	69 94		7.5YR7/4	10YR4/4	50	SL	2cabk	h	vss p	evd	along roots Stage III+	n.o.	n.o.	3vfdt	n.o.		n.o.	lapilli	roundness not possible to measure due to coating of CaCO3 lapilli 0.2-8cm
Bkb2	94 130+		10YR7/4	4/4	35	L	2masbk	sh	so po	evd	n dis bot	n.o.	n.o.	1vfdi	n.o.		n.o.	lapilli	roundness not possible to measure due to coating of CaCO3 lapilli 0.2-4cm

Summary of morphological data for soil SU1-2 described in
the surface debris-apron unit Qa2 of the U1 cone.
Visual assessment of pebble roundness (Krumbein, 1941).

Location: Cima volcanic field, N side of U1 cone, on Qa2 (apron
Elevation (feet):
Topographic Position:
Climate: Arid
Vegetation: Creosote bush, small woody shrubs, annuals

Sample Lable: CVCU1-2
Date: 3/17/88
Described by: Claire Renault
Project: Master's Thesis

Desert Pavement: None to very poor, no rock varnish

in = inside ped
out = outside ped

Horizon SU1-2	Depth (cm) -base	Boundary	Color dry	Color wet	Texture % gravel	Texture matrix	Structure	Consistence dry	Consistence wet	CaCO3 matrix	CaCO3 gravel	Clay Films	Roots	Pores	Parent Material	Comments
Av	0	2 as	10YR6.5/3;4/3		<5	SL	1mgr 1copl	so	sopo	n.o.	n.o.	n.o.	3vf	3vfdi&v	ash lapilli	lapilli .2 - 1cm roundness = .1-.2 fluvial ash in fines
Bwk	2	14 cs	10YR7/4;4/4		15	SL	1vf-fsbk 1fgr	so	sopo	ed	e on bot no coat	n.o.	3vf	2vfdi&v	ash lapilli	lapilli .2 - 3cm roundness = .3 fluvial
Bwkb	14	36 aw	10YR7/4;4/4		45	LS	1-2msbk 1f-mgr	so	sopo	ed	n dis bot Stage I	n.o.		2vfdt 3vfdi	lapilli bombs ash (fining up)	lapilli and bombs .2 - 14cm roundness = .3 fluvial
Bkb	36	81 aw	10YR7/3;4/3		60	LS	1fgr	so	sopo	es	n dis-cont bot and sides STAGE I+	n.o.	1v 3vf	3vfdi		lapilli and bombs .2 - 11cm roundness = .3
Btkqb2	81	83 cw	7.5YR8/2 10YR5/4		50	LS	m	vh	sopo		m cont bot, sides & roots dis sides, top 1/3mm lamm. bot	2nbr	n.o.	2vfdt	lapilli bombs ash	lapilli and bombs .2 - 8cm
Bk2b2	83	115+	7.5YR7/4 7.5YR7/4 10YR5/4		45	LS	m	vh	sopo		m cont bot, sides & roots dis sides, top 1/3mm lamm. bot	2nbr	n.o.	3vfdt	lapilli bombs ash	

Summary of morphological data for soil SU2-1 described in
the surface debris-apron unit Qal of the U2 cone.
Vissual assessment of pebble roundness by Krumbine (1941).

Location: Cima volcanic field, E side of U2 cone, on apron
Elevation (feet):
Topographic Position:
Climate: Arid
Vegetation: Creosote bush 0.5 - 3 m apart, few Joshua Tree, Yucca, small woody shrubs, abundant annuals
Desert Pavement: Very poorly developed, 50% bombs, 50% lapilli
Parent material: Lapilli, bombs, ash, loess

Sample Lable: CVCU2-1
Date: 1/15/88
Described by: Claire Renault
Project: Master's Thesis

in = inside ped
out = outside ped

Horizon SU2-1	Depth (cm) top	base	Boundary	Color dry	Color wet	Texture % gravel	Texture matrix	Structure	Consistence dry	Consistence wet	CaCo3 matrix	CaCo3 gravel	Clay Films	Roots	Pores	Parent Material	Comments
Av	0.5	3	as	10YR6.5/4;4/3		30	SL	1f-copl 1agr	so	sopo	evd	n.o.	n.o.	3vf 1f	3vfdv	bombs 20% lapilli 80%	roundness = .3 no bedding
Bwk	3	13	cw	10YR6/4;4/4		45	SL	1m-cosbk	sh	vsspo	esd	n dis bot	inpo&br	3vf	3vfdtki 1vfdv	bombs lapilli	lapilli .2-2cm; bombs<12cm roundness = .3; bombs are matrix supported;
Bwk2	13	26	cw	10YR7/4;4/4		40	SL	1vf-fsbk	so	sopo	esd	n-k dis bot sides	inpo	n.o.	2vfdt 3vfdi	bombs 15% lapilli 85%	lapilli .2-3cm; bombs <10cm roundness = .3 bombs matrix supported
Bk	26	43	as	10YR7/3;3/4		30	SL	1agr	so	sopo	evd	n-k dis bot	n.o.	2vf 1f	3vfdi	bombs <5% lapilli >95%	lapilli .2-4cm; bombs <7cm roundness = .3 bombs matrix supported
Btkb	43	73+		(outside of pe 10YR6/4 10YR7/4 7.5YR4/4		50	LS	3vcoabk	vh	sopo	evd n dis bo+ peds	m cont all, root casts	2nbr inpo	n.o.	1vfdt	can't tell	very thin lam. CaCO3 on top of horizon pedogen obscures sed. struc.

Summary of morphological data for soil SB-1 developed in the debris-apron of the B cone. Visual assessment of pebble roundness (Krumbine, 1941).

Location: Cima Volcanic Field, SW side of B cone, Apron (Qai)
Elevation (feet):
Topographic Position: 8.5 degree slope
Climate: Arid
Vegitation: creosote bush spaced 3-5m apart, some small woody scrubs, few dried annuals
Desert Pavement: mod-well developed, interlocking clasts composed of 30% boobs and 70% lapili

Sample Label: CVCB-01
Date: 6/22/87
Described by: Tom Skirvin & Claire Renault
Project: Master's Thesis

Horizon SB-1	Depth (cm)		Boundary	Color (ped) dry	Color wet	Texture % gravel	Texture matrix	Structure	Consistance dry	Consistance wet	CaCO3 matrix	CaCO3 gravel	Clay Films	Roots	Pores	Salt Gravel	Salt Matrix	Parent Material	Comments
AC	0	1	aw	10YR6/3	4/3	—	SL	sg	so	so,ps	es	—	no	no	no	no	no	loess	——
Av	1	6	aw	in: 10YR7/3 out: 10YR6/3	4/3 4/4	17	SiL	2vc pl	h	ss,ps	in: es out: no	—	no	2vf	3vf-m v	dis no	no	lapili	lapili 0.2-2cm; roundness 0.3
AvBtk	6	13	cw	10YR7/3	4/3	45	SL	2m-co pl 2m-c sbk	h	so,ps	e-es varries	dis n bot	4mk br 2-3m po	2vf	3vf-f v	dis no	gyp ? on out ped	lapili boobs	lapili 0.2-2cm; roundness 0.3 Boobs at bottom of horizon; 7-8cm long 5-10cm apart Horizon may represent a buried pavement.
AvBtkb	13	19	aw	in: 10YR7/3 out: 10YR8/2	4/3 7/3	25	fSL	2c-vc pl 2f-m sbk	sh-vh	ss,ps	es-ev 2f fill	cont n peds	3m-mk br	2vf	2vf dis v	no	NaCl taste	lapili	lapili 0.2-1.5cm; roundness 0.4-0.3 Possible laminar fluvial structures Pedogenesis obliterates most sed structures
Btkyb	19	26	aw	in: 10YR6/3 out: 10YR5/3	4/3 4/3	20	SL	1-2c-vc pl 1-2vf-m sbk	sh-vh	ss,ps	e-es bot of peds	dis vm bot	3-4mk br 3m po	3vf-f ped sides	3vf dis v, ir	gyp dis n bot	gyp lay out ped	lapili	Lapili 0.2-3cm; roundness 0.2-0.3 Gypsum inside and outside peds obliterates most sed structures; Brown gypsum forms laminar layers. Laminar structures of fine/coarse material (I-beds?)
Btkb	26	37	—	10YR7/3	4/4	20	LS	1m gr	so	so,po	ev fill	cont n bot	no	2-3vf	no	no	NaCl taste	lapili	lapili 0.2-1.5cm; roundness 0.2 Appears to be one cont. fine layer (sed sorted)
Bkyb	37	78	ab	10YR7/3	4/4	30	LS	sg	lo	so,po	——	cont n bot and sides	no	3vf	no	gyp bot stals	gyp stals	lapili	lapili 0.2-1cm; roundness 0.2 (roundness inacurate due to CO3) Layers (up to 15m) create a local Stage 4 carb Gypsum present as brown coatings within layers Extresely well cemented discontinuous carbonate (m bot), gypsum (top), and silica (?) forming layers Sedimentary structure obliterated by pedogenisis Horizon appears to be a colluvial sedimentary layer
Bky/Eyb	78	98	cb	in: 10YR6/3 out: 10YR8/2	5/3 5/4	55	LS	3vc pl 3vc sbk	vh	so,po	in: ev out: ev Bt. 4 Pf in 50% po	cont all (lea)	no	no	3vf-m dis ir	no	gyp top peds stl	lapili	lapili 0.2-1cm; roundness very angular 0.1 Secondary structure occurs where there is no laminar structure; Laminated peds not laterally continuous (depth varries) Stage 4 ontop of peds (lea) Beginning of airfall lapili
Bkyb'	98	105	—	in: 10YR7/3 out: 10YR8/2	6/6 6/6	50	LS	3f-m sbk 3m pl	vh	so,po	es	e on lea	no	no	no	no	gyp ? layers	lapili	lapili 0.2-1cm; roundness 0.1 airfall
Bkyb''	105	125+	—	———		—	—	sg	—	——		e-es bot	no	no	--	gyp bot		lapili	lapili 0.2-3cm, roundness 0.1 airfall

Summary of morphological data for soil SB-2 described in the surface debris-apron units Qa2 of the B cone.
Visual assessment of pebble roundness by Krumbine (1941).

Location: Cima Volcanic Field, SE side of B cone on apron (Qa2) 60m from apron/cone break in slope/m
Elevation (feet):
Topographic Position: Lowermost portion of apron; 3.5 degree slope
Climate: Arid
Vegitation: None
Desert Pavement: Moderate development

Sample Label: CVCB-2
Date: 6/26-27/87
Described by: Tom Sikrvin
Claire Renault
Project: Master's Thesis

in = inside ped
out = outside ped

Horizon SB-2	Depth (cm) top-base	Boundary (ped)	Color dry		wet	Texture % gravel	matrix	Structure Primary	Secondary	Consistence dry	wet	CaCO3 matrix	gravel	Clay Films	Roots	Pores	Salt Gravel	Matrix	Parent Material	Comments
AC	0 1	aw	10YR7/3	5/3	--	Si	sg			lo	so po	ed	--	n.o.	n.o.	n.o.	n.o.	n.o.	loess	--
Av	1 5	aw	in: 10YR7/3	5/4	20	SiL	2c-vcpl			sh	ss ps	esd	n.o.	inpo	3vf	3vf-fdv	n.o.	n.o.	lapilli	lapilli 0.2-1cm; roundness 0.4-0.3
			out: 10YR7/3	5/3																
AvBtk	5 8	aw	10YR7/3	5/4	40	L	2c-vcpl	2f-esbk		sh	so po	in: esd out: evd	dis vn bot	3npf 3npo 3nbr	3vf-f	3vfdv 3vfdi	n.o.	n.o.	lapilli	lapilli 0.2-2cm; roundness 0.3; however, difficult to asses due to pedogenesis
Bt	8 11	cwb	10YR7/4	4/4	55	L	1fgr			so	so po	evd	dis n bot	4co	2vf	n.o.	n.o.	n.o.	lapilli boabs	lapilli + boabs 0.2-9cm; roundness 0.1-0.2
Bky	11 30	awb	10YR6/3	4/4	35-40	SL	1f-esbk			so	so po	evd	dis n bot filats, <1as nods	3co	3vf	1vfdi	n.o.	n.o.	lapilli boabs	lapilli + boabs 0.2-10cm; roundness 0.1-0.2; few cemented insect burrows
AvBtkyb	30 43	awb	10YR7/3	4/4	30	LS	2f-esbk			sh	so po	evd	dis n bot	inpo 3nbr	n.o.	3vfdv	gypsum	n.o.	lapilli	lapilli 0.2-4cm; roundness 0.2-0.3 laterally discontinuous
Bkyb	43 49	asb	10YR6/3	4/3	40	LS	1fgr	2mgr		so	so po	n.o.	dis n bot	n.o.	3vf	2vfdi	gyp dis bot	n.o.	lapilli	lapilli 0.2-4cm; roundness 0.2
AvBtkyb2	49 52	asb	in: 10YR6/3	4/3	20	fSL	2f-esbk	2cpl		sh	ss ps	in: ed out: n.o.	dis n bot	inpf	3vf	3vf-fdv 3vfdi	gyp dis bot	n.o.	lapilli	lapilli 0.2-3cm; roundness 0.2-0.3
			out: 10YR7/3	4/3																
Bkb2	52 56	aw	10YR6/3	4/3	20	LfS	2vfsbk			so-sh	so po	n.o.	dis n bot; 1csf	n.o.	3vf	3vfdi	gyp dis bot	n.o.	lapilli	lapilli 0.2-2cm; roundness 0.2 possible vessicular pores
AvBtkyb3	56 70	csb	in: 10YR6/3	4/3	40	LS	2c-vcpl	2f-esbk		sh	so po	--	dis n bot pf; cont n bot	inpf	2vf	2vfdv 2vfdi	gyp dis bot	n.o.	lapilli boabs	lapilli 0.2-2.5cm; roundness 0.1-0.2 burrows (.5cm)
			out: 10YR7/3																	
Btkyb3	70 80	as	10YR7/3	4/3	30	SL	2mpr	2f-csbk		h	so ps	--	cont n all; coats on 3vf root casts	2mbr	n.o.	1vfdv 3vfdi	n.o.	gyp in pores	lapilli	lapilli 0.2-5cm; roundness -- beginning of airfall
Bkyb3	80 93	aw	10YR7/3	5/3	60	SL	1f-esbk			sh	so po	esd	cont n bot; coats on 3vf root casts	n.o.	3vf	n.c.	gyp dis bot	n.o.	lapilli	lapilli 0.2-4cm; roundness 0.1
Bky2b3	93 109	aw	10YR8/2	5/3	30	SiL	3c-vcsbk			h	vss ps	--	cont n bot; dis n sides and top	n.o.	n.o.	3vf-vdi	gyp dis bot	n.o.	lapilli	lapilli 0.2-3cm; roundness (too much CaCO3) burrows (0.3cm)
Bky2b3	109 120+	--	10YR7/3	4/3	60	LS	sg			lo	so po	esd	cont n bot	n.o.	n.o.	n.o.	gyp dis bot	n.o.	lapilli	lapilli, 0.2-4cm; roundness 0.1

Summary of morphological data for soil SE-2 described in the surface debris-apron unit Qa2 of the E cone.
Visual assessment of pebble roundness (Krumbein, 1941).

Location: Cima volcanic field, NE side of E cone, Qa2 (apron) Sample Label: CVCE-1
Elevation (feet): Date: 1/5/88
Topographic Position: Described by: Claire Renault
Climate: Arid Project: Master's Thesis
Vegetation: Creosote bush 1-2m apart, small woody shrubs, annuals

Desert Pavement: none In = inside ped
Out = outside ped

Horizon SE-2	Depth (cm) top-base	Boundary	Color dry	Color wet	Texture % gravel	Texture matrix	Structure Primary	Structure Secondary	Consistence dry	Consistence wet	CaCO3 matrix	CaCO3 gravel	Clay Films	Roots	Pores	Salt Gravel	Salt Matrix	Parent Material	Comments
Av	0 - 9	as	10YR7/4	4/4	20	coSL	1copl	1m-cgr	so	sopo	ed	n.e.	n.e.	3vf	3vfdvbi	n.e.	n.e.	lapilli ash (fining up)	lapilli .2-2cm roundness = .3 laminar bedding mod - poor sorting
Bwky	9 - 24	as	10YR7/3	5/4	35	coSL	1csbk	1m-cgr	so	sopo	ed	n dis bot	n.e.	2vf	3vfci	stls on sides	n.e.	lapilli ash (fining up)	lapilli .2-5cm roundness = .3-.2 laminar bedding mod - poor sorting
Av&Btkyb	24 - 33	as	10YR7/4	4/3	55	coSL	1msbk	1vf-fsbk	sh	sopo	ed	n dis bot	1mbr 1mpokpf	3vf 1f	3vfdv 2vfdikt	bot	fil.	lapilli ash (fining up)	lapilli .2 - 3cm roundness = .3 laminar bedding mod - poor sorting
2Bkyb	33 - 55	cs	10YR7/3	5/4	40	vcoSL	m 1fsbk		so	sopo	ed	n dis bot	n.e.	3vf 1m	3fdi 1vfdt	fil. on bot	fil.	lapilli ash (fining up)	lapilli .2 - 5cm roundness = .3 - .4 laminar bedding mod - poor sorting
2Bky2b	55 - 71	cw	10YR7.5/3	5/4	25	SL	sg		lo	sopo	esd	n dis bot	n.e.	3vf	3vfdi	fil. on bot	n.e.	lapilli boabs ash	lapilli and boabs .2 - 13cm roundness = .2 boabs matrix supported debris flow deposit (?)
3Btkyb2	71 - 85	cw	8.75YR7/4	10YR5/6	43	coSL	1m-1fpl	1f-msbk	so-sh	sopo	esd	n dis bot (dis on peds)	2mbr 1mpo	1vf	1vfdi	fil. on bot	fil.	lapilli boabs ash	lapilli and boabs .2 - 10cm roundness = .3 - .2 laminar fluvial bedding pedogen. part. obsc. bedding
3Bkyb2	85 - 112	cw	7.5YR7/4	10YR6/4	20	coSL	1co-vcsbk	1f-msbk	sh	sopo	esd	1mo cont bot dis top & side, Stage III, coats on peds	n.e.	1vf	1vfdi 3vfdt	n.e.	fil.	lapilli boabs ash	lapilli and boabs .2 - 14cm roundness = .2 no bedding visible colluvium (?)
3Bky2b2	112 - 122	cw	7.5YR6/4	8.75YR5	50	coSL	m		h	sopo	esd	1lmo cont coats on bot, dis top & sides, Stage II	n.e.	1vf	3vfdi	coats on grains	fil.	lapilli boabs ash	lapilli and boabs .2 - 11cm roundness = .1 - .2 iron ox. abund. on clasts no bedding visible colluvium (?)
3Bky3b2	122 - 144	cw	10YR7/4	5/4	50	coSL	m	1mpl	so	sopo	esd	1lmo cont coats on bot, dis top & sides, Stage II	n.e.	1vf	3vfdi	n.e.	fil.	lapilli boabs ash	lapilli and boabs .2 - 12cm roundness = .1 - .2 iron ox. abund. on clasts no bedding visible colluvium (?)
3Bkb2	144 - 157+		10YR7/4	5/4	40	SL	sg		lo	sopo	esd	n dis bot	n.e.	n.e.	3vfdi	n.e.	n.e.	lapilli ash	lapilli .2 - 5cm roundness = .1 less iron ox. and silt approaching airfall

Summary of morphological data for soil SE-1 described
in the surface debris-apron unit Qal of the E cone.
Visual assessment of pebble roundness (Krumbein, 1941)

Location: Cima volcanic field, E side of B cone, Qal (0) (apron)
Elevation (feet):
Topographic Position:
Climate: Arid
Vegetation: Creosote bush 6 m apart, woody shrubs 6 m apart, few annuals
Desert Pavement: Good, interlocking with rock varnish

Sample Lable: CVCE-2
Date: 1/6/88
Described by: Claire Renault
Project: Master's Thesis

in = inside ped
out = outside ped

Horizon SE-1	Depth (cm) top-base	Bound-dary	Color dry	Color wet	Texture % gravl	Texture matrx	Structure	Consistence dry	Consistence wet	CaCO3 gravel	Clay Films	Roots	Pores	Salt Gravel	Salt Matrix	Parent Material	Comments
Av	0 2	as	10YR7/4	4/4	5	L	2c-vcpl	sh	ss ps	n.o.	n.o.	1vf	3vfdi 3vf-adv	n.o.	n.o.	lapilli ash	lapilli 0.2-1.5cm; roundness = .3-.4
Btky	2 8	as	8.75YR7/4	4/4	5	CL	3vcpl	vh	s p	vn dis bot	1skpf 3npo	n.o.		gyp bot peds	n.o.	lapilli ash	lapilli 0.2-1cm; roundness = .3
Bky	8 20	cs	10YR6.5/4	4/4	15	SL	1f-agr	so	vss po	n dis bot	n.o.	3vf	3vfdi	gyp bot clasts	soft masses gyp	lapilli ash bombs	lapilli 0.2-7cm; roundness = .3
Bky2	20 41	as	10YR7/4	4/4	10	LS	1fgr	so	so po	n dis bot	n.o.	3vf	3vfdi	gyp fila bot clasts	n.o.	lapilli ash	lapilli .2-1.5cm; roundness = .2
Bky3	41 51	as	10YR6.5/4	4/4	7	LS	1f-agr	so	so po	n dis bot	n.o.	2vf	3vfdi	gyp fila bot clasts	n.o.	lapilli ash	lapilli .2-1cm; roundness = .2
Bky4	51 54	aw	10YR7.5/3	5/4	20	SL	3c-vcpl 1msbk	vh	vss po	Stage II+ discont. lam layers of CaCO3	n.o.	3vf-f	3vfdt 3vfdi	gyp fila bot clasts	n.o.	lapilli ash	lapilli 0.2-1.5cm; roundness = .2-.1
Bky5	54 61	cw	10YR8/4	4/4	20	LS	1fsbk	sh	so po	n dis bot	n.o.	1vf	3vfdt 3vfdi	n.o.	gyp fila	lapilli ash	lapilli 0.2-2cm; roundness = .2
2Bky	61 63	cw	10YR7.5/3	5.5/4	20	LS	2m-cpl	vh	so po	loc Stage IV in small platy layers	n.o.	3vf	2vfdt	gyp fila bot peds	n.o.	lapilli ash	lapilli 0.2-2cm; roundness = .2
2Bky2	63 127+		10YR6/4	4/4	15	LS	1-2msbk	h	so po	n dis bot	n.o.	2vf	1vfdt 2vfdi	brown gyp bot clasts	n.o.	lapilli ash bombs	lapilli .2-8cm; roundness = .3 Some quartz and Feldspar clasts approx .3cm

APPENDIX C

STATISTICAL TESTS

WILCOXON T TEST

Null Hypothesis I: The percent areal extent of debris-flow channels is the same when topographically below resistant cone slope lithologies versus non-resistant lithologies.

OBSERVATION:	0	0	0	0	11	17	33	40	50	50
RANK:	1.5	1.5	1.5	1.5	6	7	8	9	10.5	10.5

OBSERVATION CONT.:	52	54	62	69	74	79	88
RANK CONTINUED:	12	13	14	15	16	17	18

N1 = Percent debris flow below areas with no agglutinate or proto-agglutinate (underlined above).
N2 = Percent debris flow below areas with agglutinate or proto-agglutinate.

Calculated T value = 43.5
Table T value = 53

If observed T is equal or less than the tabulated value then the hypothesis that there is no difference between the sampled populations is discredited. Therefore, the null hypothesis is rejected indicating that the percentage of debris-flow activity is higher below agglutinate and proto-agglutinate than elseware on the cinder cone.

Null Hypothesis II: The areal extent of deeply incised channels is the same when topographically below resistant lithologies (agglutinate or proto-agglutinate) versus non-resistant lithologies.

OBSERVATION:	10	11	14	14	16	17	19	21	28
RANK:	1	2	3.5	3.5	5	6	7	8	9

OBSERVATION CONT.:	30	31	32	34	37
RANK CONTINUED:	10	11	12	13	14

N1 = Depth of incision below areas with no agglutinate or proto-agglutinate (underlined above)
N2 = Depth of incision below areas with agglutiante or proto-agglutinate.

Calculated T value = 17.5
Table T value = 22

The null hypothesis is rejected indicating that the depth of incision is greater topographically below exposures of agglutinate and proto-agglutinate.

APPENDIX D

TOPOGRAPHIC PROFILES

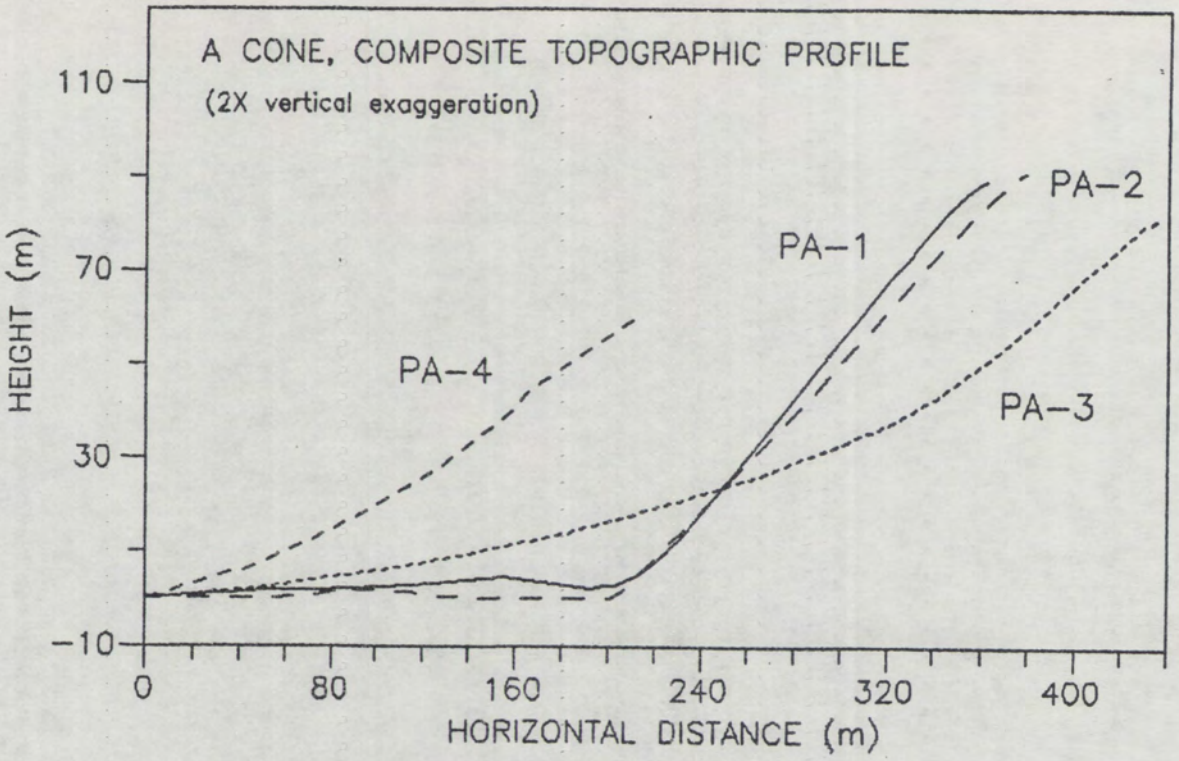
A CONE, COMPOSITE TOPOGRAPHIC PROFILE
(2X vertical exaggeration)
110
70
30
-10
HEIGHT (m)
0
80
160
240
320
400
HORIZONTAL DISTANCE (m)
PA-1
PA-2
PA-3
PA-4

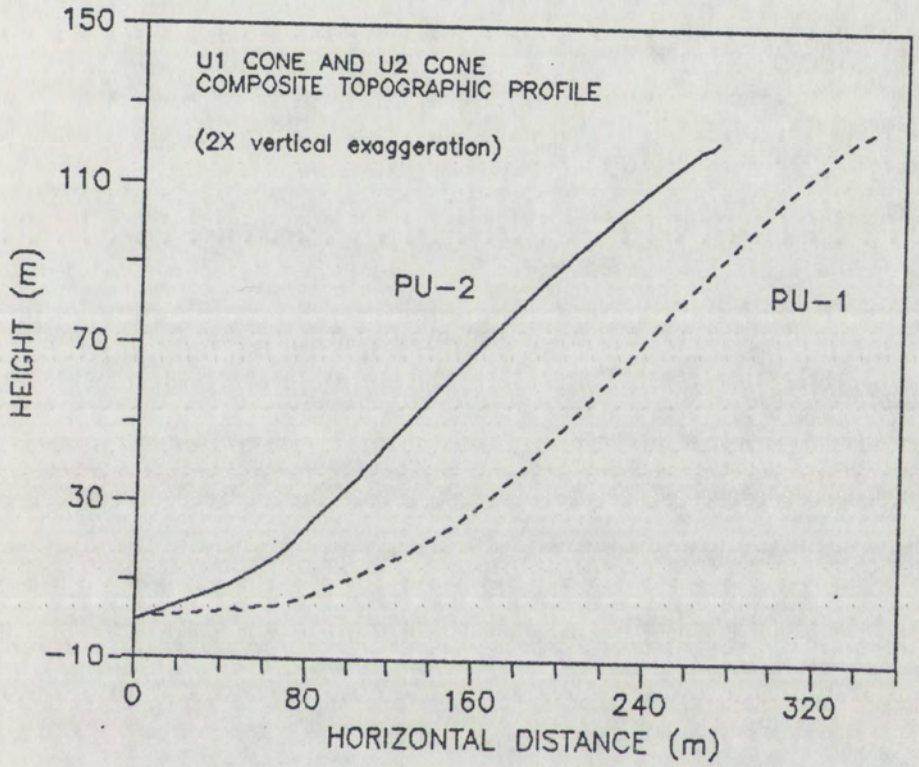
U1 CONE AND U2 CONE
COMPOSITE TOPOGRAPHIC PROFILE
(2X vertical exaggeration)
PU-2
PU-1
HEIGHT (m)
150
110
70
30
-10
0
80
160
240
320
HORIZONTAL DISTANCE (m)

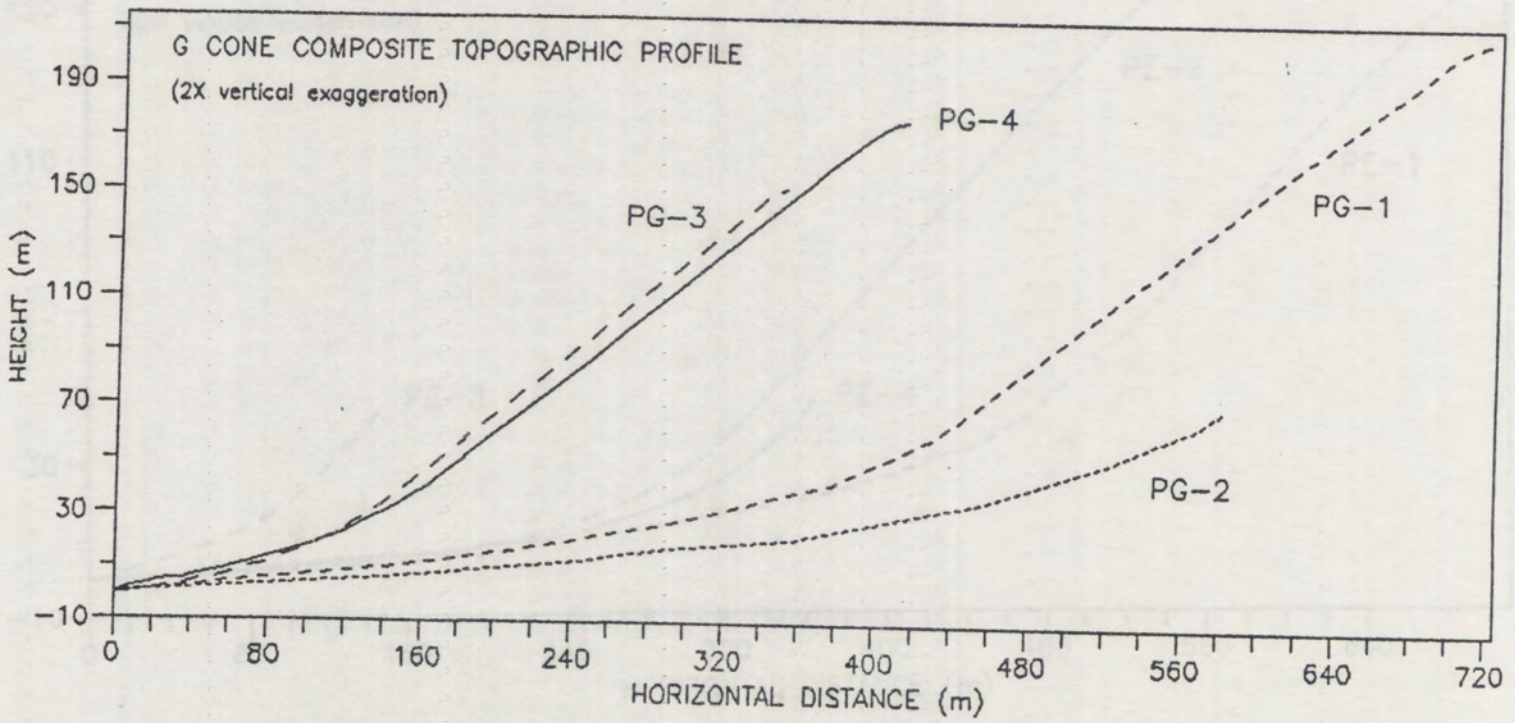
G CONE COMPOSITE TOPOGRAPHIC PROFILE
(2X vertical exaggeration)
PG-4
PG-3
PG-1
PG-2
HEIGHT (m)
190
150
110
70
30
-10
0
80
160
240
320
400
480
560
640
720
HORIZONTAL DISTANCE (m)

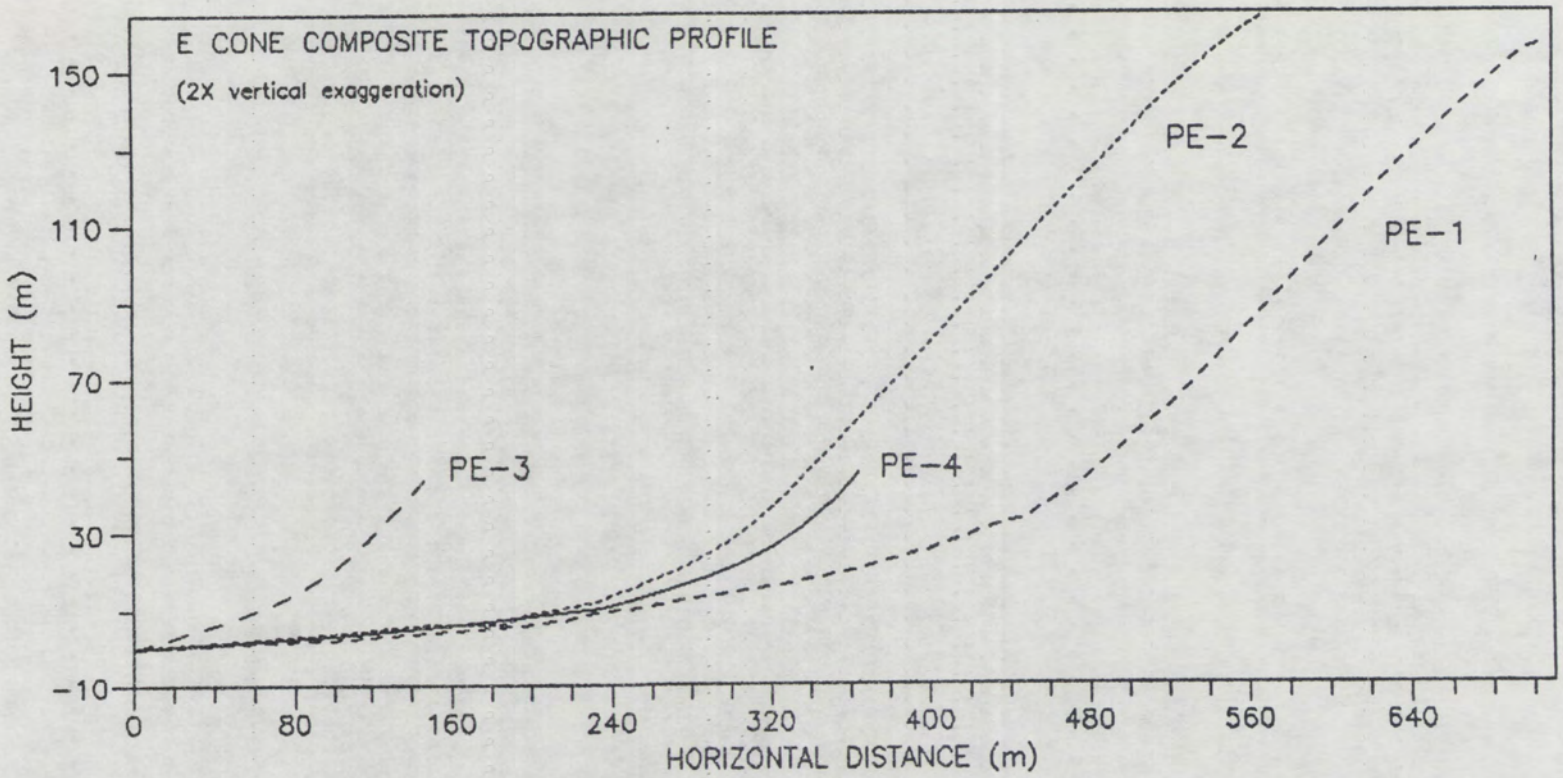
E CONE COMPOSITE TOPOGRAPHIC PROFILE
(2X vertical exaggeration)
PE-1
PE-2
PE-3
PE-4
HEIGHT (m)
150
110
70
30
-10
0
80
160
240
320
400
480
560
640
HORIZONTAL DISTANCE (m)

REFERENCES

Bird, P., 1988, Formation of the Rocky Mountains, Western United States: A continuum computer model: Science, v.239, p. 1501-1507.

Birkeland, P.W., 1984, Soils and Geomorphology: Oxford University Press, New York, 272 p.

Blackburn, E.A., Wilson, L., Sparks, R.S.J., 1976, Mechanisms and dynamics of strombolian activity: Journal of Geological Society of London, v. 132, p. 429-440.

Bockheim, J.G., 1980, Solution and use of chronofunctions in studying soil development: Geoderma, v. 24, p. 71-85.

Bloomfield, K., 1975, A late-Quaternary monogenetic volcanic field in central Mexico: Geologische Rundscjau, v. 64, p. 476-497.

Brown, D.E., Lowe, C.A., and Pase, C.R., 1980, Digitized classification for ecosystems with an illustrated summary of the vegetation of North America: United States Department of Agriculture, Forest Service General Technical Report, RM-73.

Cas, R.A.F. and Wright, J.V., 1987, Volcanic Successions, Modern and Ancient, London, Allen and Unwin, 528 p.

Chouet, B., Hanisevicz, N., and McGetchin, T.R., 1974, Photoballistics of Volcanic Jet Activity at Stromboli, Italy: Journal of Geophysical Research, v. 79, p. 4961-4976.

Colton, H.S., 1937, The basaltic cinder cones and lava flows of the San Francisco Mountain volcanic field: Museum North; Arizona Bulletin. v. 10, p. 1-49.

Colton, H.S., 1967, The basaltic cinder cones and lava flows of the San Francisco Mountain volcanic field: Flagstaff, Arizona, Museum of Northern Arizona, p. 56.

Crowe, B., Perry, F., Wells, S., McFadden, L., Renault, C., Turrin, B., Champion, D., Harrington, C., 1989, Polycyclic Volcanism: A Common Eruption Mechanism of Small Volume Basaltic Volcanic Centers of the southern Great Basin, U.S.A., Submitted to Continental Magmatism, IAVCEI General Assembly, Santa Fe, 1989, New Mexico.

Crowe, B.M., Perry, F.V., Turrin, B.C., Wells, S.G., McFadden, L.d., 1988, Volcanic hazard assessment for storage of high-level radioactive waste at Yucca Mountain, Nevada: Geological Society of America Abstracts with Programs, v. 20, p. 153.

Crowe, B., Harrington, C., Perry, F., Wells, S.G., McFadden, L.D., Renault, C.E., Turrin, B., Champion, D., 1989, (in press), Volcanic Hazard Studies for the Yucca Mountain Project, DOE Waste 1989, Tucson Az.

Dohrenwend, J.C., Wells, S.G., and Turrin, B.D., 1986, Degradation of Quaternary cinder cones in the Cima volcanic field, Mojave Desert, California: Geological Society of America Bulletin, v. 97, p. 421-427.

Dohrenwend, J.C., McFadden, L.D., and Turrin, B.D., Wells, S.G., 1984, K-Ar dating of the cima volcanic field, Mojave Desert, California: Late Cenozoic volcanic history and landscape evolution: Geology v. 12, p. 163-167.

Dorn, R.I., 1984, Geomorphological interpretation of rock varnish in the Mojave Desert, in: Dohrenwend, J.C. ed., Surficial Geology of the Eastern Mojave Desert, California: Geological Society of America 1984 Annual Meeting Guidebook, p. 150-161.

Dorn, R.I., Bamforth, D.B., Cahill, T.A., Dohrenwend, J.C., Turrin, B.D., Donahue, D.J., Jull, A.J.T., Long, A., Macko, M.E., Weil, E.B., Whitley, D.S., Zahel, T.H., 1986, Cation-ratio and accelerator radiocarbon dating of rock varnish on Mojave artifacts and landforms: Science, v. 231, p. 830-833.

Evanari, J., Yaalon,'D.H., and Gutterman, Y., 1974, Note on soils with vesicular structures in deserts: Zeitschrift fur Geomorphologie, v. 18, p. 162-172.

Farmer, G.L., Semken, S., Crowe, B., Perry, V.F., Curtis, D., DePaolo, D.J., (in press), Isotopic evidence regarding the structure and origin of subcontinental lithospheric mantle in the southern Great Basin.

Fisher, R.V. and Schmicke, H.U.,1984, Pyroclastic Rocks: Berlin: Springer-Verlag.

Gardner, V. and Dackombe, R., 1983, Sediment and Sedimentary Rock Descriptions, in: Geomorphological Field Manual, Dackombe, R.V., and Gardner, V. eds., Allen and Unwin, London, p. 105-121.

Gile, L.H., Peterson, F.F., and Grossman, R.B., 1966, Morphological and genetic sequences of carbonate accumulation in desert soils: Soils Science, v. 101, p. 347-360.

Gile, L.H., 1987, A Pedogenic Chronology of Kilbourn Hole, Southern New Mexico: I. Soils in the tuff: Soil Science Society of America Journal, v. 51, p. 74-75.

Greeley, R., and Iverson, J.D., 1986, Aeolian Processes and Features at Amboy Lava Field, California, in: El-Baz, F., and Hassan, M.H.A. eds, Physics of Desertification, Martins Nijhoff Publishers, p. 290-317.

Gutmann, J.T., 1979, Structure and Eruptive cycle of cinder cones in the Pinacate Volcanic Field and the Controls on Strombolian Activity: Journal of Geology, v. 87 p. 448-454.

Hasenaka, T., and Carmichael, I.S.E., 1985, The cinder cones of Michoean Guanajato, central Mexico: Their age, volume and distribution, and magma discharge rate: Journal of Volcanology and Geothermal Research, v. 25, p. 105-124.

Katz, M. and Boettcher, A., 1980, The Cima Volcanic Field, in: D.L. Fife and A.R. Brown eds., Geology and Mineral Evaluation of the California Desert, South Coast Geological Society, p. 236-241.

Kear, D., 1957, Erosional Stages of Volcanic Cones as Indicators of Age: New Zealand Science and Technology, v. 38B, p. 671-682.

Keiffer, G. 1971, A percu sur la morphologie des regions volcaniques du Massif Central Francais, Clermon-Feran p. 479-510.

Krumbein, W.C. 1941, Measurement and geological significance of shape and roundness of sedimentary particles: Journal of Sedimentary Petrology, v. 11, p. 64-72.

McDonald, G.A., 1972, in: Volcanos, Prentice-Hall, Englewood Cliffs, N.J., p. 183-197.